La Sapienza University of Rome Ph.D School in Behavioral Neuroscience

Ph.D Program in
Psychobiology and Psychopharmacology

Bidirectional control of dorsomedial striatum on innate avoidance behavior

Accademic year 2023/2024

Luca Fralleoni
1459551

Tutor Prof. Arianna Rinaldi

Table of Contents

Abstract

Avoidance behaviour, aimed at escaping dangerous stimuli and threatening situations, can become maladaptive when individuals avoid relatively safe situations, a hallmark of anxiety disorders. Innate avoidance, a natural aversion to ethologically relevant stimuli, involves a neural circuit in which the basolateral amygdala (BLA) and prefrontal cortex (PFC) play a central role. We have observed that both the PFC and the BLA send converging unidirectional excitatory inputs to the dorsomedial striatum (DMS), which thus may be ideally positioned to regulate the output of this circuit. Indeed, the DMS has been implicated in learned, and more recently in innate avoidance behaviours. To investigate the role of the PFC-DMS and BLA-DMS pathways in innate avoidance, we used a chemogenetic approach. CD1 male mice received a bilateral injection of AAVs expressing either the inhibitory DREADD hM4D(Gi) or the excitatory DREADD hM3D(Gq) in the PFC or BLA. Then, mice were focally injected with CNO or saline into the DMS and tested in the elevated plus maze (EPM) 30 minutes later. Inhibiting the PFC-DMS pathway did not affect the time spent in open arms of the EPM, but its activation significantly reduced anxiety. On the other hand, activation of the BLA-DMS pathway led to a reduction in the time spent in the open arms, while its inhibition had a strong anxiolytic effect. To understand why the same type of manipulation of two pathways converging in the same region generates opposite behavioral responses, we aimed to evaluate the contribution of striatal interneurons receiving direct projections from the PFC or the BLA. To this end, Ai14 mice were injected in the PFC or BLA with an anterograde virus (AAV1-hSyn-P2A-Cre-WPRE), capable of crossing the downstream synapse and infecting neurons that receive input from neurons at the injection site. Subsequently, brain sections were processed with a parvalbumin antibody to identify the percentage of double-positive striatal interneurons and verify whether a different percentage of these neurons received projections from the PFC or BLA. However, we did not observe significant differences in the percentage of parvalbumin-positive striatal interneurons receiving input from the PFC or BLA. As a final experiment, to verify how information from the PFC and BLA flows downstream of the basal ganglia, CD1 mice were injected with a viral vector expressing channelrhodopsin, while optical fibers were implanted in the GPi to specifically manipulate this projection during the EPM and OF tests. Activation of this pathway showed a reduction in time spent in the open arms of the EPM, suggesting an increase in avoidance behavior, without altering locomotion as measured in the OF. These results not only confirm the involvement of PFC-DMS and BLA-DMS projecting neurons in mice behaviour in the EPM, but also underscore that these pathways exert opposing bidirectional control over innate avoidance. Moreover, additional experimental subjects will be necessary to confirm the opposite effect of the projections does not involve a different contribution of parvalbumin-positive interneurons. Finally, this is the first evidence that information arriving in the DMS, which mediates avoidance behaviors, flows downstream to the GPi.

Abbreviations Table

Abbreviation	Meaning
adBNST	Anterodorsal Bed Nucleus of Stria Terminalis
BLA	Basolateral Amygdala
CNO	Clozapine N-oxide
CEA	Central Amygdala
COL	Cholinergic
CS	Conditioned Stimulus
D1R	D1 Dopamine Receptor
D2R	D2 Dopamine Receptor
dDG	Dorsal Dentate Gyrus
DG	Dentate Gyrus
DLS	Dorsolateral Striatum
DMS	Dorsomedial Striatum
DS	Dorsal Striatum
EP	Entopeduncolar Nucleus
EPM	Elevated Plus Maze
EZM	Elevated Zero Maze
GCs	Granule cells
GP	Globus Pallidus
Gpe	external Globus Pallidus
Gpi	Internal Globus Pallidus
HYP	Hyphothalamus
IA	iInhibitory Avoidance
IC	Inferior Colliculus
LC	Locus Ceruleus
LS	Lateral Septum
mGlur	Metabotropic Glutamatre Receptor
mPFC	medial Prefrontal Cortex
MSN	Medium spiny Neuron
OF	Open Field
ovBNST	Oval Bed Nucleus of Stria Terminalis
PAG	Periaqueductal grey
PB	Parabrachial Nucleus
PFC	Prefrontal Cortex
PV	Parvalbumin
RN	Raphe Nuclei
SC	Superior Colliculus
SN	Substantia Nigra
SNc	Substantia Nigra compacta
SNr	Substantia Nigra reticulata
SOM	Somatostatin
THAL	Thalamus
TS	Tail of the Striatum
US	Unconditional Stimulus
vBNST	Ventral Bed Nucleus of Stria Terminalis
vDG	Ventral Dentate Gyrus
vGP	Ventral Pallidum
vHPC	Ventral Hippocampus
VS	Ventral Striatum
VTA	Ventral Tegmental Area

1 Introduction

1.1 Avoidance and anxiety

Avoidance refers to any behavior aimed at evading dangerous stimuli and threatening situations. Adaptive avoidance enhances survival and fitness, whereas maladaptive avoidance reduces interaction with relatively safe stimuli, impacting social life and cognitive abilities (Arnaudova et al. 2017). Indeed, maladaptive avoidance is a cardinal symptom of anxiety disorders and related conditions such as post-traumatic stress disorder (Aupperle et al. 2010).

Anxiety is defined as an emotional reaction to vague, potential threats, characterized by prolonged arousal, heightened vigilance, and apprehension. This state results in distinct patterns of defensive behavior and autonomic responses, such as sweating, dizziness, and increased blood pressure and heart rate (Michael Davis et al. 2010; Blanchard et al. 2008; Grupe et al. 2013; Sylvers et al. 2011). Fear and anxiety can be conceptually understood as brain states triggered by external or internal stimuli, leading to specific measurable behavioral, physiological, hormonal, and autonomic responses. These responses have evolved to help organisms avoid or mitigate harm, thus ensuring survival. Fear typically arises from immediate, concrete sensory input, while anxiety is often provoked by potential, circumstantial, and anticipated threats (Davis et al. 2001; Davis et al. 2010; Blanchard et al. 2008; Grupe et al. 2013).

Anxiety disorders impact around 12.7% of the U.S. population, based on 12-month data from the 2012-2013 National Epidemiologic Survey on Alcohol and Related Conditions. Earlier research from the 2004 National Comorbidity Study indicated a 12-month prevalence of 21% and a lifetime prevalence of 34% (Kessler et al. 2012). These disorders are linked to higher healthcare usage, diminished quality of life, and impaired daily functioning. Among the most common

anxiety disorders are social anxiety disorder (13% lifetime prevalence), generalized anxiety disorder (6.2%), panic disorder (5.2%), and agoraphobia (2.6%), which often occurs alongside panic disorder. The anxiety disorders usually follow a long-term, persistent course (Kessler et al. 2012). Many individuals endure symptoms for years before seeking treatment (Bandelow et al. 2015). A meta-analysis of 43 studies revealed that anxiety rates spiked during the COVID-19 pandemic, with roughly 25% of adults reporting symptoms between 2019 and August 2020 (Santabárbara et al. 2021). Anxiety disorders rank as the second most prevalent psychiatric condition after depression and are associated with an average of 4.6 lost workdays per month, contributing to over $4 billion in workplace-related costs (Harder et al. 2016). They can also coexist with or exacerbate various medical conditions, including cardiovascular, gastrointestinal, pulmonary diseases, cancer, chronic pain, and migraines. Studies show that between 71% and 97.8% of those with anxiety disorders are misdiagnosed, and about 41% remain untreated (Vermani et al. 2011; Kroenke et al. 2007). Moreover, a recent epidemiological study has highlighted a global rise in anxiety disorder cases. In 2019, the worldwide prevalence of anxiety disorders was estimated at 4.05%. The number of affected individuals grew significantly from 1990 to 2019, increasing from 194.9 million to 301.4 million. Across all mental health conditions, the global prevalence was recorded at 12,537 cases per 100,000 people. Specifically, anxiety disorders accounted for 3,895 cases per 100,000 individuals. Compared to other major mental health conditions, anxiety disorders were considerably more common. For example, bipolar disorder had a prevalence of 511 cases, while schizophrenia affected 304 cases per 100,000 individuals (Javaid et al. 2023).

In conclusion, continued research into anxiety disorders is essential for improving public health outcomes, developing more effective treatments, and addressing the significant societal and economic impacts of these pervasive conditions.

Animal models have allowed to make significant progress in understanding the neural mechanisms that contribute to dysfunctional avoidance behavior seen in anxiety disorders. Although anxiety is a subjective experience that cannot be directly measured in animal models, a diverse array of behavioral tests have been implemented to quantify anxiety-related behavioral phenotypes. Exploratory-based tasks exploit rodents' innate avoidance of exposed, illuminated environments and their inherent drive to explore novel settings. These tasks, often referred to as approach-avoidance conflict tests, involve exposing rodents to an arena with "safe" and "aversive" zones.

Figure 1 An elevated plus maze used in behavioral studies to assess avoidance behavior in rodents. This test provides valuable insights into the behavioral responses associated with anxiety in animal models. The maze consists of two open arms and two enclosed arms, elevated from the ground. Rodents are observed for their tendency to explore the open arms (indicating reduced anxiety) versus the enclosed arms (indicating increased anxiety).

One of the most commonly used paradigms based on approach-avoidance conflict to assess avoidance and anxiety-like behavior in rodents is the elevated plus maze (EPM). The EPM is a plus-shaped maze elevated above the ground, consisting of two enclosed arms and two open arms (Fig1). The time spent into the open arm and the number of entries into the open arms are quantified, with an anxious phenotype indicated by greater avoidance of the open arms (Pellow et al. 1985). Other common approach-avoidance conflict tasks are the elevated zero maze (EZM), open field (OF) and light-dark box. In all these tasks mice with an anxious phenotype tend to spend more time in enclosed or 'safe' zones compared to controls. These tests do not require training because they take advantage of these innate tendencies, but are sensitive to locomotor deficits, so it is important to assess the effect of any treatments on locomotor activity. These tests have a high degree of face validity in that most anxiety disorders include a component of avoidance of a potentially hazardous stimulus, and they also have a good predictive value since they respond well to pharmacological treatments known to modulate anxiety in humans (Calhoon et al. 2015)(Fig2).

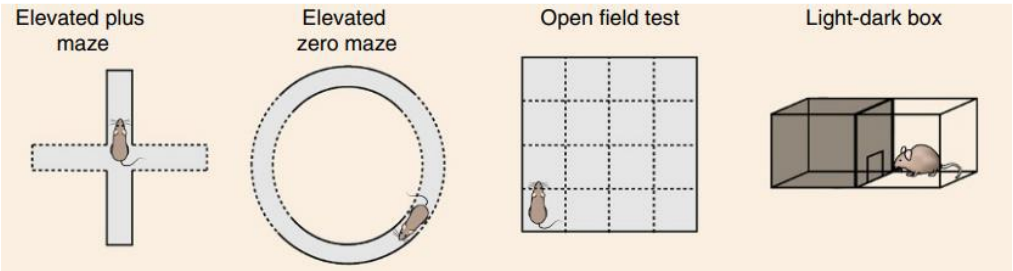

Figure 2 Validated tests to assay innate anxiety through approach-avoidance conflict task. From left to right elevated plus maze (EPM), elevated zero maze (EZM), open field (OF), light-dark box (adapted from Calhoon & Tye 2015).

1.2 Neural circuits underlying avoidance and anxiety

A substantial body of evidence indicates that avoidance and anxiety are mediated by partially overlapping neuronal circuits, which are similar in both humans and animals (Aupperle et al. 2010; Ball et al. 2022). Current research, both clinical and preclinical, suggests that anxiety disorders stem from dysfunctions within a set of highly interconnected neural circuits, with the basolateral amygdala (BLA), ventral hippocampus (vHPC), and prefrontal cortex (PFC) being key nodes (Calhoon et al. 2015; Duval et al. 2015). Using the approach-avoidance conflict task, researchers have extensively examined the roles of PFC, BLA, and vHPC activity in driving anxiety-like behavior in rodents, alongside other classic methodologies (Fig3).

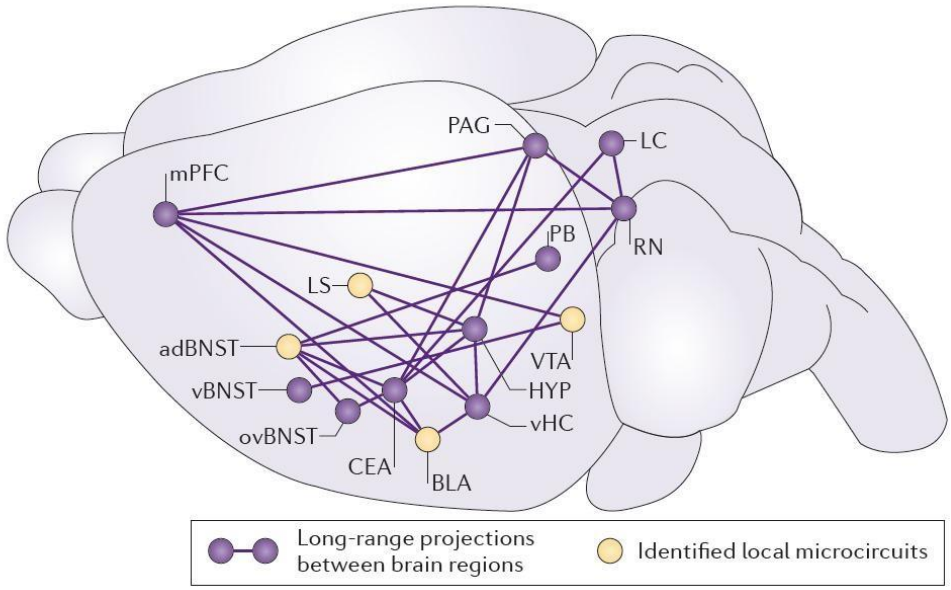

Figure 3 The anxiety network. Anxiety states are mediated by local and long-range connections between multiple brain areas. BLA, basolateral amygdala; CEA, central amygdala; vBNST, ventral bed nucleus of stria terminalis; adBNST, anterodorsal bed

nucleus of the stria terminalis; vHC, ventral hippocampus; VTA, ventral tegmental area; HYP, hypothalamus; LC, locus coeruleus; LS, lateral septum; mPFC, medial prefrontal cortex; ovBNST, oval BNST; PAG, periaqueductal grey; PB, parabrachial nucleus; RN, raphe nuclei (Tovote et al. 2015).

In vivo electrophysiology during approach-avoidance conflicts has shed light on changes in PFC neural activity when exposed to anxiety-inducing environments; specifically, theta power in the PFC increases as mice explore the enclosed arms of the EPM (Adhikari et al. 2010). Moreover, single-unit PFC neural activity has been characterized in mice during the approach-avoidance conflict in the EPM. Some neurons preferentially fire in the open arms, while others preferentially fire in the closed arms or center. Additionally, neurons that fire in the open arm also fire when the enclosed arm is made aversive with bright light, indicating that PFC neurons encode aversive environmental features rather than just location (Adhikari et al. 2011).

The amygdala was one of the first brain structures implicated in anxiety behaviors. Larger amygdala volumes correlate with increased anxiety in humans (Machado-de-Sousa et al. 2014). Patients with social anxiety disorder show heightened amygdala activation during anticipatory anxiety compared to healthy individuals (Boehme et al. 2014). In rodents, amygdala activation is observed following exposure to anxiogenic contexts (Silveira et al. 1993; Butler et al. 2012), and pharmacological inactivation of the amygdala produces an anxiolytic effect in the elevated plus-maze (Moreira et al. 2007). Tonic activity in certain BLA neurons correlates with anxiety-like behavior in the EPM and OF (Wang et al. 2011). The role of the amygdala in avoidance behavior has emerged from optogenetic manipulation rather than local pharmacological inactivation and lesion studies. Indeed, manipulation of the central nucleus of the amygdala, but not the BLA, is required for the avoidance of open spaces (Moreira et al. 2007; Carvalho et al.

2012). However, these results may reflect compensatory changes following drug infusion or lesions. Fortunately, new tools like optogenetic manipulation, which is quick and reversible, allow researchers to overcome these limitations. Optogenetic activation of the entire BLA has been shown to augment anxiety (Tye et al. 2011).

Studies suggest that the vHPC plays a crucial role in the pathogenesis of mood and anxiety disorders. The vHPC has long been associated with regulating behavior during approach-avoidance conflict (Bryant et al. 2020). In adult rodents and humans, the subgranular zone of the dentate gyrus (DG) continuously generates new granule cells (GCs) (Cameron et al. 2001). Recent findings have demonstrated the significant role of adult-born and mature GCs in regulating anxiety. Increased neurogenesis in the DG reduces corticosteroid-induced anxiety-like behaviour (Hill et al. 2015), whereas inhibition of hippocampal neurogenesis increases anxiety-related behaviors (Revest et al. 2009). Important studies have proposed that adult-born GCs in the ventral DG (vDG), but not the dorsal DG (dDG), are key in mediating anxiety-related behaviors. In mice, increasing neurogenesis in the vDG prevents social defeat-induced anxiety-like behaviors by inhibiting the activity of mature GCs. Conversely, chemogenetic silencing of adult-born GCs leads to avoidance behavior in the social interaction test and decreased center exploration in the OF (Anacker et al. 2018). However, another study from the same group found that optogenetic activation of mature vDG GCs relieves anxiety (Kheirbek et al. 2013).

Furthermore, recent studies highlight the causal role of connectivity between the PFC, vHPC, and BLA. The vHPC sends dense projections to the rodent PFC (Vertes et al. 2004). Chemogenetic inhibition of these projecting neurons decreases anxiety-related avoidance in the EPM and OF. Additionally, optical inhibition of vHPC-PFC reduces theta synchrony in this circuit and disrupts PFC

task-specific firing patterns in the EPM (Padilla-Coreano et al. 2016; Parfitt et al. 2017).

In contrast to the vHPC-PFC circuit, tract-tracing studies have demonstrated reciprocal connectivity between the PFC and BLA. Long-range afferent input from the amygdala to the PFC comes exclusively from the BLA, whereas the PFC sends top-down projections to multiple amygdala nuclei, including the lateral, basal, basomedial, and central amygdala (Gabbott et al. 2005; Vertes et al. 2004). Similar to the vHPC-PFC circuit, a subset of neurons within the BLA has been shown to track anxiety-like behavior in the EPM and OF (Wang et al. 2011). Glutamatergic signals from the BLA to pyramidal neurons in the ventral CA1 control innate anxiety behaviors in the elevated plus maze and open field tests. Activation of this pathway increases anxiety, while its inhibition reduces anxiety (Degroot et al. 2004; Felix-Ortiz et al. 2016). Furthermore, optical activation of BLA terminals in the PFC increases avoidance in the EPM and OF, while inhibition produces the opposite effects (Felix-Ortiz et al. 2016).

Collectively, the studies discussed above strongly suggest that the amygdala and vHPC are both involved in mediating anxiety-related behavior. However, the contribution of the specific connection between these two regions has been poorly understood. To study the BLA-vHPC circuit, light-sensitive opsins were expressed in glutamatergic BLA projection neurons, and an optical fiber was positioned above BLA axon terminals within the vHPC for precise illumination. Phasic light activation of channelrhodopsin-expressing BLA terminals within the vHPC transiently and significantly increased anxiety-related behavior in the OF and EPM. Conversely, light inhibition of BLA terminals in the vHPC reduced anxiety-like behavior in the OF and EPM (Felix-Ortiz et al. 2013).

The notion that a distributed network of interconnected brain regions modulates anxiety is not new and has been suggested previously (Papez 1995). Nonetheless, future studies will identify all the components of this network and dissect the function of each projection.

1.3 The striatum

The basal ganglia are a collection of subcortical nuclei that play a role in various functions such as motor control, learning, decision-making, and reward (Packard et al. 2002; Schultz et al. 1997; Yin et al. 2006).

In human studies, the name of basal ganglia refers generally to the *striatum*, the subthalamic nucleus and the substantia nigra. From an anatomical perspective, the basal ganglia consist of a group of brain structures that includes the caudate nucleus (commonly termed dorsal striatum – DS), putamen, nucleus accumbens (Nac – or ventral striatum –VS), globus palludus (GP), subthalamic nucleus and substantia nigra (SN) (Goodman and Packard 2016). Although simplified, the same compartimentalization is also observed in rodents. It can be distinguished the globus pallidus, corresponding to external GP (GPe), while the internal GP (GPi) is equivalent (in terms of inputs and outputs) to the entopeduncolar nucleus (EP), (Fig 4).

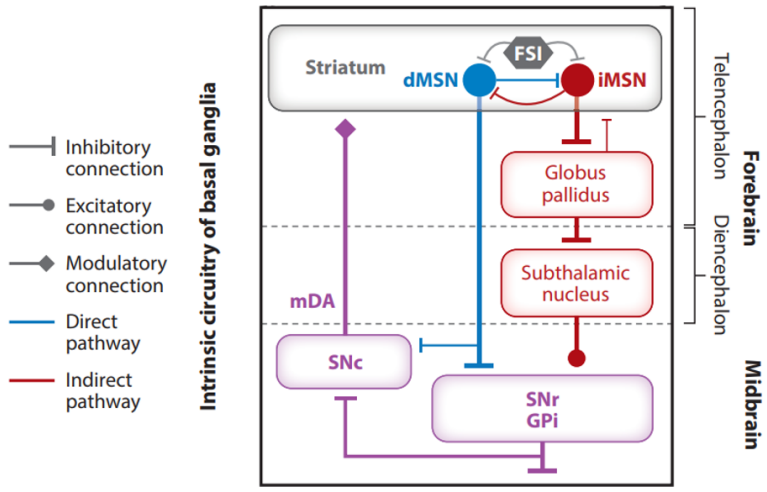

Figure 4 Schematic representation of basal ganglia circuits (Adapted from Park et al. 2020).

Each individual structure is constituted by macroscopically different subnuclei in the human brain (Groenewegen et al. 2003). Thus, the striatum includes the caudate nucleus, putamen and nucleus accumbens; the pallidum consist of GPi and GPe and the ventral pallidum (vGP); the subthalamic nucleus appears, macroscopically, as an undivided morphological unity; the SN has a clearly distinguishable pars compacta (SNc) and pars reticulata (SNr) (Groenewegen et al. 2003). All these subcortical regions are highly interconnected with each other and play an important role in regulating various aspects of psychomotor behavior (Charara et al. 2003).

The reason for including the caudate nucleus, putamen, and Nac in the striatum is that all three nuclei have similar histological, neurochemical end connectional characteristics (Groenewegen et al. 2003).

The striatum serves as the primary input structure of the basal ganglia, receiving glutamatergic signals from both the cortex and the thalamus (Hunnicutt et al. 2016). The striatum is characterized by various neuronal populations: the vast majority of striatal neurons (95%) correspond to medium spiny neurons (MSN). They are GABAergic projecting neurons characterized by high spine density and electrophysiologically by a negative resting potential and low firings rates in vivo (Cepeda et al. 2008). They are divided in two distinct populations by their D1/D2 dopamine receptors expression and by their downstream projection targets (Kita et al. 1988; Gerfen et al. 2011). Thus, MSNs projecting to the GPe participate in the indirect striatoplallidal pathway and are characterized by D2 dopamine (D2R) receptor, while MSNs innervating the GPi, or entopeduncular nucleus, and the SNr form the direct striatonigral pathway and are characterized by D1 dopamine (D1R) receptor.

Furhtermore, striatal MSNs projecting through the indirect pathway are known to contain the neuropeptide encephalin, whereas the neuropeptides substance P and dynorphin are expressed in those MSNs projecting directly to the GPi and SNr (Lanciego et al. 2012). The electrophysiological activity of MSNs depend in part from convergent excitatory inputs to become "active" (Groenewegen et al. 2003). MSNs process excitatory glutamatergic inputs first through AMPA and kainate receptors and then NMDA receptors, once cells are depolarised. Throughout all the extension of the striatum MSNs exhibit mostly a common set of membrane properties, such as hyperpolarised resting membrane potentials and strong inward rectification (Voorn et al. 2004).

Furthermore, several classes of GABAergic interneurons have been described. Striatal parvalbumin (PV) and somatostatin (SOM) GABAergic interneurons are the most studied. They show distinct electrophysiological and morphological properties that can be used to identify each class (Tepper et al. 2010). Furthermore, PV interneurons are more likely to target direct-pathway MSNs than indirect-pathway MSNs, indicating a possible mechanism for quick, pathway-specific regulation of striatal output pathways (Gittis et al., 2010). Cholinergic striatal interneurons (COL) make a further class of inhibitory striatal interneurons and like GABAergic interneurons have their own features (Zhou et al. 2002). These neuronal populations show a regular distribution along the mediolateral Dorsal striatum axis, except for PV ad COL interneurons that show a higher density in the lateral part (Kita et al. 1990; Fino et al. 2018; Gangarossa et al. 2013; Matamales et al. 2016). Indeed, some recent studies have divided the DS in two regions, dorsomedial (DMS) and dorsolateral (DLS) striatum (fig5). Classifying DS into DLS and DMS is mainly based on behavioural studies and the lack of anatomical boundaries between these regions has led to look for differences in terms of connectivity, synaptic plasticity and neuronal distribution.

Nevertheless, some electrophysiological and cellular studies have reported that the DMS and DLS can be considered as distinct regions.

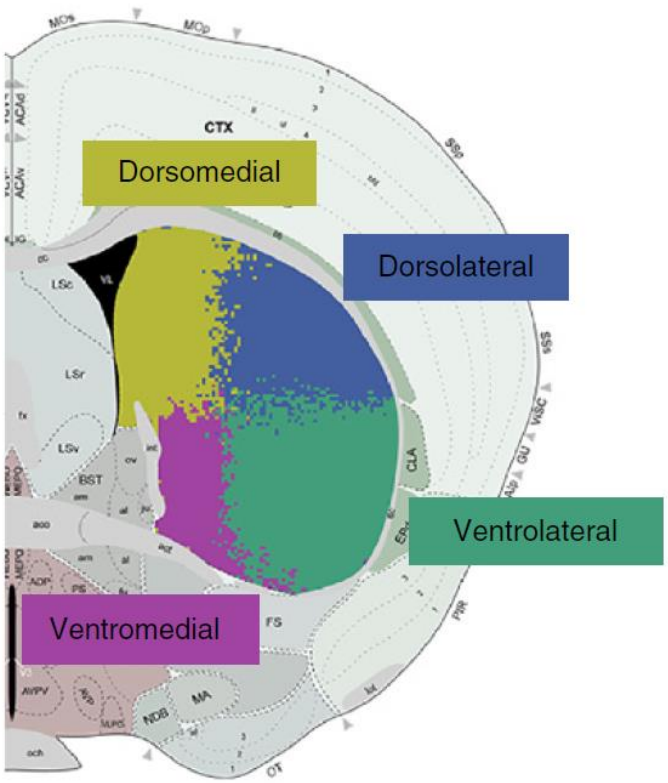

Figure 5 Diagram illustrating the division of territories within the dorsal striatum (Hintiryan et al. 2016)

Cortes reports how DMS and DLS MSN display distinct electrophysiological properties and slow wave oscillation features. These differences are robust enough to classify MSNs in DMS or DLS cells with ≈90% accuracy by a machine-

learning approach in order to predict their position. Furthermore, slow wave oscillation activity in DMS and DLS correlate with their own input cortical areas suggesting this spontaneous activity heterogeneity within dorsal striatum is partly due to cortical afferents (Alegre-Cortés et al. 2021). PV, SOM and COL interneurons display characteristics depending on striatal territory. As mentioned above, PV and COL interneurons have a higher density in DLS whereas SOM show a regular distribution. COL interneurons display different responses in DS following SNc dopaminergic neurons stimulation. They show two distinct responses: the first one is a pause in spontaneous neuronal activity whereas the second one is a brief pause followed by a burst of action potentials. The former response is a peculiarity of DMS COL interneurons and it is due to activation of D2R following dopamine release from SNc inputs while the second one has been described only in DLS and it is due to activation of D2R and metabotropic glutamate receptors (mGluR) following co-release of dopamine and glutamate from SNc terminals (Cai et al. 2018). This different regulation of DMS and DLS by SNc dopaminergic neurons may be fit with the distinct nigrostriatal circuits described by Lerner (Lerner et al. 2015).

These different spontaneous and evoke neuronal activity along mediolateral DS axis reflect the different innervations (fig6). Cortical and thalamic projections are the most important excitatory inputs into dorsal striatum. Hintiryan has reported distinct cortical innervations into DS. The DMS primarily receives inputs from limbic and association cortices, including the PFC while the DLS primarily receives inputs from the motor and somatosensory cortices, such as M1/2 and S1/2 (Hintiryan et al. 2016). Furthermore, the DMS, but not DLS, receives projection from BLA (Hintiryan et al. 2021), a region known to be critical for associating sensory stimuli with aversive events.

Therefore, despite anatomical boundaries are absent between DMS and DLS, these regions display sharp features that make them independent territories and could explain their heterogeneity in striatal-dependent behaviours.

The extended demonstrations of anatomical segregated inputs in dorsal striatum has suggested that these connections impose a functional organization and its anatomical and neurochemical heterogeneity mirrors the heterogeneity of functions which the striatum is implicated. Even though many other investigations regarding the role of striatum need to be done, most of the evidences reported seems to suggest that the two parts of the DS are essential element of neural system involved in processing cognitive informations. Traditionally, most of the studies on striatum has been driven by researching the role of this structure in relation to motor function and skills (Yin et al. 2009; Cui et al. 2013). However in the last decades, new literature reports a more extensive repertoire of functions for this brain region, challenging the idea that striatal region is confined to the motor domain. In fact, it has been suggested that striatal circuitries are not only responsible for the motor learning, but they might be relevant also for learning and memory processes as (S-R)/habit learning (Packard et al. 2002), instrumental learning (Yin et al. 2004) spatial memory (De Leonibus et al. 2003; De Leonibus et al. 2005), behavioral/cognitive flexibility (Ragozzino et al. 2002), spatial/non-spatial navigation (Devan e White 1999; Lee et al. 2008).

1.4 Focus on the DMS in avoidance behavior

The DMS has been thoroughly investigated for its vital role in stimulus-response learning, which involves a sensory cue consistently eliciting a motor response (Packard and Knowlton 2002). However, the DMS's role in learned avoidance is not completely clear.

In the inhibitory avoidance (IA) test, animals learn to evade an environment where they previously encountered an aversive stimulus (US, such as a foot-shock) by staying in the brightly lit side of a two-compartment chamber (passive avoidance paradigm) or by moving to the opposite side compartment after a CS presentation (active avoidance paradigm). In this paradigm, animals must suppress their natural avoidance behavior, i.e., their tendency to avoid bright and open areas.

The involvement of the DS in IA has been recognized since the 1960s. Various studies in rodents have shown that electrolytic or chemical disruption of the caudate nucleus impairs the acquisition and retention of the passive IA task (Kirkby et al. 1968; Prado-Alcalá et al. 1975; Chavez et al. 1995). A significant deficit in the consolidation of a passive IA task has also been observed following the inhibition of transcription and translation in DS (Prado-Alcalá et al. 2017). Interestingly, while foot-shock alone does not alter the number of dendritic spines of MSNs in the DLS and DMS, intensive IA training induces a notable increase in spine density proportional to the foot-shock intensity.

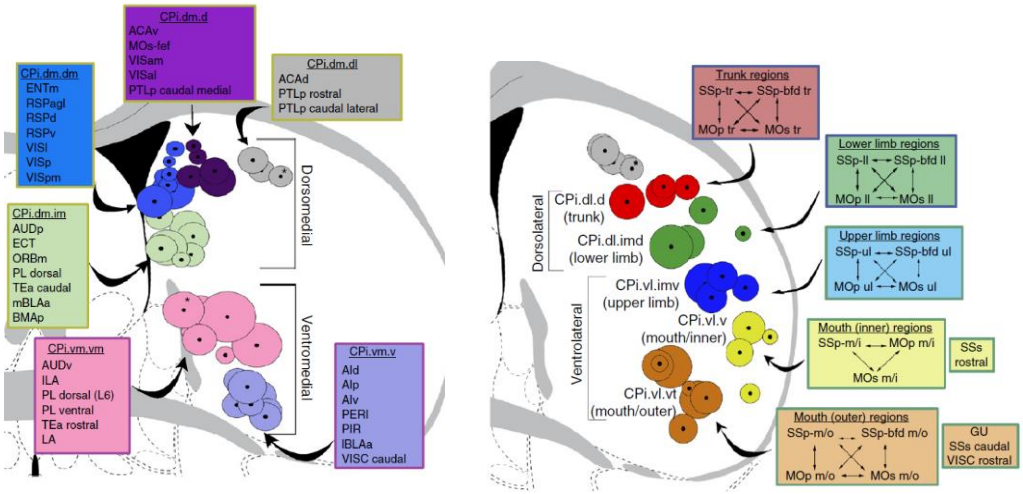

Figure 6 Different inputs to the medial striatum (left) and lateral striatum (right)(Adapted from Hintiryan et al. 2016)

The learning-induced increase in dendritic spines in DS may represent a cellular mechanism underlying the consolidation and persistence of memory storage (Bello-Medina et al. 2016).

Lesion studies have also shown that DS plays a crucial role in the active avoidance task (Kirkby et al. 1974). Wendler and collegues demonstrated a differential involvement of DS subregions since lesions of DLS impaired early acquisition, whereas DMS lesions affected the late phases of learning and extinction. The exact striatal circuit resulting in active avoidance behavior remains unclear (Wendler et al. 2014). Using chemogenetics and optogenetics, Hormigo and collaborators recently discovered that the SNr, the primary DS output, modulates the avoidance response to the CS. Inhibition of SNr firing facilitates active avoidance during tone presentation, while SNr excitation blocks the response. According to their proposed circuit model, the CS-driven avoidance behavior may engage a multisynaptic loop that originates within and returns to the superior

colliculus via the SNr (Hormigo et al. 2016). The superior colliculus detects sensory stimuli and sends information to the striatum via the posterior intralaminar nucleus (Linke et al.1999; Krout et al. 2001). Once activated by CS, the striatal direct pathway MSNs may suppress the SNr and consequently disinhibit its projections to the superior colliculus and the mesencephalic locomotor central pattern generators, thereby promoting active avoidance behavior (MacKay-Lyons et al. 2002)

Emerging evidence suggests that the DMS, particularly the D2R-expressing MSNs, plays a significant role in innate avoidance behavior in the EPM and OF. Using fiber photometry, LeBlanc and colleagues demonstrated that D2 MSNs activity increases as mice enter anxiogenic areas of these tasks. Additionally, they showed that optogenetic stimulation of D2 MSNs promotes avoidance of open areas in both tasks, while chemogenetic inhibition of D2 MSNs reduces avoidance behavior. Interestingly, knocking out the D2R on COL interneurons or dopamine neurons did not affect the mice's performance in exploratory tasks, suggesting that DMS indirect pathway neurons are critical for evoking avoidance behavior (LeBlanc et al. 2020).

Recent research indicates that PFC–DMS projections may play a more crucial role in regulating avoidance. Using fiber photometry recordings in both male and female mice during the EZM task, Loewke and collegues observed heightened neural activity in frontostriatal projection neurons during exploration of the anxiogenic open arms. Additionally, optogenetic experiments showed that this frontostriatal projection preferentially excites postsynaptic D1 receptor-expressing neurons in the DMS and causally controls innate avoidance behavior (Loewke et al. 2021). Furthermore, the BLA neurons projecting to the DMS, primarily targeting dopamine D1 receptor-expressing neurons, significantly overlap with the neuronal population that responds to aversive predator stress, a widely used anxiogenic

stressor. Specific optogenetic activation of the BLA-DMS circuit induced a strong anxiety response followed by compulsive grooming (Lee et al. 2024).

Furthermore, The DS primarily consists of MSNs that predominantly express either D1R or D2R. D1 MSNs project directly to the SNr and are known as direct pathway MSNs. These D1 MSN projections to the SNr exhibit a topographical organization, with anterior DS D1 MSNs projecting medially, while D1 MSNs from the posterior DMS/DLS and TS project laterally (Hedreen et al. 1991). On the other hand, D2 MSNs indirectly project to the SNr via the GPe and subthalamic nuclei, forming the indirect pathway (DeLong et al. 1990; Bertran-Gonzalez et al. 2010).

Activation of these two MSN populations often results in opposing behavioral effects (Lenz and Lobo 2013). Both the GPe and SNr have been implicated in avoidance behaviors (Ipser et al. 2013; Hormigo et al. 2016; Almada et al. 2018; LeBlanc et al. 2020). The SNr sends projections to various regions involved in the fear response, including the superior colliculus, inferior colliculus, and periaqueductal gray (Castellan-Baldan et al. 2006). Together, these pathways position the DMS to integrate sensory input and aversive stimuli, thereby modulating responses to aversive experiences. The administration of dopaminergic antagonists of D1R and D2R in the DMS produced respectively decrease and an increase in anxiety behaviour (Nguyen et al. 2019).

2 Aim of the study

Avoidance encompasses any behavior intended to evade dangerous stimuli and threatening situations. Adaptive avoidance enhances survival and fitness, whereas maladaptive avoidance impairs interaction with relatively safe stimuli, impacting social life and cognitive functions (Arnaudova et al. 2017). Indeed, maladaptive avoidance has been recognized as a key symptom of anxiety disorders and related conditions such as post-traumatic stress disorder (Aupperle et al. 2010).

For over a century since the initial discovery that temporal lobe structures regulate emotional behaviors, our knowledge of the neural mechanisms underlying anxiety and avoidance was primarily derived from insights obtained through lesion and inactivation studies. Although these foundational studies identified crucial areas involved in the regulation of anxiety, such as the BLA, the bed nucleus of the stria terminalis (BNST), the vHPC, and the PFC, advancements in understanding the roles of these regional macrocircuits in this emotional state remained limited (Calhoon e Tye 2015; Duval et al. 2015; Papez 1995). The ability to expand our understanding of the brain regions involved in the network that regulates avoidance and anxiety-like behaviors would provide a more comprehensive perspective, giving us the way for more targeted and personalized treatments, whether pharmacological or therapeutic. To expand a network involved in the regulation of a specific behavior, a good starting point could be to determine whether certain regions are more interconnected than others with those already known to regulate that behavior. In this regard, the DS appears to be a particularly interesting candidate, as it seems to be anatomically well integrated within the classical network that regulate anxiety-like behavior and innate avoidance. From a functional point of view, the DS has been extensively studied for its essential role

in stimulus-response learning, but whether the DS contributes to avoidance behavior is not fully understood.

The DS is composed of DMS, DLS and a posterior portion (tail of the striatum, TS) (Hunnicutt et al. 2016). The DLS receive inputs primarily from motor and somatosensory cortices. The TS receives primary information from sensory cortices (Hunnicutt et al. 2016; Hintiryan et al. 2016). Interestingly, the DMS subdivision receives direct excitatory projection from BLA and PFC, regions implicated in anxiety (Hunnicutt et al. 2016; Hintiryan et al. 2016; 2021). The DMS is predominantly composed of MSNs that project to SN and GP. Both GP and SN have been shown to play a role in aversive behavior (Ipser et al. 2013; Hormigo et al. 2016; Almada et al. 2018). Furthermore, recent evidences suggest that the DMS could integrate sensory and aversive informations and modulate aversive response (Leblank et al., 2020; Loewke et al. 2021; Lee et al. 2024).

With the aim to identify new regions that integrate into the established network responsible for regulating innate avoidance and anxiety-like behaviors, we focused on the DMS, rather than other striatal subregions such as the DLS or the tail of the striatum. The DMS was chosen first of all due to its anatomical inputs from the BLA and the PFC, and its outputs to the GP and SN. From a functional point of view, the DMS is known to play a role in learning the association between stimuli and outcomes and in decision-making (Packard et al. 2002; Balleine et al. 2007). DMS lesions impair goal-directed behavior, leaving the animal's behavior stimulus-driven and habitual. In contrast, DLS lesions inhibit the formation of habits, leaving the animal's behavior under the control of anticipated goals (Burton, Nakamura, and Roesch 2015), potentially the DMS playing a central role in modulating decision and goal-oriented action to avoid new and learned situations. Recent evidence suggest also a possible role of DMS in avoidance behavior (Nguyen et al. 2019; LeBlanc et al. 2020; Loewke et al. 2021).

Based on these anatomical and functional evidence, we set out to investigate the role of specific inputs from PFC and BLA to DMS in innate avoidance behavior in CD1 outbred mice. Mice are one of the most widely used animal models in scientific research. Their genetic similarity to humans makes them a tool for studying biological processes and diseases. Furthermore, within the broader category of mice used in research, outbred strains play an important role. They show higher genetic variability that enhances the reliability and applicability of research findings. This variability makes them more representative of natural populations, which is particularly useful for studies requiring a range of genetic responses.

Our first aim was to confirm whether PFC and BLA projecting neurons converge in the DMS and identify the specific subregion of the DMS that receives these converging projections. To this aim, CD1 mice were injected in DMS with retrograde tracers and the presence of labelled neurons was evaluated in PFC and BLA.

The second aim was to investigate the role of PFC-DMS and BLA-DMS pathways in avoidance behavior. We employed a chemogenetic approach to specifically manipulate PFC-DMS and BLA-DMS projecting neurons and measured anxiety-like behaviour in the EPM. Furthermore, to evaluate if these projections interact in differentially with striatal interneurons, Ai14 mice were injected in PFC or BLA with an anterograde transynaptic tracer and then, immunohistochemistry for Parvalbumin interneurons was performed in striatal region.

The third aim was to explore the role of downstream DMS pathways in innate avoidance behavior. The DMS can engage connections with the midbrain neurotransmitter system indirectly by projecting to the GPi, thereby regulating the activity of the Lateral Habenula. The Lateral Habenula is known for its role in modulating neurotransmitter systems in the midbrain (Wallace et al. 2017; Zhao

et al. 2015). These midbrain nuclei are particularly noteworthy because they not only contribute to avoidance behavior but also have significant projections to the PFC and the BLA (Muller et al. 2009; Tang et al. 2020; Bariselli et al. 2016; Albert et al. 2014). This forms a potential closed feedback system, where the interactions between the DMS, midbrain nuclei, and regions such as the PFC and BLA continuously influence each other. For this reasons, we focused on the GPi, using an optogenetic approach to specifically manipulate DMS-GPi projecting neurons, measuring anxiety-like behaviour in the EPM.

3 Materials and methods

3.1 Subjects

Male outbred CD1 mice, 8-15 weeks old, weighing 40-60g were used for anatomical, chemogenetic and optogenetic experiments. They were supplied from a colony maintained at Sapienza University of Rome, obtained from Charles River breeding pairs. Mice were housed in groups of 2-4 per cage (26.8 x 21.5 x 14.1 cm) or 5-8 per cage (42.5 x 26.6 x 18.5 cm) in the animal facility of the Department of Biology and Biotechnology "Charles Darwin", Sapienza University of Rome, Italy. Only male mice were used for behavioral experiments to compare our result with the current literature. Male and female Ai14 Cre-reporter mice (B6.Cg-Gt(ROSA)26Sortm14(CAG-tdTomato)Hze/J; The Jackson Laboratory), 8-15 weeks old, weighing 30-40g, were used to study parvalbumin-positive interneurons. They were supplied from a colony maintained at Sapienza University of Rome and housed in groups of 2-4 mice per cage (26.8 x 21.5 x 14.1 cm). All animals were maintained at a constant temperature (21±2°C) and humidity (45-60%), on a 12h light/dark cycle (lights on at 07:30) with *ad libitum* access to food (Global Rodent Diet, Envigo) and water. All behavioral procedures were performed during the light period (9:00-18:00). Procedures were conducted under the authorization N. 967/2018-PR and N.843/2023-PR from the Italian Ministry of Health, according to Italian (DL.116/92) and European laws and regulations on the use of animals in research, and NIH guidelines on animal care. The experimental unit in all the experiments is the animal. Mice were assigned to the different experimental groups in a randomized manner.

3.2 Stereotaxic surgery procedures

Stereotaxic injections were performed on 7 to 9 weeks old CD1 male mice anesthetized with isoflurane (4%) (Iso-Vet, Piramal) using a tabletop isoflurane anaesthesia system (Harvard Apparatus, USA) and secured on a stereotaxic apparatus (David Kopf Instruments, USA). Isoflurane (3-5%) was delivered together with 0.6 L of oxygen per minute produced by an oxygen generator. Waste gases were evacuated through an active scavenger (Harvard Apparatus, USA) provided with a canister of activated charcoal to absorb the excess anaesthetic gas. Charcoal canisters were weighed before and after surgery and replaced as needed. Animal's eyes were protected with a drop of Recugel (Bausch and Lomb GmbH, Berlin) and a warming lamp (230W) was placed 50cm above the mouse to avoid hypothermia due to anaesthesia. The respiration rate and general conditions of the mice were constantly monitored during surgeries. Once the head was secured, the scalp of the mouse was disinfected with Betadine (10%, Medapharma, Italy) and then longitudinally incised with a scalpel to expose the skull. The stereotaxic coordinates of lambda and bregma, two skull reference points created by the intersection of the sagittal suture with, the lambdoid and coronal sutures, respectively, were measured and kept on the same horizontal plane (±0.2 mm). Bregma coordinates were then used to calculate the coordinates of the injection or implant site according to the mouse brain atlas (Paxinos and Franklin, 2019). A small hole was then drilled in the skull at the intended injection/implant site to allow access to the brain. Paracetamol (Tachipirina, Angelini), as an anti-inflammatory treatment, was administered via the drinking water on the day of surgery and for the following two days, at a dose of 2 mg/kg, to ensure analgesia.

3.2.1 Striatal input characterization

CD1 male mice were unilaterally injected with a retrograde AAV vector expressing mCherry under control of the synapsin promoter (AAVrg-hSyn-mCherry) or fluorogold (Cas 223769-64-0, Santa Cruz Biotechnology) in DMS (Injection coordinates relative to bregma: AP= +0.9mm; ML= ±1.3 mm; DV= -3.1 mm). Fluorogold is a fluorescent dye used to trace neural circuits and study neuronal connectivity. When Fluorogold is administered in a brain area, it is absorbed by neurons and axon terminals at the injection site. After absorption, it is transported retrogradely along the axons to the neuron's cell body, allowing for the tracing of the input pathways of that brain area (Schmued et al. 1986).The volume of injection was 0.20 µL per side. The injection was performed with the use of calibrated glass micropipettes connected to a syringe, with slow manual pressure applied over 2 minutes. Following the infusion, the pipettes were kept in place for an additional 5 minutes, allowing viral diffusion and preventing backflow, before being slowly retracted. Afterward, the scalp was sutured with a surgical thread and then animals were allowed to recover for 3 weeks before perfusion.

3.2.2 Chemogenetics

CD1 male mice were bilaterally injected with an AAV vector expressing either the inhibitory DREADD hM4D(Gi) (AAV2-hSyn-hM4D(Gi)-mCherry) or the excitatory DREADD hM3D(Gq) (AAV2-hSyn-hM3D(Gq)-mCherry) under control of the synapsin promoter in PFC (Injection coordinates relative to bregma: AP= +1.8mm; ML= ±0.4 mm; DV= -2.3 mm) or BLA (Injection coordinates relative to bregma: AP= -1.4 mm; ML= ±3.3 mm; DV= -4.9 mm). The volume of injection was 0.20 µL per side. Control mice were injected with saline (NaCl 0.9%). The injection was performed with the use of calibrated glass micropipettes connected to a syringe,

with slow manual pressure applied over 2 minutes. Following the infusion, the pipettes were kept in place for an additional 5 minutes, allowing viral diffusion and preventing backflow, before being slowly retracted. Afterward, the scalp was sutured with a surgical thread and the animals were allowed to recover for 3 weeks before undergoing cannulas implant surgery. Two stainless-steel guide cannulas (diameter 0.50/0.25 x 7mm) were bilaterally implanted in DMS at the following coordinates relative to bregma: AP= +0.9 mm; ML= ±1.3 mm; DV= -1.2 mm. The guide cannulas were anchored to the skull using dental acrylic cement (Ilic, Italy). Mice were allowed to recover for 1 week before the behavioral procedures.

3.2.3 Optogenetics

CD1 male mice were bilaterally injected with an AAV vector expressing the excitatory opsin Channelrhodopsine under the control of the synapsin promoter (AAV5-hSyn-hChR2(H134R)-EYFP) in DMS (Injection coordinates relative to bregma: AP= +0.9mm; ML= ±1.3 mm; DV= -3.1 mm). The volume of injection was 0.20 µL per side. The viral injection was performed with the use of calibrated glass micropipettes connected to a syringe, with slow manual pressure applied over 2 minutes. Following the infusion, the pipettes were kept in place for an additional 5 minutes, allowing viral diffusion and preventing backflow, before being slowly retracted. After the infusion, custom-made optic fiber cannulas (200-nm core diameter; 0.39NA, Thorlabs) were lowered over the internal globus pallidum (AP=-0.9 mm, ML=±2.0 mm, DV=-4.6 mm) and secured to the skull with dental cement (Lang Jet Repair, Ravell). A screw (diameter 1mm x length 2mm, Ruglamzhip) was fixed to the animal's skull to secure the stability of the head cap. Mice were allowed to recover for 3 weeks before the behavioral procedures.

3.2.4 Striatal interneurons characterization

Ai14 mice were unilaterally injected with an anterograde AAV vector expressing Cre under control of the synapsin promoter (AAV1-hSyn-P2A-Cre-WPRE) in PFC (Injection coordinates relative to bregma: AP= +1.8mm; ML= ±0.4 mm; DV= -2.3 mm) or BLA (Injection coordinates relative to bregma: AP= -1.4 mm; ML= ±3.3 mm; DV= -4.9 mm). The volume of injection was 0.20 µL per side. The injection was performed with the use of calibrated glass micropipettes connected to a syringe, with slow manual pressure applied over 2 minutes. Following the infusion, the pipettes were kept in place for an additional 5 minutes, allowing viral diffusion and preventing backflow, before being slowly retracted. Afterward, the scalp was sutured with a surgical thread and the animals were allowed to recover for 3 weeks before perfusion.

3.2.5 Viral vectors

For the striatal input characterization, we used an adeno associated virus of serotype 2-retro (AAVrg), a modified AAV2 serotype able to infect terminal axons and go back to soma (Tervo et al. 2016), to express the reporter mCherry (AAVrg-hSyn-mCherry; 7×10^{12} vg/mL). It was obtained from Addgene repository (#114472-AAVrg; Addgene, MA, USA, https://www.addgene.org/114472; Fig7).

For chemogenetic manipulations, we used an adeno associated virus of serotype 2 (AAV2) expressing the inhibitory DREADD hM4D(Gi) fused with mCherry (AAV2-hSyn-hM4D(Gi)-mCherry; 7×10^{12} vg/mL; gift from Brian Roth) or excitatory DREADD hM3D(Gq) (AAV2-hSyn-hM3D(Gq)-mCherry; 3×10^{12} vg/mL; gift from Brian Roth), obtained from Addgene repository (#50475-AAV2 and #50474-AAV2; Addgene, MA, USA, https://www.addgene.org/50475; https://www.addgene.org/50474; Fig8).

For optogenetic manipulations, we used an adeno associated virus of serotype 5 (AAV5) expressing the excitatory channelrodopsin (AAV5-hSyn- hChR2(H134R)-EYFP; 7×10^{12} vg/mL; gift from Karl Deisseroth), obtained from Addgene repository (#26973-AAV5; Addgene, MA, USA, https://www.addgene.org/26973; Fig 9). The H134R mutation of Channelrhodopsin enhances the channel's ionic conductance and reduces desensitization, resulting in a stronger and more sustained current in response to light. This allows for more efficient and prolonged neuron depolarization. By slowing the channel's closing after activation, the mutation extends the duration of the channel's opening, thereby increasing the length of neuronal depolarization. With greater light sensitivity, it provides a more robust and sustained response, making it an ideal tool for optogenetic experiments that require continuous or long-lasting stimulation. In short, Channelrhodopsin H134R is an optimized version of the native protein, designed to improve channel stability and efficiency under light exposure, making it especially useful for experiments involving optogenetic neuromodulation (Nagel et al. 2005).

Different AAV serotypes have revealed distinct patterns of transduction within the nervous system. In general, AAV1,2 and 5 exhibit higher transduction frequencies than other serotypes in all regions injected within the CNS (Asokan et al. 2006). These serotypes are known to also have the ability to infect glial cells. However, the use of the hSyn promoter helps to limit expression to neurons, reducing expression outside of neuronal cells (Kügler et al. 2003).

For characterization of striatal microcircuits, we used an adeno associated virus of serotype 1 (AAV1-hSyn-Cre-WPRE.hGH; 7×10^{12} vg/mL; gift from James M. Wilson (#105553-AAV1; Addgene, MA, USA, https://www.addgene.org/105553; Fig10). AAV1 vectors exhibit anterograde trans-synaptic spread properties. AAV1-Cre from transduced presynaptic neurons effectively and specifically drives Cre-dependent transgene expression in selected postsynaptic neuronal targets, thus allowing axonal tracing and functional manipulations of the latter input-

defined neuronal population. AAV1 appears not to spread beyond the first-order downstream neurons, thus facilitating a more conclusive interpretation of

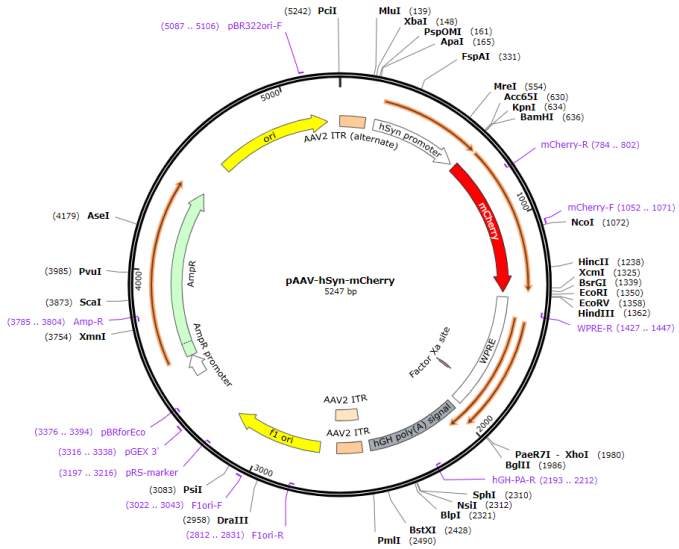

Figure 7 Viral construct of AAVrg-hSyn-mCherry used in anatomical experiment

anatomical connectivity results. One limitation of using AAV1 for anterograde trans-neuronal studies, however, is the fact that AAV1-Cre can be also transported in the retrograde direction, as has been reported. Application should therefore be limited to pathways that do not contain reciprocal connections between targeted pre- and postsynaptic regions (Zingg et al. 2017).

A

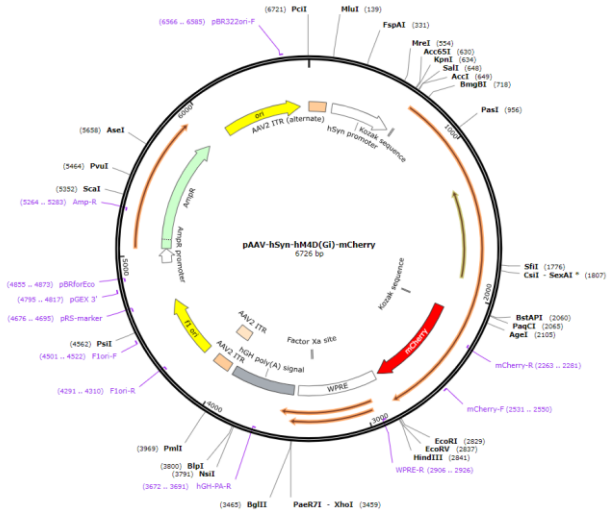

B

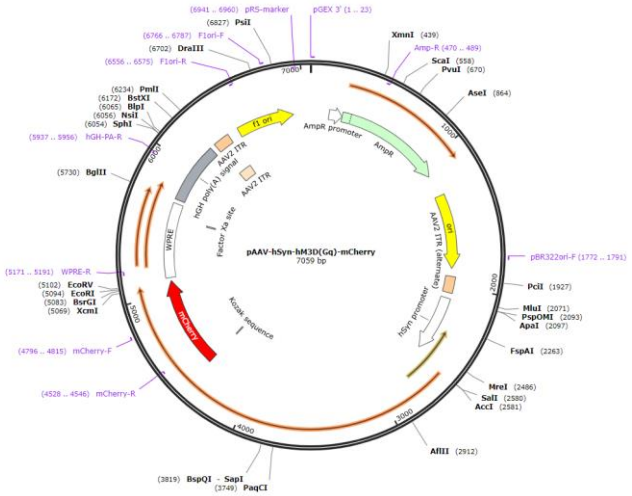

Figure 8 (A) Viral construct of AAV2-hSyn-hM4D(Gi)-mCherry used in chemogenetic inhibition (B) Viral construct of AAV2-hSyn-hM3D(Gq)-mCherry used in chemogenetic activation.

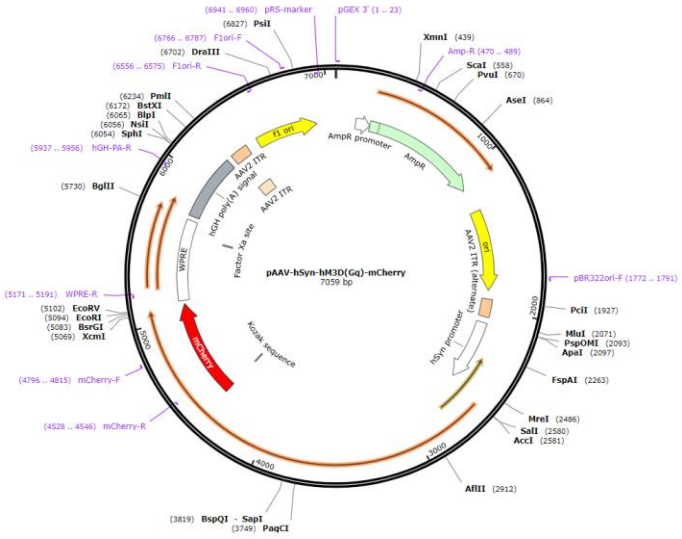

Figure 9 Viral construct of AAV5-hSyn-hChR2(H134R)-EYFP used in optogenetic activation

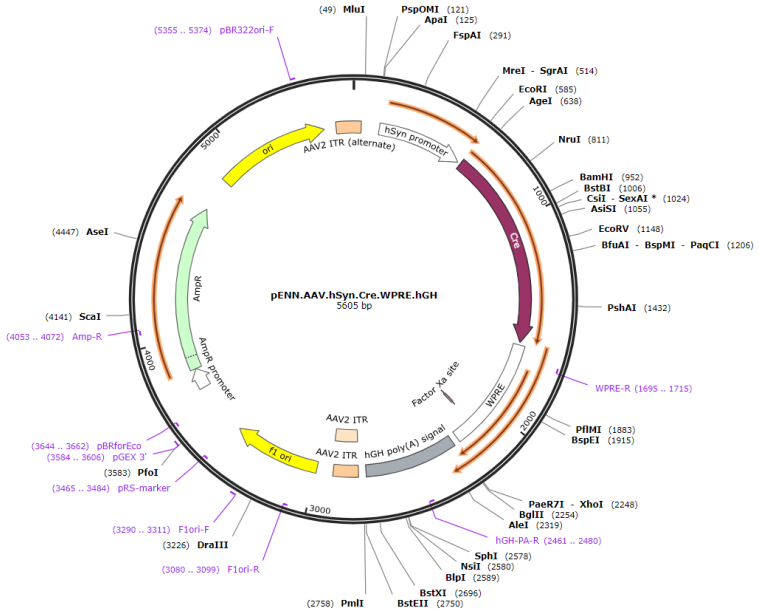

Figure 10 Viral construct of AAV1-hSyn-Cre-WPRE.hGH used in striatal interneurons characterization

3.3 CNO Focal injection

Clozapine N-oxide (CNO) is a synthetic drug used as a ligand to activate DREADD receptors (Armbruster et al. 2007). To specifically manipulate PFC-DMS and BLA-DMS projections, CNO (Sigma Aldrich, USA) was diluted at a concentration of 10 mM in saline 0.9%, and focally administered 30min before testing in the elevated plus maze, based on previous evidence showing that CNO delivered on axon terminals robustly silences synaptic release within minutes, without significantly reducing axonal action potential propagation, and this reverses within 1–4 hr (Stachniak et al. 2014). Mice were gently restrained to insert into the guide cannulas an injection needle (length: 7.0 mm; diameter: 0.25 mm) connected with a plastic tube to a 1 µL Hamilton syringe. The dose was chosen based on previous literature (Torromino et al. 2019). The volume of injection was 0.2 µL per side, administered over two minutes. During CNO infusion, mice were free to move in the holding cage. After the injection, the needle was kept in place for an additional minute. Control mice were subjected to the same procedure, but were administered with saline at physiological concentration (NaCl 0.9%).

3.4 Elevated plus maze (EPM)

The EPM is often regarded as a straightforward technique for evaluating the anxiety response and approach-avoidance conflict of rodents. There is a wide range of possible applications for the elevated plus maze. For example, it can be utilized for the prescreening of newly developed pharmacological agents intended for the treatment of anxiety-related disorders. Additionally, the anxiolytic and anxiogenic effects of various pharmacological agents, substances of abuse, and hormones can be explored. Furthermore, the elevated plus maze is a useful behavioral assay to investigate the brain regions and mechanisms that underlie

anxiety behavior. In fact, this apparatus has been employed as a model for unconditioned anxiety for more than two decades, and currently, there are over 2,000 research papers associated with this subject (Walf et al. 2007).

The apparatus was made of black Plexiglas and consisted of two open and two closed arms connected by a central square platform (5 x 5 cm); each arm was 5 cm wide and 35 cm long and the closed arms were surrounded by 15 cm high black walls. Furthermore, the open arms have a small outer edge of approximately 2 mm in height to provide tactile feedback to the animal during the test. (Fig 11 A). The maze was positioned 50 cm from the ground and placed in a mildly lit room (100lux), with white curtains all around. Each mouse was placed on the central platform facing the open arm and allowed to freely explore the apparatus. Between consecutive tests, the apparatus was cleaned with 70% ethanol solution. The time spent in open and closed arms and total distance were later manually scored from the recorded videotapes using ANY-maze (ANY-maze v.7.1, Stoelting Co., USA). The mouse was considered inside a specific compartment when all four paws were inside the compartment.

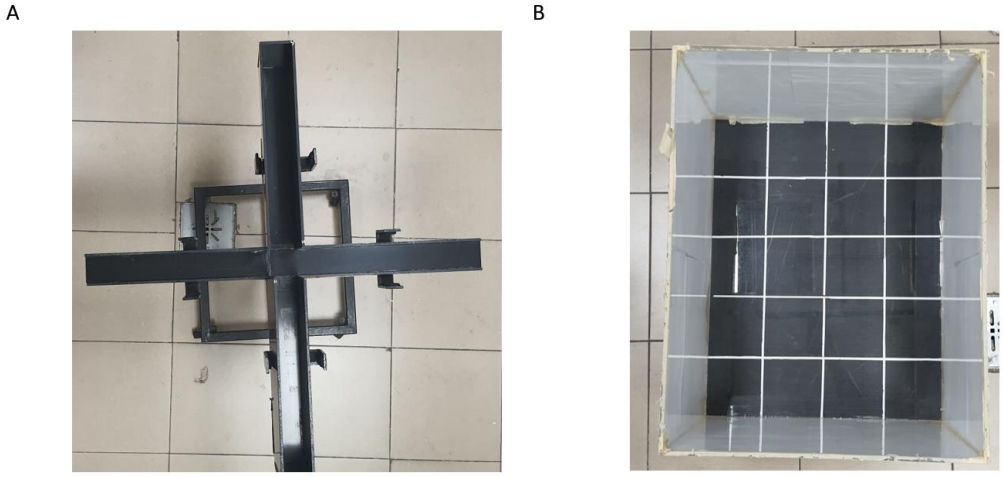

Figure 11 Images of EPM **(A)** and OF **(B)** apparatus used in these experiments.

3.4.1 Chemogenetics

All animals were handled for 5 minutes each day for the 5 days leading up to the test. On the day of the test, they were allowed to acclimate in the testing room for 30 minutes. Each mouse was isolated in a waiting cage for 30 minutes following CNO administration, then it was placed on the central platform of the EPM facing the open arm and allowed to freely explore for 5 minutes.

3.4.2 Optogenetics

All animals were handled for 5 minutes each day for the 5 days leading up to the test. On the day of the test, they were allowed to acclimate in the testing room for 30 minutes. Each mouse was isolated in a waiting cage for 30 minutes, then the implanted optic fiber cannulas were connected to a blue-light laser (CNI laser 100 mW – laser optogenetics 470 + 594 nm) through a 2-m optic fiber (Thorlabs) and 1x2 rotary joint splitter (RJ2 – Thorlabs). The optical fibers conductance were measured using a digital optic power and energy meter (PM100D - Thorlabs) before the animal's surgery. The animal was then placed on the central platform of the EPM facing the open arm and allowed to freely explore for 14 minutes. The stimulation protocol consisted of a 2 min baseline laser-off period followed by three 2 min-epochs alternating laser on/off (1–1.5 mW, 10 Hz, 5 ms pulse width, PulserPlus TTl Pulse Generator, Prizmatix). Between consecutive tests, the apparatus was cleaned with 70% ethanol solution.

3.5 Open field (OF)

The OF is widely used to assess exploratory behavior and overall activity in both mice and rats, allowing for the measurement of both the quality and quantity of activity. Several behavior can be recorded and analyzed, such as the distance traveled, the duration of movement, instances of rearing, and fluctuations in activity over time. Additionally, the OF is frequently utilized to evaluate the sedative, toxic, or stimulant effects of various drugs. Consequently, the OF assesses multiple aspects of behavior beyond mere locomotion. The OF allows for the measurement of various behavioral parameters that are indicative of the level of anxiety in mice. In particular, it is possible to measure the time spent in the center of the apparatus and the time spent near the walls. Anxious animals tend to remain along the edges of the arena, avoiding exploring the central area, which is perceived as a more exposed zone and, therefore, where they are more vulnerable. (Gould et al. 2009).

The apparatus was made of Plexiglas and consisted of rectangular arena (35 x 50 cm) with a black floor surrounded by 40 cm-high white walls (Fig 11 B). The apparatus was placed in a mildly lit room (100lux), with white curtains all around. Each mouse was placed in the center of the apparatus and allowed to freely explore it for 14min. Between consecutive tests, the apparatus was cleaned with 70% ethanol solution. The time spent in center and in the periphery of the arena (7 cm from the wall) and the total distance travelled by the animals were automatically scored from the recorded videotapes using ANY-maze (ANY-maze, Stoelting Co., USA). The mouse was considered inside a specific compartment when all four paws were inside the compartment. All animals were handled for 5 minutes each day for the 5 days leading up to the test. On the day of the test, they were allowed to acclimate in the testing room for 30 minutes. Each mouse was isolated in a waiting cage for 30 minutes, then the implanted optic fiber cannulas

were connected to a blue-light laser (CNI laser 100 mW – laser optogenetics 470 + 594 nm) through a 2-m optic fiber (Thorlabs) and 1x2 rotary joint splitter (RJ2 – Thorlabs). The optical fibers were measured using a digital optic power and energy meter (PM100D - Thorlabs) before the animal's surgery. The animal was placed in the center of the apparatus and allowed to freely explore for 14 minutes. The stimulation protocol consisted of a 2 min baseline laser-off period followed by three 2 min-epochs alternating laser on/off (1–1.5 mW, 10 Hz, 5 ms pulse width, PulserPlus TTl Pulse Generator, Prizmatix).

3.6 Brain tissue collection and sectioning

To visualize virus expression for chemogenetic, optogenetic and striatal input characterization, animals were deeply anesthetized and quickly transcardially perfused with 50mL of saline solution (0,9%) followed by 50mL of formaldehyde solution (50-00-0, Sigma-Aldrich, USA) 4% in saline phosphate buffer 0.1M (PBS). Brains were removed, stored overnight in formaldehyde solution (4%) at 4° C and then transferred to a 30% sucrose solution (57-50-1, Sigma-Aldrich, USA) for at least 48h. Subsequently, 40µm coronal sections were cut with a cryostat and stored at -20°C in anti-freezing solution (NaH_2PO_4-H_2O 1.59 ml/mL, Na_2HPO_4 5,47 mg/mL, NaCl 9 mg/mL, PVP-40 10 mg/mL, sucrose 300mg/mL, and ethylene glycol 0.3 ml/L in distilled H_2O). Brain sections were cryo-preserved in 24 well-plates until the immunofluorescence analysis was performed. Brains of mice that underwent stereotaxic viral infusion were collected and sectioned in the same way, but during sectioning, one in two slices were mounted on gelatin-coated slides and coverslipped with Fluoromont with dapi (F6057, Sigma-Aldrich, USA) to evaluate viral expression or fluorogold spread throughout the brain.

3.7 Images acquisition

To visualize viral expression for chemogenetic, optogenetic and striatal input characterization, as well as fluorogold, when perfectly dry and cleaned from the excess of mounting medium, the slides were analyzed using a Nikon Eclipse TE300 fluorescence microscope. Images of the regions of interest (PFC, BLA, DMS) were acquired at 2X (Nikon Plan UW 2x/0.06, 696x520 pixel) magnification. For the striatal input characterization the regions of interest were acquired at both 2x (Nikon Plan UW 2x/0.06, 696x520 pixel) and 10x (Nikon S Fluor 10x/0.50, 2560x1920 pixel) magnification. For the expression of the AAV2 retrograde tracer in striatal input characterization the acquisition has been performed also at 40x (Nikon Plan Fluor 40x/1.30 magnification. A minimum of 10 images per animal were acquired every 80 µm for the TRITC, FITC and DAPI channels. Sections from the striatal interneurons characterization experiment were analyzed using a ZEISS LSM900 confocal microscope. Images of the DMS were acquired at 20X (Plan Apocrhomat 20x/0.8 M27) magnification and pinhole 1.00AU/22 um. To capture the entire region, 20 images per hemisphere were acquired, which were then stiched to create a single image (1526x2539 pixel). For each animal, a minimum of 4 sections spaced 80 µm apart were acquired for the Tomato, AlexaFluor488 and DAPI channels and 7 seven consecutive optical slices (z-stacks) were taken per hemisphere, with each slice in the z-stack spaced 4–4.5 µm apart.

3.8 Histological verification of viral expression and cannula/fiber optic placement

After collecting the sections, the correct positioning of the injection, as well as the viral diffusion, were verified. Viral placement was schematized for each subject on coronal sections of the mouse brain atlas (Paxinos and Franklin 2019) with the use of Adobe Illustrator (Adobe Systems Incorporated, USA). Viral expression quantification was performed for each subject on the section with the highest fluorescent signal. Firstly, we defined a set of regions of interest (ROIs), using as a template the schematic drawings of the mouse brain atlas at different antero-posterior coordinates (Paxinos and Franklin 2019). Each ROI delineated the area of the target regions (PFC, BLA or DMS). Then, with Adobe Illustrator software (Adobe Systems Incorporated, USA) we overlaid the image of the section with the highest fluorescent signal with onto the ROI of the corresponding antero-posterior coordinate, to calculate the percentage of virus expression within and outside the target area. Mice were included only if robust bilateral expression (>50% of the total region of interest) was observed inside the ROI. For animals injected in the PFC, only those showing virus expression outside the ROI that covered no more than 10% of the total area of the primary motor cortex were included, as this is a region projecting to the DMS. Expression outside the ROI in regions that do not project to the DMS was considered irrelevant for the experimental results.

Regarding the placement of cannulas in DMS, only animals meeting all the following criteria were included: antero-posterior coordinate between bregma +1.10 and +0.38; medio-lateral coordinate between bregma +/- 1.0 and +/- 2.0; dorso-ventral coordinate between bregma -2.0 and -4.0.

Regarding the placement of the optic fiber in the GPi, only animals meeting all the following criteria were included: antero-posterior coordinate between bregma -1.06 and -1.58; medio-lateral and dorso-ventral coordinate: only animals with the

optic fiber placement positioned outside the GPi but no more than 0.1 µm from the dorsal perimeter of the structure were included.

3.9 Immunofluorescence staining for striatal interneurons characterization

To remove the anti-freezing solution from brain slice of Ai14 mime, sections were rinsed in PBS 0.1M (6 x 10 min). The following immunofluorescence protocol was then applied:

1. 1h at room temperature in PBS 0.1M-Triton-100 0.2% (PBST);
2. 1h at room temperature in PBST-Normal Goat Serum (NGS) 5%;
3. Incubation with mouse anti-Parvalbumin primary antibody (P3088, Sigma-Aldrich) 1:2000 in PBST-NGS 5%, overnight at 4°C;
4. 3x5 min washes in PBST;
5. Incubation with goat anti-mouse secondary antibody conjugated with Alexa Fluor 488 1:500 in PBST-NGS 5% (#4488, Jackson Immunoresearch) for 1h at room temperature;
6. 3x5 min washes in PBS 0.1M.

The sections were then mounted on gelatin-coated or polarazied slides, coverslipped with Fluoromont with Dapi (F6057, Sigma-Aldrich, USA) and left to dry.

3.10 Cell counting for striatal interneuron characterization characterization

For each animal we acquired a z-stack on 4 sections of DMS and for both emisphere. We used Fiji software for image analysis. As each z-stack was made

of 7 seven consecutive optical slices spaced 4–4.5 µm apart, each stack was converted into a single image using the Zproject plugin based on the max intensity tool. Double labelled cell whitin the DMS were manually counted. The number of double-labelled cells was reported as percentage of total Tomato positive cells.

3.11 Statistical analysis

Based on the inclusion criteria mentioned above for the neuroanatomical analysis, the rate of inclusion for each experimental group is reported in Table 1. Exclusion rates were primarily linked to the technical complexity of the experimental design. Specifically, in chemogenetic experiments, the dual surgery requirement and the natural variability in virus expression resulted in inclusion rates lower than expected. Furthermore, only animals that covered a total distance of more than 3 meters in the EPM for chemogenetic and optogenetic experiments were included. All statistical analysis was performed using GraphPad Prism software 8.4.3 (TIBCO Software Inc., USA). Comparison between control and experimental groups for open, center and closed arm time in EPM as well as distance travelled in EPM and OF were analyzed using independent student's t-test or one-way anova for repeated measure. Regarding the statistical analysis of cell counts for the striatal interneuron characterization experiment, the percentage of double-positive cells in the DMS was compared between animals injected with the anterograde virus in the BLA and PFC using an independent student's t-test. To assess whether the data were normally distributed, the Graphpad Prism 8.4.3 Shapiro-Wilk normality test was used, before proceeding to the parametric statistical analysis. Data collection and analysis were conducted with the experimenter blinded to experimental groups to prevent bias. The level of significance was set at $p<0.05$.

A summary timeline of the temporal frequency of the experiments conducted in this study is shown in Figure 12.

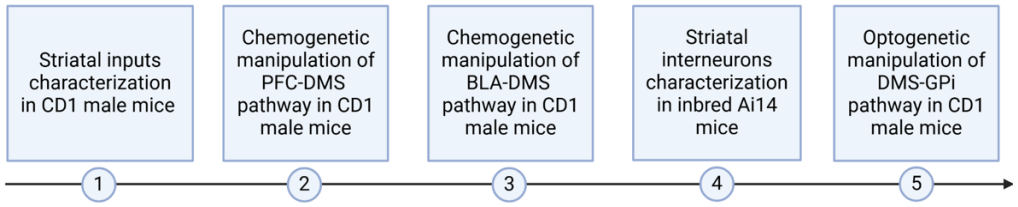

Figure 12 A temporal schematic representation of the experiments.

TABLE 1

Group	Total animals	Included animals	Description
Striatal input characterization	6	n=3	Fluorogold injection in DMS
Striatal input characterization	6	n=3	AAV2rg injection in DMS
Chemogenetic experiment	41	n=8	inhibitory DREADD + CNO in PFC
Chemogenetic experiment	42	n=10	inhibitory DREADD + Saline in PFC
Chemogenetic experiment	40	n=10	excitatory DREADD + CNO in PFC
Chemogenetic experiment	41	n=7	excitatory DREADD + Saline in PFC
Chemogenetic experiment	30	n=9	inhibitory DREADD + CNO in BLA
Chemogenetic experiment	30	n=7	inhibitory DREADD + Saline in BLA
Chemogenetic experiment	34	n=7	excitatory DREADD + CNO in BLA
Chemogenetic experiment	34	n=7	excitatory DREADD + Saline in BLA
Striatal interneuron characterization	4	n=3	AAV1 injection in PFC
Striatal interneuron characterization	7	n=2	AAV1 injection in BLA
Optogenetic experiment	19	n=4	AAV5 injection in PFC + EPM test
Optogenetic experiment	19	n=3	AAV5 injection in PFC + OF test

Table1 Total and included animals for each experimental groups

4 Results

4.1 Striatal input characterization: DMS receives converging inputs from PFC and BLA in CD1 mice

In recent years, significant efforts have been made to characterize striatal inputs from various cortical and subcortical regions. In particular, it is now clear that the DMS receives unidirectional projections from both the PFC and the BLA (Hintiryan et al. 2016; 2021; Hunnicutt et al. 2016). However, most of the literature has produced these findings by focusing on inbred C57Bl/6J strains, limiting the understanding of the striatal network to this specific model. In particular, the use of outbred strains allows for greater genetic variability, thereby reducing the influence of specific effects that might arise from a particular genetic background. This approach is more likely to reflect what could occur within a heterogeneous population. Firstly, we aimed to confirm that the DMS receives projections from the PFC and the BLA in the outbred CD1 strain. Furthermore, given that the DMS receives inputs from various brain regions along its anteroposterior axis (Hintiryan et al. 2016), it was important to identify the specific region of the DMS that receives converging projections from both the PFC and the BLA. To confirm that the intermediate DMS in CD1 mice receives inputs from both the PFC and BLA, we used several retrograde tracers (Fig 13).

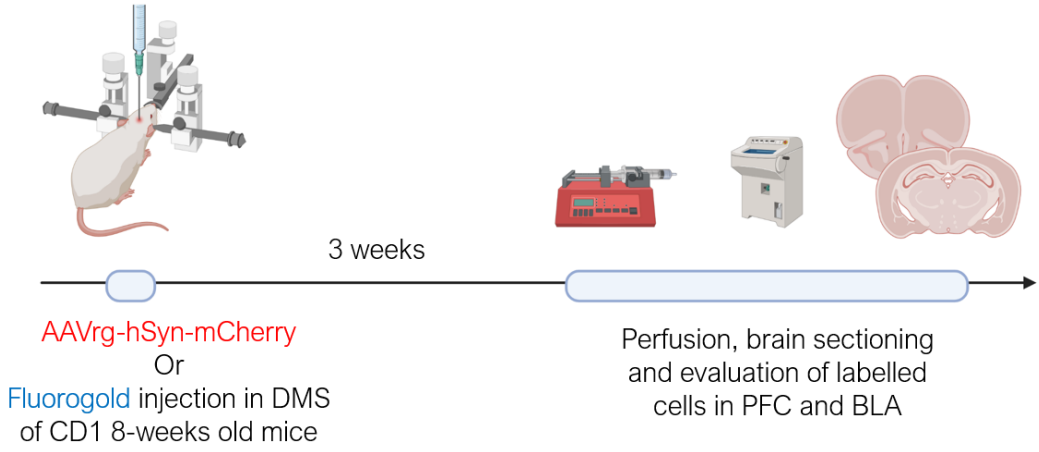

Figure 13 Experimental timeline for the striatal inputs characterization.

First, mice were bilaterally injected with fluorogold in DMS and labelled cells were detected both in PFC and BLA (Fig 14).

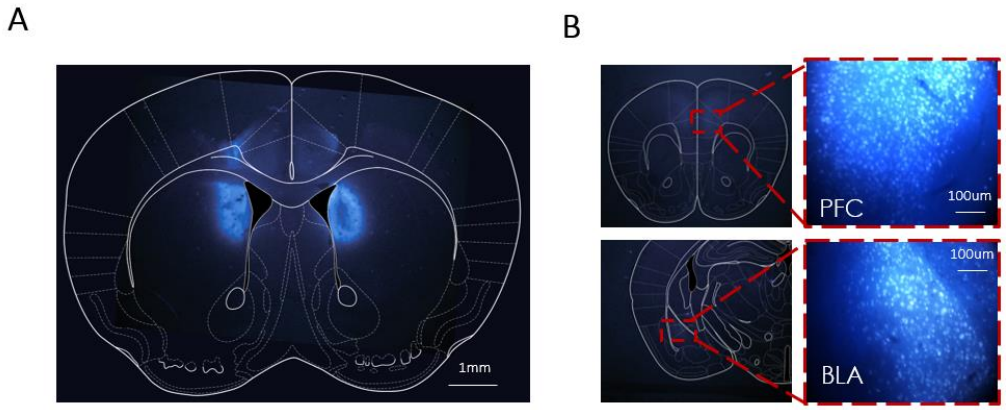

Figure 14 Representative image showing fluorogold diffusion in DMS (A, 2x magnification, n=3) and labelled cell in PFC and BLA (B, 10x magnification). A schematic drawing of the corresponding section from the PFC and BLA was superimposed onto the image.

To confirm the pathways showed by fluorogold and to restrict transgene expression exclusively to neurons that could be targeted in subsequent chemogenetic experiment, we injected in DMS a retrograde viral vector (AAV2rg-hSyn-mCherry) to express mCherry under the control of hSyn promoter (Kügler, Kilic, and Bähr 2003) and we assessed the presence of labelled neurons in PFC and BLA. In agreement with the data obtained with the fluorogold tracer, labelled neurons were detected in both regions (Fig15). Together, these data confirm that both PFC and BLA projecting neurons send convergent projections within the DMS.

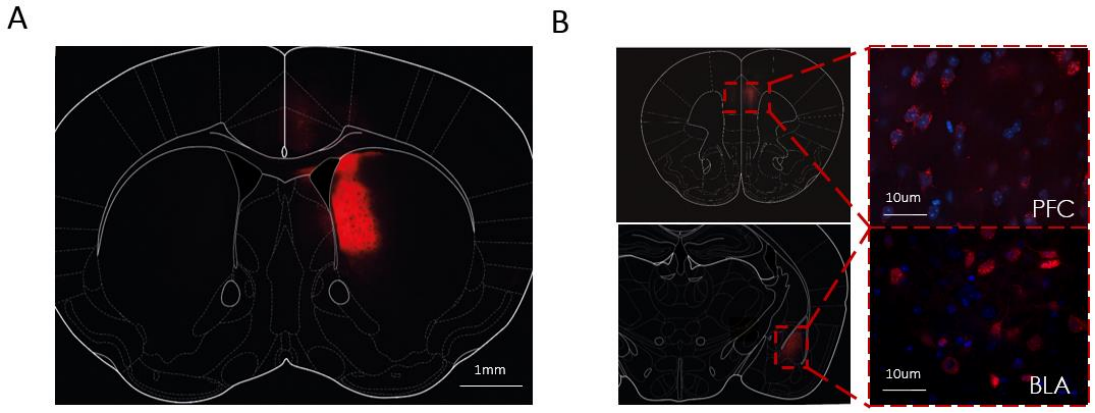

Figure 15 Representative mCherry expression in DMS (A, 2x magnification, n=3) and labelled neurons in PFC and BLA (B, 40x magnification). A schematic drawing of the corresponding section from the PFC and BLA was superimposed onto the image.

4.2 Chemogenetic activation of PFC–DMS projection neurons reduces approach–avoidance behaviour, while inhibition has no effect

From the literature, we know that optogenetic inhibition of the PFC-DMS pathway induces an increase in anxiety-like behavior as tested in the EZM, whereas its activation produces an anxiolytic effect (Loewke et al. 2021). However, these findings present some critical issues. In fact, the use of optogenetic in a test like the elevated zero maze could induce learning mechanisms typical of conditional place preference due to pathway stimulation within the experimental apparatus. For this reason, we opted for an approach that allowed us to manipulate the pathway continuously during the test delivering CNO 30 minutes before the beginning of the test, avoiding the occurrence of aversive or approach behaviors toward a specific area of the apparatus. Additionally, the study by Loewke and colleagues used inbred C57Bl/6J strains while we tested the effect of PFC-DMS manipulation in CD1 mice. Therefore, to evaluate the role of PFC-DMS projecting neurons in innate avoidance behavior, mice were bilaterally injected with inhibitory or excitatory DREADDs in the PFC, and guide cannulas were implanted in the DMS. This approach allowed us to specifically manipulate PFC terminals in DMS by delivering CNO directly into the DMS, 30 minutes before the elevated plus maze test (fig16).

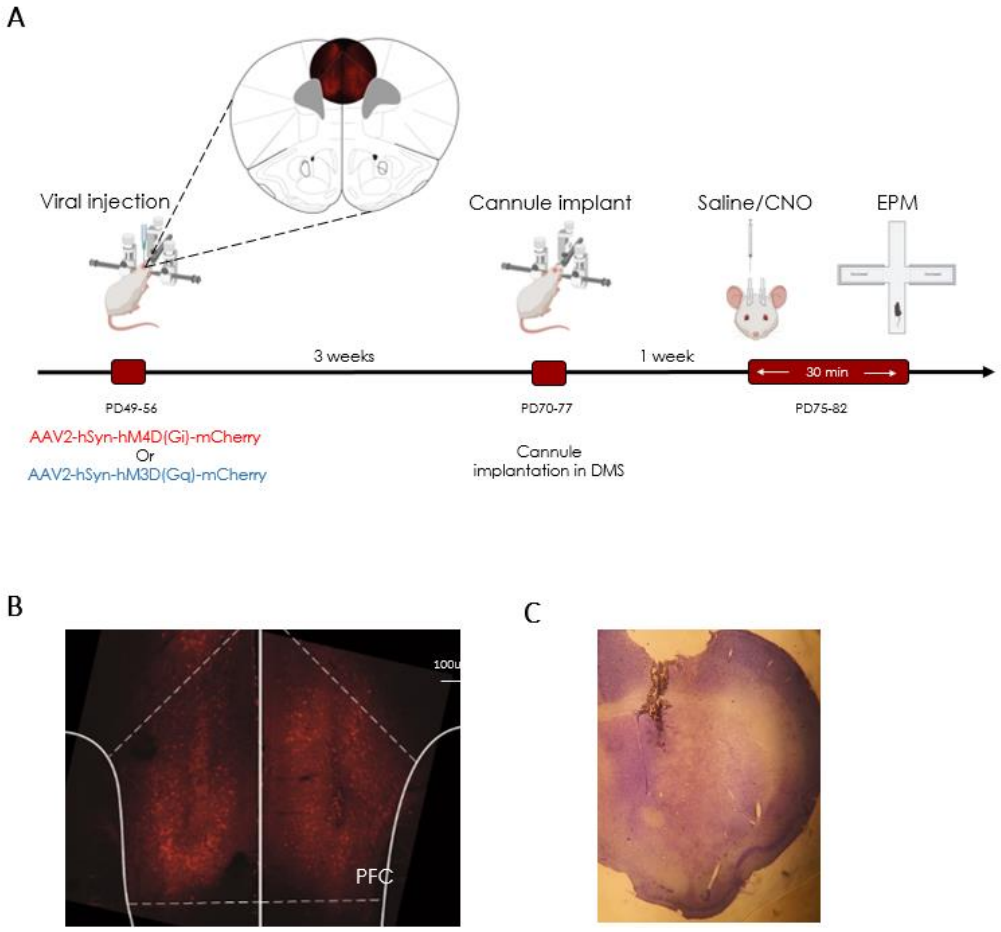

Figure 16 (A) Schematic diagrams of the experimental timeline used in this study. **(B)** Representative image viral expression in PFC. **(C)** Representative image of CNO injection site in DMS.

The inhibition of the PFC-DMS pathway (Fig. 17 A) did not affect avoidance behavior. There were no significant differences in the time spent in the open and closed arms, the center, or the distance travelled in the CNO group compared to the control group (Fig17 B-F; OA time, t=0.08179, df=16, p=0.935; CA time, t=0.3270, df=16, p=0.747; Center time t=0.7675, df=16, p=0.454; Distance, t=0.6274, df=16, p=0.539; unpaired two-tailed t-test).

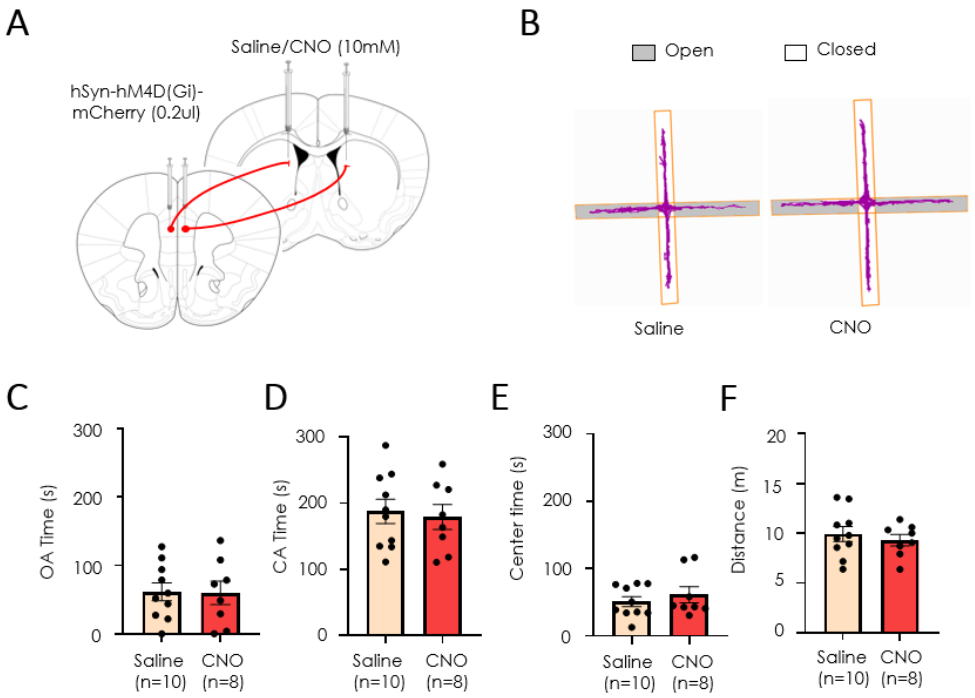

Figure 17 (A) Schematic representation of the experimental approach used to inhibit the PFC-DMS pathway. **(B)** Representative tracking plot of distance travelled by saline and CNO animals in the EPM. **(C-E)** The saline and CNO groups spent the same amount of time in the various zones of the apparatus. **(F)** There were no differences in distance travelled between the two groups. Bars represent mean ± SEM, while the dots indicate the values for each individual animal.

In contrast, the activation of the same pathway (Fig18 A) led mice to spend significant more time in the open arms and spend less time in the center of the apparatus; however, this data did not reach statistical significance (Fig18 C-E; OA time, t=2.670, df=15, p=0.017; CA time, t=0.6610, df=15, p=0.518; Center time, t=2.018, df=15, p=0.061; unpaired two-tailed t-test). Although the CNO group travelled a greater distance than the control group, this effect seems to be specific to the open arms, indicating that the manipulation likely doesn't affect overall movement or locomotion (Fig18 F-H; Distance, t=2.633, df=15, p=0.018; OA Distance, t=2.348, df=15, p=0.033; CA Distance, t=0.7276, df=15, p=0.478).

Taken together, these findings suggest that the PFC-DMS pathway plays a role in regulating innate avoidance behavior without impacting overall locomotion.

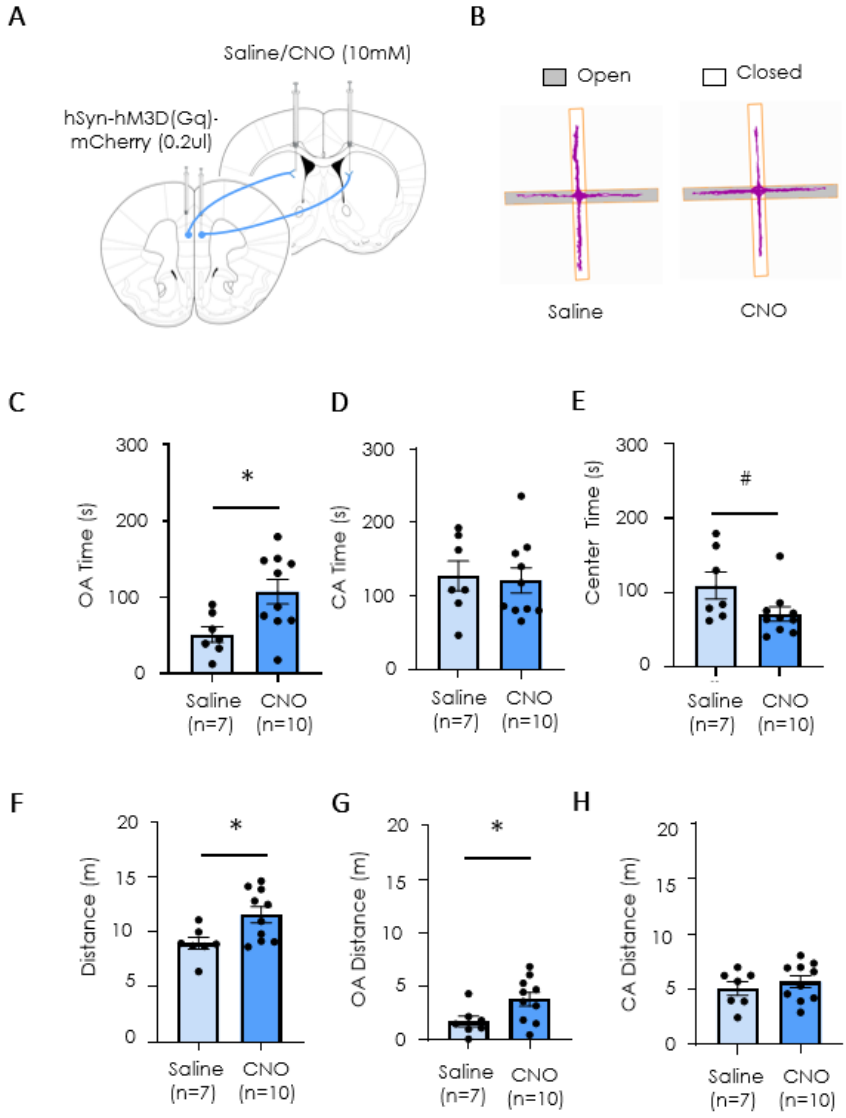

Figure 18 (A) Schematic representation of the experimental approach used to stimulate the PFC-DMS pathway. **(B)** Representative tracking plot of distance travelled by saline and CNO animals in EPM. **(C-E)** The CNO group spent more time in OA and less in the center (# p=0.06) of the apparatus compared to the control group. **(F-H)** Differences in distance travelled between the two groups were specific for the OA. *p<0.05 (t-test). Bars represent mean ± SEM, while the dots indicate the values for each individual animal.

4.3 Chemogenetic manipulation of BLA–DMS projection neurons bidirectionally controls avoidance behaviour

Given the well-established role of the BLA in modulating avoidance behaviors (Machado-de-Sousa et al., 2014; Boehme et al., 2014; Silveira et al. 1993; Moreira et al., 2007), we hypothesized that the BLA-DMS pathway might also contribute to this behavior. To test this hypothesis, we employed chemogenetics to manipulate the BLA-DMS pathway in CD1 mice, assessing their behavior in the EPM. While recent work using optogenetic activation of this pathway demonstrated increased avoidance behaviors in the EPM (Lee et al., 2024), at the time we conceived and conducted our experiment, there was no evidence in the literature linking the BLA-DMS pathway to innate approach-avoidance behavior. For this reason, we decided to evaluate the involvement of the BLA-DMS projection in innate avoidance behavior using a chemogenetic approach, leveraging inhibitory and excitatory DREADDs.

Briefly, mice were bilaterally injected with inhibitory or excitatory DREADDs in the BLA, and guide cannulas were implanted in the DMS. CNO was delivered into the DMS 30 minutes before the EPM test (fig19 A).

The inhibition of the BLA-DMS pathway (Fig20 A) significantly increased the time spent in the open arms and reduced the time spent in the closed arm (Fig 20 C-D; OA time, t=2.230, df=14, p=0.042; CA time, t=2.636, df=14, p=0.019, unpaired two-tailed t-test). There were no significant differences in the time spent in the center, or the distance travelled between the CNO group and the control group (Fig20 E-F; Center time, , t=0.8147, df=14, p=0.428; Distance, t=0.4852, df=14, p=0.635, unpaired two-tailed t-test).

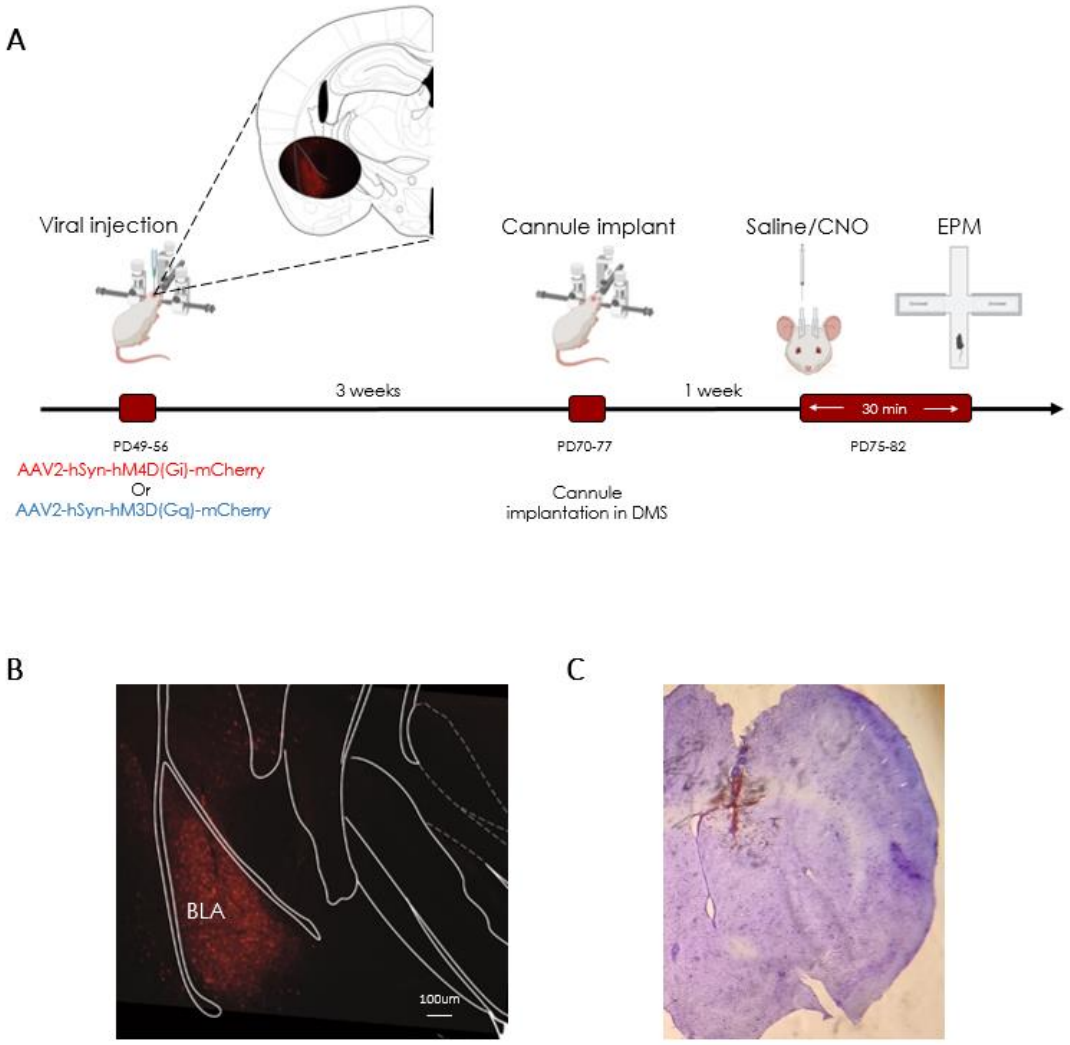

Figure 19 (A) Schematic diagrams of the experimental timelines used in this study. (B) Representative image of viral expression in BLA. (C) Representative image of CNO injection site in DMS.

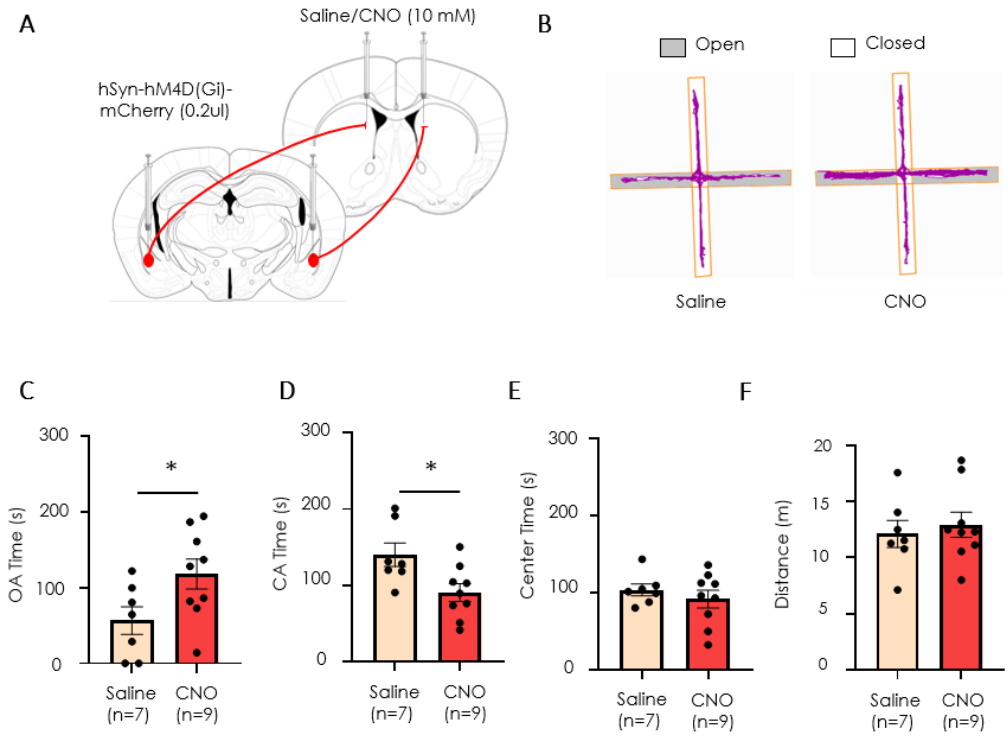

Figure 20 (A) Schematic representation of the experimental approach used to inhibit the BLA-DMS pathway. **(B)** Representative tracking plot of distance travelled by saline and CNO animals in the EPM. **(C-D)** The CNO group spent more time in OA and less in the closed arms of the apparatus compared to the control group. **(E-F)** There were no differences in the time spent in the center and distance travelled between the two groups. *p<0.05 (t-test). Bars represent mean ± SEM, while the dots indicate the values for each individual animal.

In contrast, the activation of the same pathway (Fig21 A) led the mice to spend significant less time in the open arms (Fig21 C; OA time, t=2.756, df=12, p=0.017, unpaired two-tailed t-test). There were no significant differences in the time spent in the closed arms, in the center, or the distance travelled between CNO Group and the control group, despite the time spent in CA is very close to statistical significant (Fig21 D-F; CA time, t=1.998, df=12, p=0.068; Center time, t=0.7178, df=12, p=0.486,; Distance, t=1.601, df=12, p=0.135, unpaired two-tailed t-test).

Together, these data suggest that the BLA-DMS pathway bidirectionally affects anxiety-like behavior in EPM.

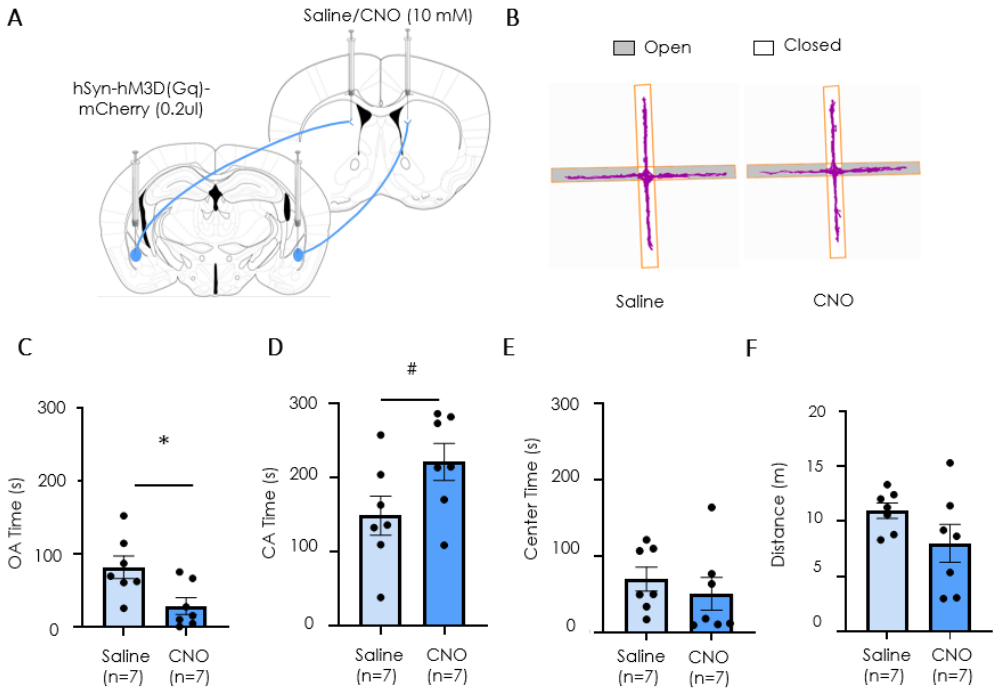

Figure 21 (A) A schematic representation of the experimental approach used to stimulate the BLA-DMS pathway. (B) Representative tracking plot of distance travelled by saline and CNO animals in the EPM. (C-D) The CNO group spent significantly less time in OA and more in the CA (# p=0.06) of the apparatus. (E-F) There were no differences in the time spent in the center, nor in the distance travelled between the two groups. *p<0.05 (t-test). Bars represent mean ± SEM, while the dots indicate the values for each individual animal.

4.4 Both PFC-DMS and BLA-DMS pathways contact Parvalbumin interneurons in DMS

The results from the chemogenetic experiments, suggest that BLA-DMS and PFC-DMS projections could influence avoidance behavior acting on the same circuit, but in opposite directions. While it has been shown that both pathways principally contact D1-MSNs, rather than D2-MSNs, indicating their prevalent engagement with the direct striatal pathway (Loewke et al. 2021; Lee et al. 2024), it remains unclear why they produce opposing behavioral effects. One possible explanation is that striatal interneurons may play distinct roles in modulating this pathway.

The striatum comprises four major classes of interneurons: (1) cholinergic neurons; (2) GABAergic neurons containing calretinin (CR); (3) GABAergic neurons containing parvalbumin (PV); and (4) GABAergic neurons containing somatostatin (SOM), neuropeptide Y (NPY), and neuronal nitric oxide synthase (NOS) (Marín, Anderson, and Rubenstein 2000). In particular, parvalbumin interneurons preferentially target direct-pathway MSNs over indirect-pathway MSNs, suggesting a potential mechanism for rapid pathway-specific regulation of striatal output pathways (Gittis et al. 2010). Our aim was to determine whether this class of interneurons could be differently involved in the PFC-DMS and BLA-DMS circuits within the DMS.

Ai14 mice were unilaterally injected in either the PFC or the BLA with the anterograde viral vector AAV1-hSyn-P2A-Cre-WPRE, a trans-synaptic serotype. This experimental approach allowed labelling of DMS neurons that receive projections from BLA or PFC by expressing the Cre-dependent reporter dtTomato. Brain sections from these mice were then processed for immunofluorescent labelling of parvalbumin interneurons in DMS (Fig 22). Finally, neurons with double labelling for dtTomato and parvalbumin were identified and counted.

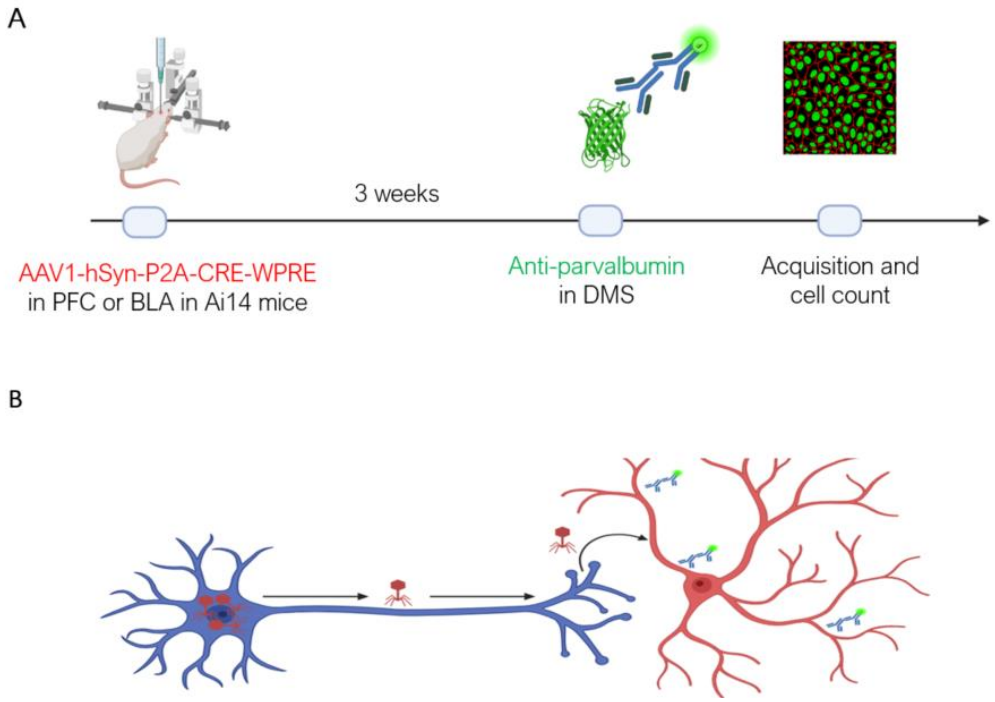

Figure 22 (A) Schematic diagrams of the experimental timelines used in this study. (B) A schematic representation of the technique used to obtain double-labeled cells. AAV1 is capable of being transported in an anterograde manner and crossing the synapse, allowing it to infect postsynaptic cells, which will appear red thanks to the Tomato reporter. Subsequently, immunohistochemistry for parvalbumin allows green labeling (using AlexaFluor488) of parvalbumin-positive cells. Parvalbumin-positive cells that are also labeled in red by the Tomato gene will then be considered double-labeled cells.

The percentage of Tomato positive cells also positive for parvalbumin showed no significant differences between animals injected with AAV1-hSyn-P2A-Cre-WPRE in PFC or BLA (Fig23 A-C; t=2,901, df=3, p=0.062, unpaired two-tailed t-test). Nonetheless, the data is very close to significance; therefore, it will be essential to increase the number of experimental subjects.

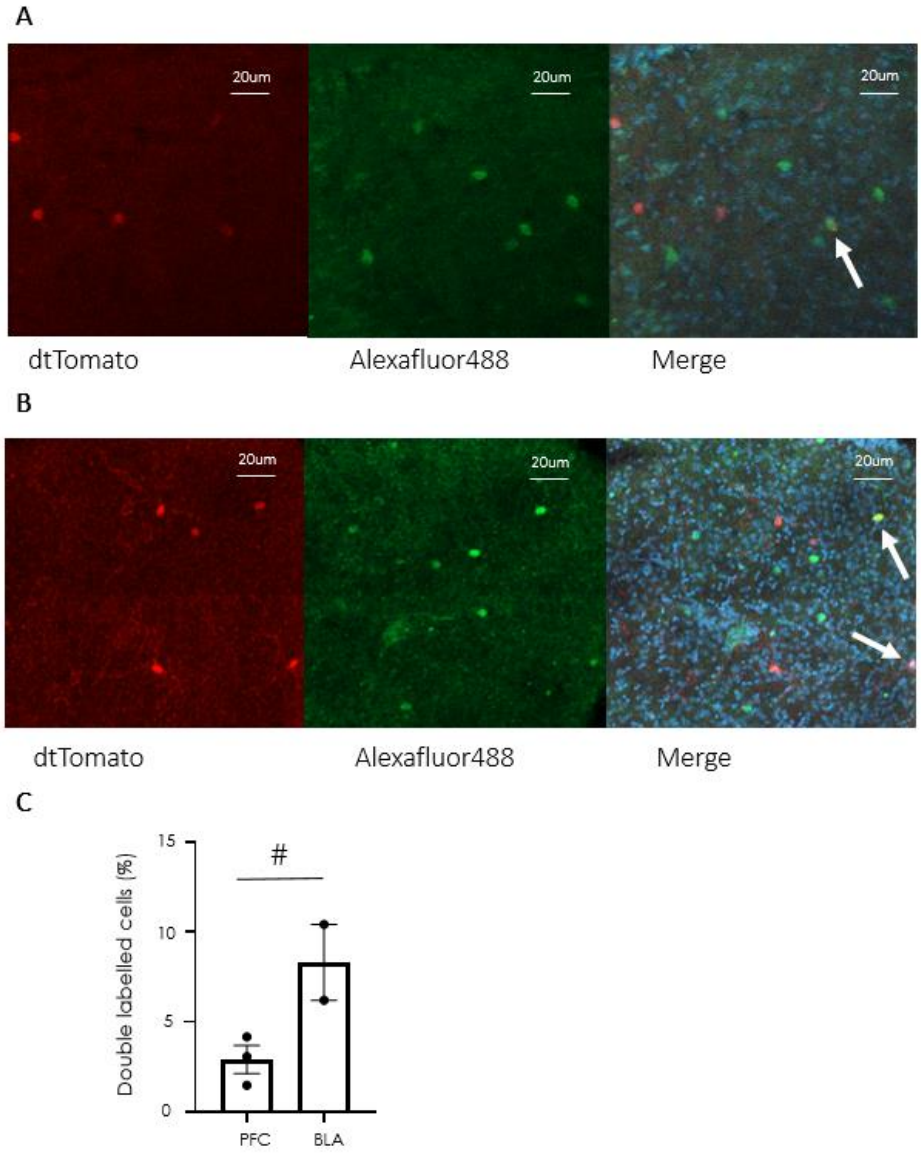

Figure 23 (A) Representative images of neurons that receive direct projection from the PFC (red), parvalbumin positive cells (green) and double labelled cells (yellow) in DMS. (B) Representative images of neurons that receive direct projection from the BLA (red), Parvalbumin positive cells (green) and double labelled cells (yellow) in DMS (20x Magnification). White arrows indicate double-labelled cells (C) The percentage of Tomato positive cells also positive for parvalbumin was not significantly different between animals injected with AAV1-hSyn-P2A-Cre-WPRE in PFC, despite the data is very close to statistical significant (#p=0.06), (n=3) or BLA (n=2).

4.5 Optogenetic activation of the DMS-GPi pathway increased avoidance behavior

Our data suggest that the signals mediating avoidance behavior originating from the PFC and BLA reach the striatum, which plays a role in controlling avoidance behavior. To further understand how this information is within downstream circuits once it reaches the basal ganglia, we aimed to explore the role of subsequent pathways in approach-avoidance behavior.

MSNs of the direct pathway express D1R and primarily project to the substantia SNr, while also providing strong inputs to the EP, the rodent equivalent of the GPi. In contrast, indirect-pathway MSNs express D2R and primarily project to the GPe (Wall et al. 2013). Specifically, the D1 pathway projecting to the GPi is particularly interesting because it has been shown that GPi neurons receiving striatal projections then project to the lateral habenula, thereby modulating its activity (Wallace et al. 2017). The activation of the LHb promotes active, passive, and conditioned behavioral avoidance by modulating GABAergic nuclei in the midbrain, suggesting that the endogenous activity of LHb glutamatergic inputs transmits information related to aversion (Stamatakis et al. 2012). For this reason, we focused specifically on DMS-GPi projections.

Mice were bilaterally injected with AAV5-hSyn-hChR2(H134R)-EYFP in the DMS, and optic fibers were implanted in the GPi, delivering laser stimulation during testing in the elevated plus maze and open field (Fig. 24). Since the stimulation of this pathway will lead to the activation of the striatal projections of the MSNs to the GPi, the final effect on the modulation of the downstream region will be inhibition, as GABA is released from the MSN terminals in the GPi.

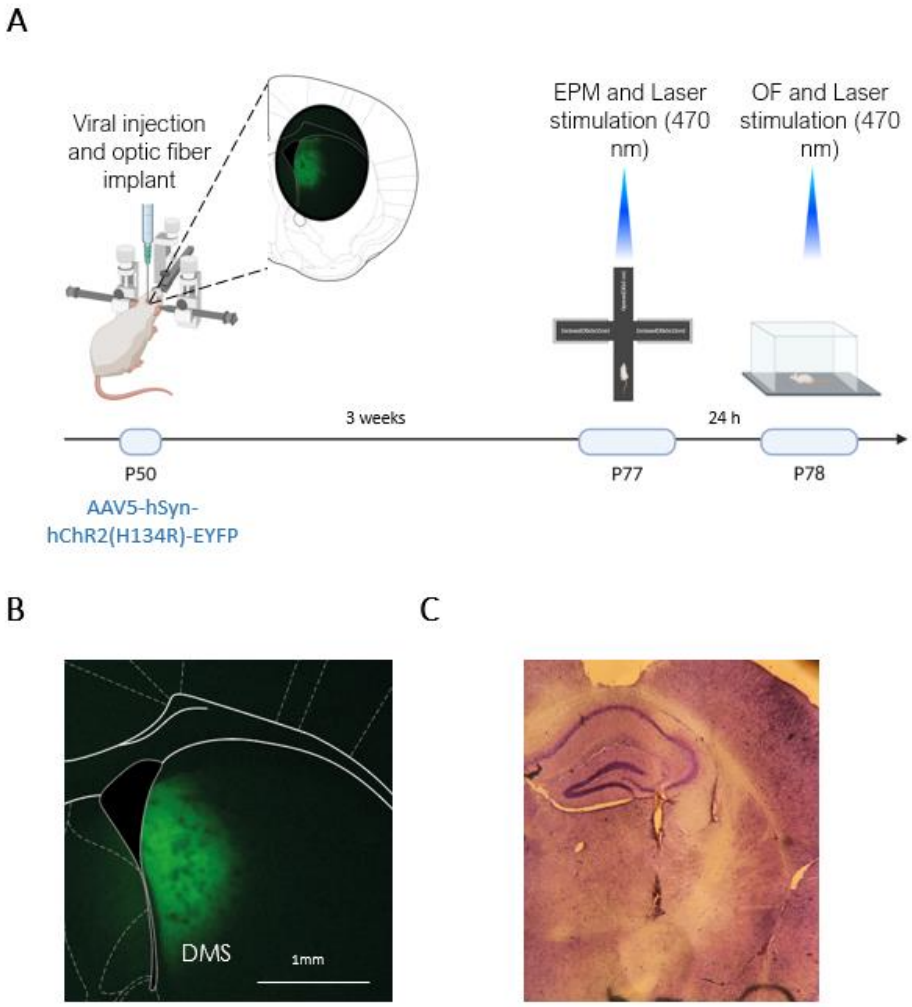

Figure 24 (A) Schematic diagrams of the experimental timelines used in this study. **(B)** Representative image of viral vector expression in DMS. **(C)** Representative image of fiber optic placement in GPi.

Preliminary results showed that the activation of the DMS-GPi pathway (Fig25 A) on avoidance behavior strengthens as the intervals progress, suggesting a potential cumulative effect of the manipulation. Additionally, laser stimulation significantly reduced the time spent in the open arms compare to baseline. In contrast, despite the closed arm time it very close, it doesn't reach statistical

significant. Therefore, more animals may be needed to achieve statistical significance. (Fig 25 B-F; OA time $F(6,18) = 6.662$, $p = 0.035$; Tukey's posthoc: $p= 0.016$ (Baseline vs On3); CA time $F(6,18) = 4.402$, $p= 0.059$, One-way RM ANOVA; Total OA, $t=6.024$, $df=3$, $p=0.009$; Total CA time, $t=0.5028$, $df=3$, $p=0.649$; Total Center time, $t=1.707$, $df=3$, $p=0.186$, paired two-tailed t-test). There were no significant differences in the total distance travelled during the ON intervals compared to OFF intervals, suggesting that the activation of DMS-GPi pathway is not affecting locomotion. (Fig25 G; Total distance paired two-tailed t-test, $t=2.232$, $df=3$, $p=0.111$).

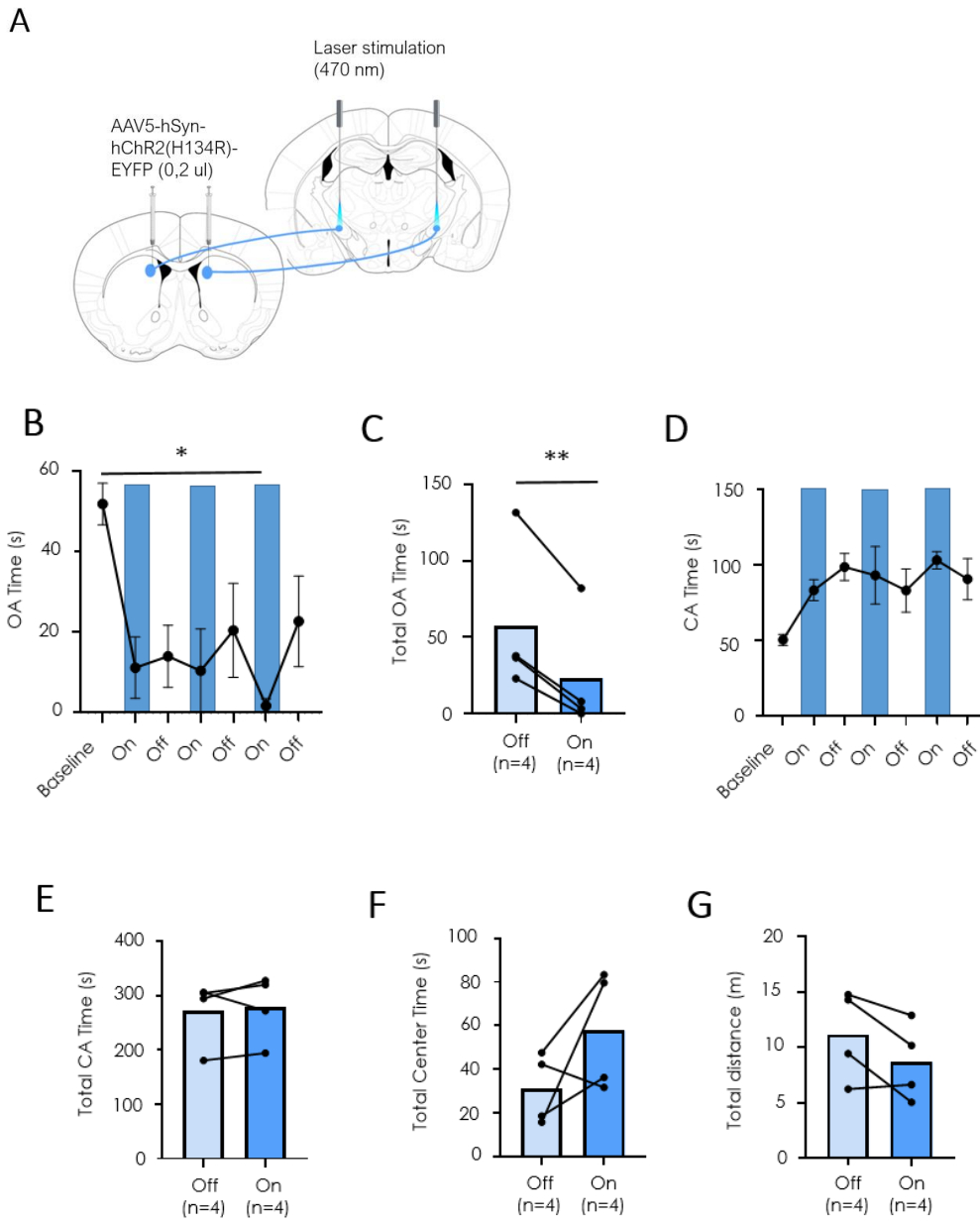

Figure 25 (A) Schematic representation of the experimental approach used to manipulate the DMS-GPi pathway. **(B-E)** During stimulation, mice spent less time in OA and the data shows a tendency to increase the time spent in closed arms of the apparatus (p=0.0598). **(F-G)** No differences were observed in the time spent in the center and the distance travelled. One-way RM ANOVA, Tukey's posthoc *p<0.05; Paired two-tailed t-test **p<0.01. Bars represent mean ± SEM.

To confirm that DMS-GPi pathway activation did not affect locomotion, mice were tested in the OF 24h after the end of the EPM. In according with the distance travelled detected during EPM, mice did not alter their locomotion during stimulation, and as expected the distance travelled progressively decreased with habituation to the OF (Fig26 A; Distance One-way RM ANOVA $F(6,12) = 9.422$, $p=0.048$). Furthermore, there were no differences in the total distance travelled in OF (Fig26 B; Total distance paired two-tailed t-test, $t=0.8315$, $df=2$, $p=0.493$).

These data suggest that the information guiding avoidance behavior, could flow from the DMS to the GPi, and that, in particular, the activation of this projection may stimulate avoidance behavior in rodents.

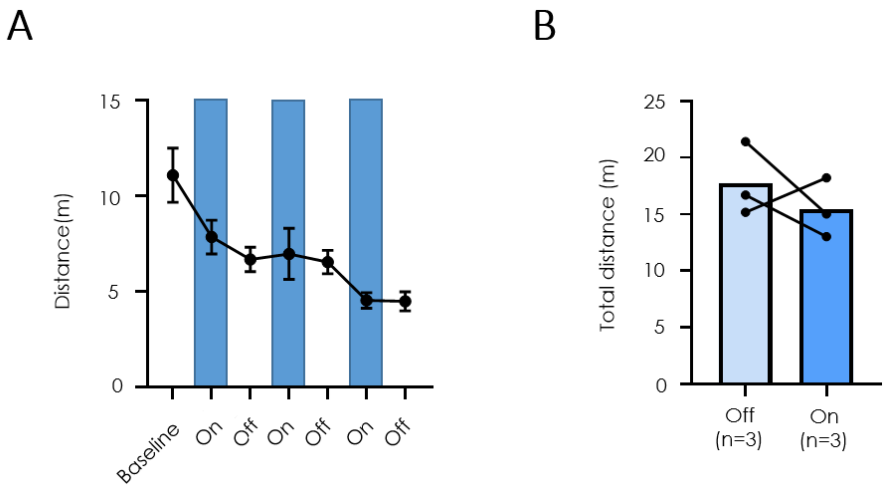

Figure 26 (A) During the test, locomotor activity in the OF decreased progressively. **(B)** Laser stimulation did not affect the total distance travelled in the OF. Bars represent mean ± SEM,

5 Discussion

In this study, we showed that in male CD1 mice, the PFC and BLA send converging projections to the DMS and that these projections are involved in the regulation of innate avoidance behavior. Specifically, excitation of the PFC-DMS pathway reduced avoidance behaviors toward the open arms in the EPM. In contrast, activation of the BLA-DMS pathway increased avoidance behaviors, while inhibition of this pathway induced an anxiolytic effect. Additionally, we collected preliminary evidence that the two pathways might contact differentially parvalbumin-positive striatal interneurons in Ai14 mice. Finally, we showed that a downstream striatal output, the DMS-GPi projection, could play a role in the regulation of innate avoidance behavior in CD1 mice as its activation exhibited an anxiogenic effect.

The knowledge of projections from the PFC and BLA to the DMS is well-established in the literature. In recent years, Hintirayan and collaborators have shown that the DMS primarily receives inputs from limbic and association cortices, including the PFC, while the DLS mainly receives inputs from motor and somatosensory cortices, such as M1/2 and S1/2 (Hintiryan et al. 2016). Additionally, the DMS, but not the DLS, receives projections from the BLA (Hintiryan et al. 2021). To verify if our target region within the DMS receives inputs from both the PFC and BLA, we used several retrograde tracers. Our results confirmed and extended the existing literature by showing not only that both PFC and BLA neurons project to the DMS in CD1 mice, but also that they project to the same subregion within the DMS. The dorsomedial striatum has a considerable anteroposterior extent, and the regions projecting into the DMS are quite diverse along this axis. We observed that inputs from the PFC and BLA reach the intermediate portion of the dorsal striatum, confirming data already present in the literature on different mouse strains (Hintiryan et al. 2016). This is a relevant

aspect from an anatomical perspective, as it becomes evident that inputs from regions of interest for avoidance behavior converge within the same area of the DMS.

Inhibiting the PFC-DMS pathway did not alter avoidance behavior in the EPM, whereas activating the same pathway significantly increased the time spent in the open arms. These results were only in part consistent with a previous study by Loewke and collaborators, which demonstrated that optogenetic stimulation of the PFC-DMS pathway increased the time spent in the open sections of the EZM while inhibition of the same pathway decreased time in the open sections, thereby increasing anxiety-like behavior (Loewke et al. 2021). While activation of the PFC-DMS pathway showed similar effects on anxiety-like behavior in both studies, inhibition did not yield the same results. The discrepancies observed with inhibition of the PFC-DMS pathway could be due to methodological differences. Indeed, optogenetic allows real-time neuronal manipulation, but the animal's position in the apparatus during light stimulation may have affected behavior, potentially leading to a conditional place preference rather than modulating innate avoidance behavior, an aspect that is not explored in the experiment by Loewke and colleagues (Loewke et al. 2021). In particular, it would be necessary to verify whether the animals were light-stimulated always when they were in the closed arms or in the open arms, to evaluate if stimulation within a specific area could induce aversion or approach behaviors toward that area.

However, the technique we employed also presents some limitations. Using focal CNO does not rule out the possibility of affecting passing fibers in the DMS. To address this issue and demonstrate that manipulating the PFC-DMS pathway specifically impacts anxiety-like behavior, further experiments are needed. These should employ viral vector-based approaches that selectively target projections from the prefrontal cortex terminating in the DMS. For instance, injecting

retrograde viral vectors expressing Cre in the DMS, along with Cre-dependent DREADDs in the PFC, followed by focal administration of CNO, would allow for specific manipulation of the pathways of interest.

Inhibiting the BLA-DMS pathway significantly increased the time spent in the open arms, while activating the same pathway led to significantly less time spent in the open arms. These findings indicate that the BLA-DMS pathway bidirectionally affects avoidance behavior in the EPM. Our results were confirmed by a study published very recently, which showed that optogenetic activation of the BLA-DMS pathway reduced the time spent in the open arms in the EPM (Lee et al. 2024), and provided the first evidence that inhibition of this pathway reduces anxiety-like behavior.

It is also important to emphasize how the data produced by chemogenetic experiments can be integrated into the existing literature about D1R and D2R. The administration of dopaminergic antagonists of D1R and D2R in the DMS produced respectively decrease and an increase in anxiety behaviour (Nguyen et al. 2019). These data suggest a clear distinction between the effects of the direct and indirect striatal pathways on avoidance behavior. However, it is crucial to note that focal administration of antagonists does not clarify whether the action is at the pre- or post-synaptic level, making it challenging to determine if the direct and indirect pathways are genuinely involved or if the modulation occurs presynaptically, indirectly affecting both pathways. Indeed, some studies indicate that the presence of dopaminergic innervation at the presynaptic level in the striatum significantly modulate inputs in the striatum (Wang et al. 2002; Tritsch et al. 2012). In fact, if modulation occurs at the presynaptic level, the effects observed by Nguyen following the administration of dopaminergic antagonists would align with the results from our experiments since the chemogenetic manipulation in our experiments occurs exclusively at the presynaptic level. This would not be

surprising, given that DREADDs are modified muscarinic metabotropic receptors, and although they exhibit different intracellular signaling pathways, it has been observed that some of these pathways are shared with dopaminergic metabotropic receptors. Some DREADDs, can activate the adenylate cyclase pathway, increasing cyclic AMP levels and leading to enhanced cellular excitability. Other DREADDs can activate pathways that reduce cAMP levels, similar to D2 receptors, resulting in opposite effects (Armbruster et al. 2007; Farrell et al. 2013; Urban et al. 2015).

The data presented, along with existing literature, indicate that both the PFC-DMS and BLA-DMS pathways are involved in anxiety-like behavior. However, it remains unclear why the same manipulation of two projections terminating in the same region results in opposite behavioral effects. A first hypothesis is that the pathways could act on different types of DMS neurons, namely the D1-MSN and D2-MSN. However, it has been shown that activation of the PFC-DMS and BLA-DMS pathways both lead to activation of D1-MSNs rather than D2-MSNs, suggesting that they primarily engage the direct striatal pathway (Loewke et al. 2021; Lee et al. 2024). Furthermore, D1-MSNs of mice that underwent prolonged activation of the BLA-DMS circuit exhibited a significantly higher AMPA/NMDA ratio, suggesting changes in the synaptic plasticity of these connections and thus their direct involvement (Lee et al. 2024). We therefore hypothesized that the contrasting effects of these two pathways on anxiety-like behavior might be due to different contributions of striatal interneurons in modulating these projections. If one of the two pathways, both glutamatergic, makes contact with a larger number of interneurons, the opposite effect on the direct striatal pathway could be justified, as a greater contribution from the interneurons might lead to reduced depolarization of the MSNs. In our preliminary experiment the difference between the percentage of parvalbumin-positive neurons that receive projection from PFC or BLA did not reach significance despite the p-value being close to 0.05

(p=0.062), thus our data does not allow to draw a definitive conclusion about the possible role of parvalbumin interneurons. Our study has important technical limitations that could explain the lack of a significant effect. Firstly, our experimental groups were too small, so it would be necessary to increase the sample size to determine if the observed difference is truly insignificant. Another important factor is the uneven distribution of males and females in the two groups. In fact, while the PFC group consists entirely of male mice, the BLA group is made of one male and one female. As there are no data in the literature about sex differences in interneuron numbers, we cannot rule out that this variable may affect the validity of our findings. Finally, our analysis focused on only one class of striatal interneurons, the parvalbumin-positive interneurons, because they show a preference for targeting the direct-pathway rather than indirect-pathway MSNs, indicating a possible mechanism for the rapid, pathway-specific regulation of striatal output pathways (Gittis et al. 2010). Without evaluating other classes of striatal interneurons, we cannot exclude the possibility that other cells may play a significant role in modulating the two pathways.

Activation of the DMS-GPi pathway significantly reduced the time spent in the open arms. These preliminary findings suggest that information related to avoidance behavior, once reaching the basal ganglia, flows from the DMS to the GPi, and that activation of this projection may increase innate avoidance behavior in rodents. This study provides the first evidence suggesting that the DMS-GPi projection may be involved in regulating anxiety-like behavior. However, it is important to emphasize that the significant difference between the ON and OFF intervals alone is insufficient to conclusively establish the role of this projection in anxiety-like behavior. First of all, introducing a reporter-only control group will be necessary to verify these findings. Additionally, it will be important to determine if stimulation in a particular area of the apparatus will provoke aversion or approach behaviors, inducing a like-conditional place preference effect (Tzschentke et al.

1998; Huston et al. 2013). To achieve this, light stimulation will be applied to the animals while they occupy either the closed or the open arms, and their behavioral responses will be subsequently assessed.

In 2020 LeBlanc also demonstrated the potential role of the DMS downstream pathways (LeBlanc et al. 2020). In particular, removing D2Rs from iMSNs (but not dopaminergic or cholinergic neurons) decreased the time mice spent in the open areas of the EZM and OF in Drd2KO mice. Disrupting the output of iMSNs with low levels of optogenetic stimulation also increased avoidance, while inhibition of iMSNs via DREADD receptors reduced it. These data, clearly showing the involvement of the DMS-GPe pathway and thus the D2-MSNs, although they may seem inconsistent with our experiments about DMS-GPi pathway, actually further enrich the picture that places the DMS at a crucial point for the control of innate avoidance behavior. In fact, the data produced by LeBlanc about DMS-GPe and our experiment on DMS-GPi are not mutually exclusive; on the contrary, it becomes clear how the DMS can integrate in the anxiety network in multiple ways, giving rise to various circuits that can integrate external information and generate the correct behavioral output.

In conclusion, our experiment provides additional support for the involvement of the DMS in avoidance behavior and further integrates this structure into the canonical circuits that have long been considered key in the regulation of anxiety-like behavior. Specifically, the DMS may act as a connecting structure between the PFC and the BLA, which project to the DMS, and certain midbrain nuclei that are also involved in avoidance behaviors (Challis et al. 2013; Bortolanza et al. 2010; C. Nguyen et al. 2021). In fact, the DMS could connect to these nuclei both directly, via the direct pathway such as the SN, and indirectly by sending projections to the GPi, thereby modulating the activity of the lateral habenula. (Wallace et al. 2017), known for its modulatory activity on the dopaminergic,

serotonergic, and GABAergic nuclei of the midbrain, such as the SN, VTA, and Raphe nuclei (Zhao et al. 2015; Hu et al. 2020). These nuclei are particularly interesting because, in addition to being involved in avoidance behaviors, they project to the PFC and the BLA (Muller et al. 2009; Tang et al. 2020; Bariselli et al. 2016; Albert et al. 2014). In this way, the DMS could integrate into the network, facilitating the formation of a closed circuit in which all the involved regions are highly interconnected and modulated by one another, allowing the midbrain nuclei to influence the higher centers.

The role of the striatum in avoidance behaviors integrates with its other functions through its participation in complex neural circuits that regulate not only the response to avoidance but also motivation, motor control, and decision-making. The striatum receives input from various brain areas, including the PFC and the BLA(Hintiryan et al. 2016; 2021), which are involved in risk assessment and emotions (Dixon et al. 2017; Davis et al. 2001). This allows the striatum to integrate information related to adverse situations and adapt behavior accordingly. The striatum plays a fundamental role in learning associations between stimuli and outcomes (Packard and Knowlton 2002). In avoidance behaviors, negative experiences can be stored, influencing future decisions and enhancing the ability to avoid similar situations. Furthermore, the striatum is crucial for motor control (Vink et al. 2005), facilitating the behavioral responses necessary for avoidance. This implies that, in addition to decision-making, the striatum also coordinates physical actions to implement those decisions. In summary, the role of the striatum in avoidance behaviors is deeply interconnected with its other functions, allowing for effective integration of emotional, cognitive, and motor information to respond appropriately to potentially harmful situations.

Since the DMS is involved in controlling behaviors related to dangerous situations, its activity can influence emotional responses, contributing to increased avoidance and anxiety. Understanding this mechanism could contribute toward the

development of therapeutic interventions for anxiety disorders. In fact, research on the DMS in avoidance behaviors may have significant clinical implications, particularly for the treatment of anxiety disorders, making the modulation of the DMS a therapeutic target.

Additionally, DMS activity might also influence social behaviors, as avoidance may manifest in social contexts. Understanding the role of the DMS in these dynamics could provide valuable insights for addressing anxiety-related social issues.

6 Appendix

6.1 Specific patterns of neural activity in the hippocampus after massed or distributed spatial training

Centofante E, Fralleoni L, Lupascu CA, Migliore M, Rinaldi A, Mele A. Specific patterns of neural activity in the hippocampus after massed or distributed spatial training. Sci Rep. 2023 Aug 16;13(1):13357. doi: 10.1038/s41598-023-39882-0. PMID: 37587232; PMCID: PMC10432541.

Specific patterns of neural activity in the hippocampus after massed or distributed spatial training

Eleonora Centofante[1,2], Luca Fralleoni[1], Carmen A. Lupascu[2], Michele Migliore[2], Arianna Rinaldi[1] & Andrea Mele[1]✉

Training with long inter-session intervals, termed *distributed training*, has long been known to be superior to training with short intervals, termed *massed training*. In the present study we compared c-Fos expression after massed and distributed training protocols in the Morris water maze to outline possible differences in the learning-induced pattern of neural activation in the dorsal CA1 in the two training conditions. The results demonstrate that training and time lags between learning opportunities had an impact on the pattern of neuronal activity in the dorsal CA1. Mice trained with the distributed protocol showed sustained neuronal activity in the postero-distal component of the dorsal CA1. In parallel, in trained mice we found more active cells that tended to constitute spatially restricted clusters, whose degree increased with the increase in the time lags between learning trials. Moreover, activated cell assemblies demonstrated increased stability in their spatial organization after distributed as compared to massed training or control condition. Finally, using a machine learning algorithm we found that differences in the number of c-Fos positive cells and their location in the dorsal CA1 could be predictive of the training protocol used. These results suggest that the topographic organization and the spatial location of learning activated cell assemblies might be critical to promote the increased stability of the memory trace induced by distributed training.

Training that includes long intervals between training sessions is termed *spaced* or *distributed training*, and has long been known to be superior to training that includes short intervals, termed *massed training*. Although this phenomenon is ubiquitous over a great variety of organisms and learning tasks[1–5] and despite its relevance for education, therapy, and advertising, its neurobiological underpinnings are still poorly understood. Findings in humans as well as in laboratory rodents support the view that *distributed practice* does not affect acquisition of information but it rather yields to better retention of memory at remote time intervals[6–9], suggesting that longer time intervals between training stimuli might impact upon the consolidation process by increasing the efficiency of information storage[10,11]. Experimental evidence supports this view demonstrating that distributed stimuli have a better efficacy in activating molecular pathways important for memory[10,12]. For example, in *Drosophila* it has been found that distributed but not massed training trials are able to generate distinct waves of MAPK activity[13]. Similar effects have also been observed after continuous or intermittent 5-HT activation on CREB transcription in Aplysia[14]. Coherently, findings in rodents demonstrate that ERK1/2 signaling pathway but also CREB and PP1 expression have differential sensitivity to changes in the frequency of training trials in different learning tasks[15–18].

Individual learning experiences have been shown to induce activity in a sparse population of neurons. This original population of neurons, however, evolves over time and over subsequent stimulations, and such changes are crucial for the formation of a stable memory trace[19,20]. The features of this dynamic process have begun to be outlined. For example it has been shown that the relative excitability of a subset of neurons increases the probability that those neurons will participate to the memory trace[21]. Interestingly integration at a cellular level between successive stimuli should occur within a limited time window to promote the formation of a more stable memory[22]. Also relevant to us is the observation that over subsequent trainings, the cell ensembles required for retrieval of remote memories differ from those activated by the initial learning stimulus, suggesting a time dependent reorganization of the cellular populations underlying the memory trace[20]. Interestingly, this reorganization process might follow rules promoting topological changes in the cell ensemble embedded into the memory trace to form clusters of cells with coordinated activity[23,24].

[1]Department of Biology and Biotechnology 'C. Darwin' - Centre for Research in Neurobiology 'D.Bovet', Sapienza University of Rome, P.Le A. Moro, 5, 00185 Rome, Italy. [2]Institute of Biophysics, National Research Council, Palermo, Italy. ✉email: andrea.mele@uniroma1.it

In this framework we asked whether and how changes in the frequency of training in the spatial version of the Morris water maze (sMWM) might affect cell activity, focusing on the dorsal CA1 (dCA1) of the hippocampus (HPC), with the working hypothesis that different patterns could be observed after massed and distributed learning experiences. To this aim we compared mice trained with a massed protocol with mice trained with a distributed protocol that has been shown to induce a more stable spatial memory[9]. In the massed group, six training sessions were administered consecutively with an intersession interval of 10 to 15 min. The distributed training procedure consisted of the same number of sessions but distributed over three consecutive days, with a 4 h within-day interval. In these training conditions both groups show similar performance when tested 24 h after the last training session but only mice trained in the distributed protocol are able to recall the correct platform location when tested 14 days after training[9]. To assess changes in the pattern of cell activity we focused on the dCA1 of the HPC for its critical role in spatial memory[25] but also because it has been shown to exhibit a high functional heterogeneity[26–31]. c-Fos expression in the dCA1 was assessed after learning with the two training protocols, comparing differences in the pattern and stability of the topographical organization of labeled neurons. The analysis demonstrated different regional distribution of c-Fos positive cells in massed and distributed trained mice. Moreover, the findings support the view that distributed training promotes increased clustering and topographical stability in learning activated cells.

Results

Massed and distributed trained mice learn to locate the platform successfully. No differences were found in the learning curve of the groups trained with massed (mMWM) or distributed (dMWM) Morris water maze protocol (Fig. 1a) on either latency (two-way repeated measures ANOVA: session $F_{(5,55)} = 8.322$, $p < 0.0001$; training protocol $F_{(1,11)} = 0.1476$, $p = 0.7082$; session x training protocol $F_{(5,55)} = 0.3382$, $p = 0.8876$) or

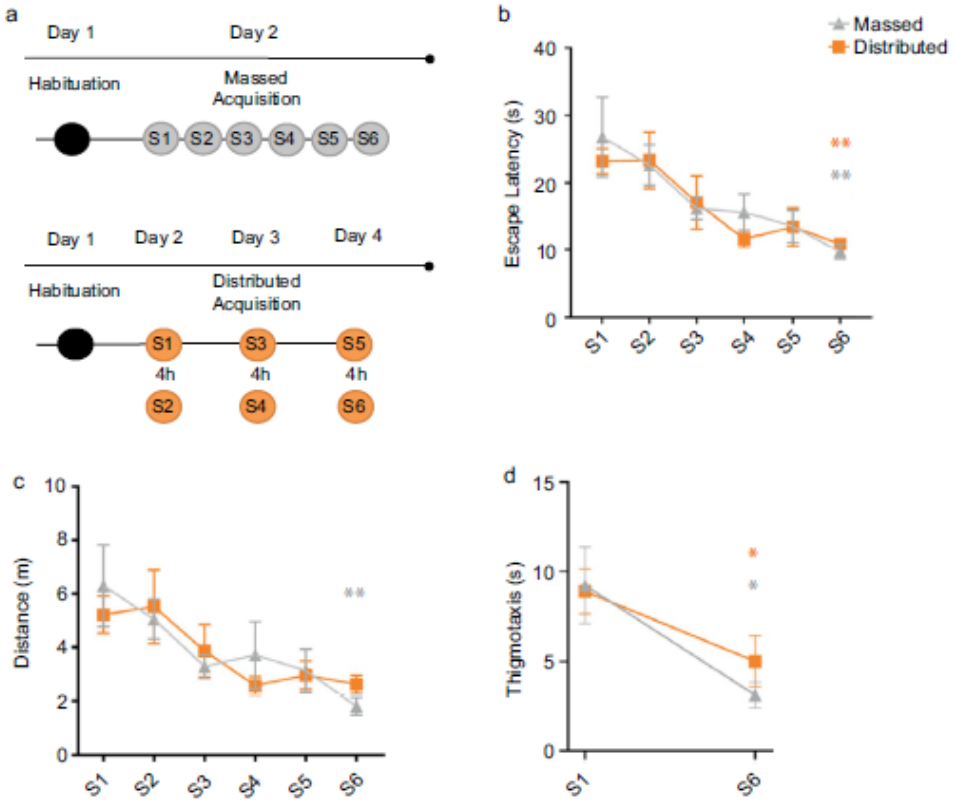

Figure 1. Learning curves for mice trained in the spatial version of the MWM with massed or distributed training protocols. (**a**) Timeline of the two MWM training procedures. (**b**) The graph shows the escape latency to reach the platform during training in the MWM in the massed (grey; N = 6) and in the distributed (orange; N = 7) groups (**$p \leq 0.01$, S1 vs. S6, massed and distributed, Tukey HSD). (**c**) The graph shows the distance travelled during training in the MWM in the massed and distributed groups (**$p \leq 0.01$, S1 vs. S6, massed, Tukey HSD). (**d**) The graph shows the time spent in thigmotaxis in S1 and S6 for both massed and distributed groups (*$p \leq 0.05$, S1 vs. S6, massed and distributed, paired t-test). Graphs represent mean ± SEM.

distance (two-way repeated measures ANOVA: session $F_{(5,55)} = 5.636$, $p = 0.0003$; training protocol $F_{(1,11)} = 0.02189$, $p = 0.8851$; session x training protocol $F_{(5,55)} = 0.5393$, $p = 0.7456$), in agreement with what has been previously reported[9,32]. Further analysis confirmed that both mMWM and dMWM trained mice progressively reduced the latency (one-way repeated measures ANOVA mMWM: $F_{(5,25)} = 4.194$, $p = 0.0066$; dMWM: $F_{(5,30)} = 5.706$, $p = 0.0008$) and the distance to reach the platform, (one-way repeated measures ANOVA mMWM: $F_{(5,25)} = 2.793$, $p = 0.0388$; dMWM: $F_{(5,30)} = 3.530$, $p = 0.0125$), demonstrating that both groups were able to correctly acquire the task (Fig. 1b,c).

A thigmotactic strategy is often deployed by animals in the initial stages of the acquisition as an alternative to a spatial strategy[33] therefore the comparison of the thigmotactic behavior in S1 and S6 in the two experimental groups was used to assess increased proficiency at this spatial task. The statistical analysis revealed a significant difference between S1 and S6 for both groups (mMWM: $t_{(5)} = 2.301$, $p = 0.0349$; dMWM $t_{(6)} = 2.478$, $p = 0.0240$, paired t-test), demonstrating that with training progression mice reduced the time spent doing thigmotaxis (Fig. 1d).

Learning induced c-Fos activity in the dCA1 shows subregional specificity depending on the training protocol. To investigate changes of c-Fos expression after massed and distributed training in the MWM we focused on the CA1 of the dorsal hippocampus, because it has been shown to be critical for spatial MWM acquisition[25]. To perform a spatially detailed count of c-Fos positive cells from the pyramidal cell layer, we draw up to 12 contiguous regions of interest (ROIs) on each section of c-Fos-stained dCA1, as shown in Fig. 2a,b. The mean number of c-Fos positive nuclei per ROI in the dCA1 was higher in trained mice (mMWM: 26.6 ± 5.6; dMWM: 29.3 ± 3.0) compared to controls (20.4 ± 2.4), although the difference did not reach statistical significance (one-way ANOVA: $F_{(2,24)} = 1.988$, $p = 0.158$). Next, we analyzed the pattern of expression of c-Fos positive nuclei along the antero-posterior and proximo-distal axes of dCA1, in light of their significant functional heterogeneity[26–30] (Fig. 2a,b). To this aim, we generated 3D heatmaps reproducing the number of c-Fos positive cells in each ROI within the dCA1. As shown in Fig. 3a control mice exhibited an overall lower number of activated cells, compared to the massed and the distributed groups, and a fairly homogenous distribution throughout the dCA1. On the contrary, the number of c-Fos positive cells was not evenly distributed in mice trained in the MWM. Moreover, the analysis revealed regional differences depending on the intertrial interval used to train the mice. In particular, the massed trained mice showed higher level of expression in the medio-proximal portion of dCA1 (Fig. 3b) while mice trained with the distributed protocol revealed higher levels in the postero-distal component of the dCA1 (Fig. 3c). To deepen our analysis and quantitatively compare c-Fos activity in mice trained with the two protocols we grouped the ROIs along the antero-posterior and proximo-distal axes (see "Methods"). The one-way ANOVA revealed significant differences in the mean c-Fos counts in the postero-central and postero-distal regions (training protocol: $F_{(2,24)} = 3.15$, $p = 0.062$ for the postero-distal region; $F_{(2,22)} = 3.618$, $p = 0.044$ for the postero-central; $F_{(2,22)} = 3.607$; $p = 0.044$ for the postero-proximal; $F_{(2,24)} = 1.222$, $p = 0.312$ for the medio-distal; $F_{(2,24)} = 1.751$, $p = 0.195$ for the medio-central; $F_{(2,23)} = 3.216$, $p = 0.058$ for the medio-proximal; $F_{(2,23)} = 0.101$; $p = 0.905$ for the antero-distal; $F_{(2,23)} = 0.690$, $p = 0.512$ for the antero-central) (Fig. 3d). The post-hoc analysis confirmed a significant difference between mice trained with the distributed

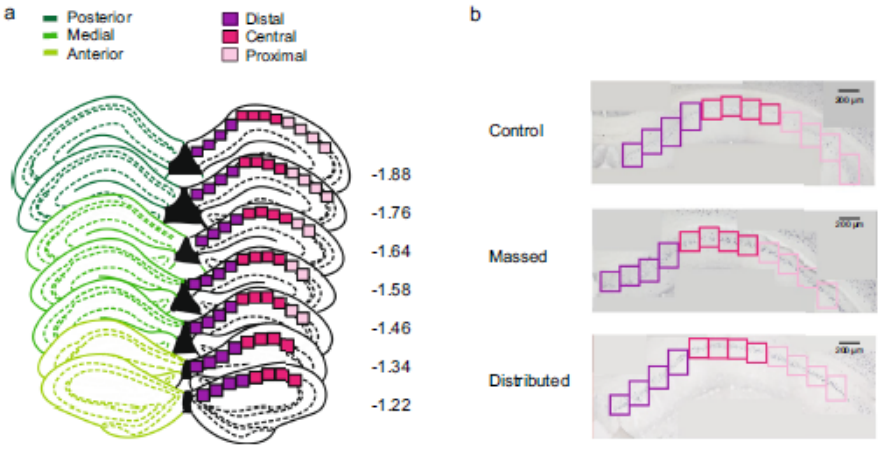

Figure 2. Schematic representation of dCA1 reconstruction. (**a**) Schematic representation of antero-posterior (dark green = posterior; green = medial; light green = anterior) and proximo-distal axes (dark pink = distal; pink = central; light pink = proximal) along dCA1. Numbers indicate anteroposterior coordinates relative to bregma (in mm, according to[54]). (**b**) Representative posterior dCA1 sections from control, massed and distributed mice, stained for c-Fos. The boxes along the proximo-distal axis represent the position of the ROIs used to count c-Fos positive cells.

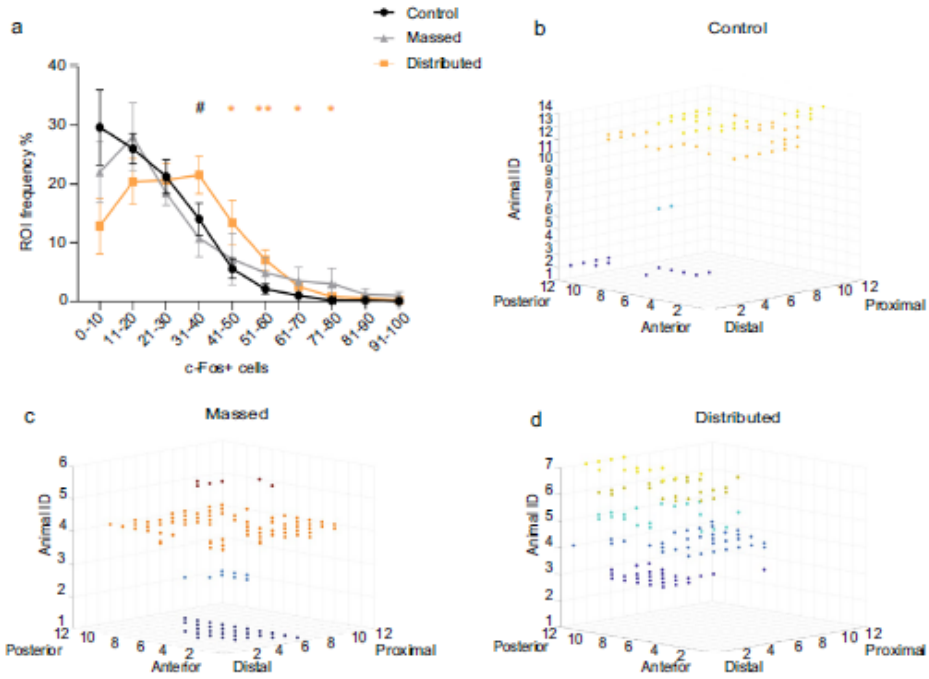

Figure 4. ROIs frequency and 3D distribution of ROIs expressing high number of c-Fos positive cells. (**a**) The graph shows the frequency of ROIs with different number of c-Fos$^+$ cells [U = 5, (31–40); U = 22, (41–50) interval; U = 14, (51–60) interval; U = 22, (61–70) interval; U = 18, (71–80) interval. * $p \leq 0.05$; ** $p \leq 0.01$ distributed versus control; # $p \leq 0.05$ massed versus distributed, Mann–Whitney. (**b-d**) 3D representation of ROIs clusters defined as the ROIs expressing high levels of c-Fos + cells (≥ 40) neighboured at least 5 similar ROIs (c-Fos + ≥ 40) separately for each experimental subject of the (**b**) control, (**c**) massed and (**d**) distributed groups. Each color represents one animal.

Considering the mean of c-Fos positive cells per ROI in controls (c-Fos$^+$ = 23) as a threshold for all the three groups, we searched for ROIs activated over the threshold with the same topological position in at least 5 out of 6 animals in the massed, 6 out of 7 in the distributed and 13 out of 14 in the control group. We could not find any above-threshold ROI sharing the same position in the animals of the control group (Fig. 5a), this held true even considering shared ROIs in only 5 out of 14 mice of the control group. Conversely this analysis revealed that 4 above-threshold ROIs and 11 above-threshold ROIs shared the same position in in the massed and the distributed group, respectively (Fig. 5b,c). Coherently with the regional activation induced by the training protocols, these common ROIs were specifically localized in the medial compartment of dCA1 for the massed and in the posterior portion of dCA1 for the distributed group, as shown in the 3D reconstruction in Fig. 5.

These results led us to ask whether these characteristic activation patterns could be robust enough to predict the training procedure. We computed accuracy using a Quadratic Discriminant (QD) classifier, a supervised machine-learning algorithm for data classification. When trained with all the variables (see "Methods"), the algorithm showed a remarkable capability to discriminate between massed and distributed trained animals (accuracy = 78%). Notably, when we repeated the procedure adding the control group the level of accuracy decreased (accuracy = 41.4%), pointing out how the absence of a specific c-Fos expression pattern in the control group reduced the discrimination ability of the algorithm. The analysis of feature importance highlighted that the most informative variable was the antero-posterior coordinate (section number) confirming that subregional differences in the level of c-Fos activity in the trained animals was a critical feature to distinguish the groups (Fig. 6).

Discussion

In the present study we contrasted c-Fos expression after massed and distributed training in the spatial version of the MWM to outline possible differences in the learning induced pattern of neural activation in the dCA1 of the HPC in the two training conditions. Three main results were obtained: 1. Distinct regional distribution of c-Fos positive cells after massed and distributed training; 2. Increased clustering of cell activity in mice trained with the distributed as compared to mice trained with the massed protocol; 3. Increased stability across animals of spatially patterned organization of distributed training induced active cells assemblies. Moreover, using a

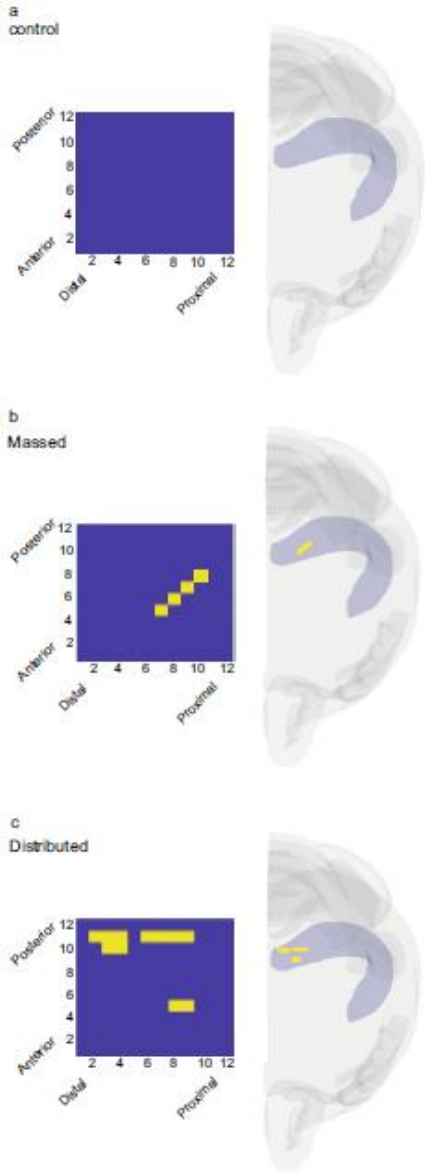

Figure 5. ROIs above threshold with shared position in the different experimental groups. (**a**) Controls, (**b**) massed and (**c**) distributed. Right panels, 3D brains reconstruction showing the localization of the shared above-threshold ROIs (yellow ROIs) within the dCA1.

Quadratic Discriminant algorithm we found that differences in the number of c-Fos positive cells and their location in the dCA1 could be predictive of the training protocol used.

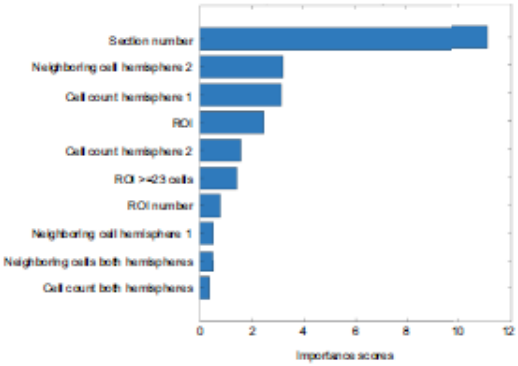

Figure 6. Machine-learning based classification of the training procedure. Histogram depicts the relative importance of the top 10 features (Section number, Neighboring cell hemisphere 2, Cell count hemisphere 1, ROI, Cell count hemisphere 2, ROIs ≥ 23cells, ROI number, Neighboring cell hemisphere 1, Neighboring cell both hemispheres, cell count both hemispheres) in the Quadratic Discriminant model (Kruskal–Wallis algorithm features importance scores).

It is well known for many types of learning that distributed training, involving longer inter-trial intervals, leads to a more robust memory formation as compared to massed training[2,5,6,9]. In the present study we compared massed and distributed training in the spatial version of the MWM. Two different training protocols were used, a within day protocol in which the six training sessions are massed with a 5–10 min inter-trial interval, and an across-three-days protocol that has been recently demonstrated to increase memory stability[9], reproducing the increased memory performance observed in humans when inter-repetition lags increase[11]. Independently on the training protocol, mice of the two groups reduced the distance and the time to reach the platform. Consistently with previous evidence[5,8,9,32,34,35] distributed training did not affect learning, as there was no difference in terms of the total distance moved and the latency to find the platform as the sessions progressed. These finding are in agreement with the suggestion that the ability of distributed training to increase memory cannot be attributed to an effect of the training protocol on learning, but rather on the consolidation process[9–11].

Although we could not find any behavioral differences in the acquisition phase, marked differences could be detected in the pattern of c-Fos expression in the dCA1 of the HPC depending on the training protocol. Analysis of c-Fos labeled cells did not highlight significant differences in the overall number of active cells between the two experimental groups, however we found a change in the regional distribution of c-Fos labeled cells. Our analysis revealed that increasing lags between learning opportunities changes the pattern of activity over the proximo-distal axis as well as over the antero-posterior axis of dCA1. In massed trained mice, in fact, we observed a higher number of c-Fos expressing cells in the medio-proximal component of the CA1, while distributed training induced activity was found mainly in the postero-distal domain of the CA1. Although the hippocampal networks sustaining memory within the CA1 are traditionally viewed as constituted by homogeneous populations of cells, heterogeneity has been demonstrated both at a structural and a functional level[36–38]. The structural heterogeneity is well established based on the differential projections from the entorhinal cortex, with the lateral part projecting preferentially to the distal component of the CA1 and the medial part projecting mainly to the proximal CA1[38,39]. The cellular compactness and width of the deep and superficial CA1 pyramidal cells sublayers also show a regionalization, decreasing and increasing respectively along the proximo-distal axis[26]. This structural heterogeneity is paralleled by functional differences on the proximo-distal axis. Relevant to us is the finding that cells in the distal component display a higher place field accuracy compared to those in the proximal component[28]. Such a functional gradient is paralleled by an opposite radial gradient in the place field stability[27] and in the recruitment of CA1 pyramidal neurons during HPC sharp wave ripples[40], suggesting a higher dynamicity and accuracy of cells in the proximal CA1 as compared to those in the distal component that would show a coarse representation of the environment but with a higher steadiness[26]. Interestingly the different pattern of activity in mice trained with the massed or the distributed protocols suggest a progressive shift along the proximo-distal axis with the increased time lag between learning opportunities. The proximal component is indeed activated after massed training, whereases the distal is activated after a distributed training (Fig. 3). This result would be consistent with behavioral evidence in rodents and humans that memory representation after distributed learning is more stable than after massed learning[9,11].

The second interesting observation raised by the quantification of c-Fos labeling was that the topographic distribution of learning activated cells in the dCA1 varies depending on the training protocols. In particular the analysis performed revealed a group difference in the number of ROIs expressing higher c-Fos labeling. This observation, together with the clustering of ROIs expressing a high number of c-Fos positive cells in the distributed groups, as compared to control mice or mice trained with the massed protocol, strongly suggests a training protocol dependent clustering of learning activated cells. Two different lines of evidence support the possibility of a learning induced clustering of cell activity. A handful of electrophysiological studies for example reported a cluster type organization of place cells, demonstrating that neighboring pyramidal cells in the CA1

have overlapping place fields[41–43], but see also[44]. More relevant are findings relative to the organization of IEGs labeled cells after training, demonstrating increased IEGs activity in adjacent cells, in the CA1, after exposure to a novel environment and tighter clusters when exposure to the same environment is repeated[45,46]. A similar learning dependent increase in clustering of active cells was observed also in the dorsal striatum as instrumental learning progresses[24]. Although a causal role of such clustering in memory formation has never been established, our findings support this hypothesis, by showing that it is more pronounced increasing the time interval between sessions when the stability of the memory trace is enhanced.

Finally, we also found a difference in the stability of the topographic distribution of activated ROIs in the three experimental groups. A few studies addressed the question relative to the topography of learning activated cells in the HPC as well as in other brain regions[47–49]. The increased topographic stability of active cells assemblies we found comparing the two training protocols is in agreement with previous evidence demonstrating a spatially patterned organization of amygdala neurons activated by training in a fear conditioning task[47,48] as well as fMRI data reporting a stable topography of activation for specific memories in the human HPC[50,51]. Thus our data support the hypothesis that increased stability of the memory trace might depend on the spatial location of active cell assemblies within dCA1[47,51]. Finally, we were able to discriminate mice trained with the different training protocols based on a quadratic discriminant algorithm for data classification, using information relative to the pattern of expression of learning induced c-Fos positive cells. These findings suggest that optimization of memory might depend upon specific hippocampal neuronal population codes that vary depending on the stability of the memory trace. It should be mentioned, that we analyzed c-Fos expression in the dHPC after training in the spatial version of the MWM, however, increased IEGs expression in the hippocampal complex has been reported also after training in the cue version of the task, although a causal role of this activity in memory has been debated[52,53]. In the future, it would be very interesting to test whether the changes in cell ensemble activation we observed in the present study could be generalized to the training frequency rather than the specific information to be acquired.

It has been hypothesized that the memory stability induced by distributed training depends on a more efficient stabilization of the memory trace[10]. The evidence presented in this study suggests that the topographic organization and the spatial location of learning activated cell assemblies might be relevant to this process. Moreover, it supports the view that activity in the distal component of the dCA1 might be important in determining the stability of the representation.

Materials and methods

Subjects. The experiments were conducted on naïve CD1 male mice (Charles River, Italy). Mice were 8 weeks old, weighting 34–38 g, at the onset of the experiments. Animals were always housed in groups of three mice in standard cages (26.8 × 21.5 × 14.1 cm), with water and food ad libitum, under a 12 h light/dark cycle (7 a.m./7 p.m.) and constant temperature (22 ± 1 °C). Behavioral training and testing were conducted during the light period (from 9:00 am to 5:00 pm). The maximum effort was made to minimize animal suffering. Procedures were conducted under the authorization N. 450/2018-PR from Italian Ministry of Health, according to Italian (DL.116/92) and European laws and regulations on the use of animals in research, and NIH guidelines on animal care.

Morris water maze. The apparatus consisted of a circular pool (110 cm diameter and 40 cm high) filled up to 5 cm from the edge with water at 22 ± 1 °C. To allow mice tracking, water was black-colored with non-toxic paint (Giotto, Italy). Black curtains surrounded the pool, and several visual cues were attached on them at the distance of round 50 cm from the pool. A white light (100W) was positioned above the apparatus facing the ceiling. Four additional lights (1.9 W) were positioned facing the cues to light them up. The pool was ideally divided into four identical quadrants. Four starting positions (labeled N, S, E, and W) were located equidistantly around the edge of the maze. A Plexiglas platform (10 cm diameter), covered with wire mesh to avoid slipping, was positioned 20 cm away from the pool wall in one of the four quadrants. The quadrant where the platform was kept during the training was randomized and was named the "Target" quadrant, whereas the other three quadrants were named "Right", "Left" and "Opposite", relative to the Target.

Mice of each group were handled for 3–4 min/day, for 5 consecutive days, before the beginning of the experiments. The spatial version of the Morris Water Maze task (MWM) consisted of two different phases: familiarization and training (Fig. 1a). The familiarization phase was the same for both the massed (mMWM) and the distributed (dMWM) protocols and consisted of one session of three consecutive trials (intertrial interval: 20 s). During the familiarization phase, no cues were attached on the curtains and the platform protruded 1.5 cm above the water surface. During the training phase, the platform was submerged 0.5 cm beneath the surface of the water and visual cues were attached on the black curtains surrounding the pool. The mMWM consisted of six consecutive training sessions (intersession interval: 10–15 min) of three trials (intertrial interval: 20 s), whereas dMWM consisted of six training sessions distributed over 3 days, with 2 sessions per day (intersession interval: 4 h) of three trials (intertrial interval: 20 s)[9]. In each trial, animals were randomly released from one of the three non-target quadrants. Mice in mMWM were kept in their holding cage for 1 h before the starting of the training sessions, whereas mice in dMWM were kept in their holding cage for 1 h before each training session. During intersession intervals, mMWM mice returned to their holding cage until the next session. Control animals were kept in their holding cage for the whole length of training sessions.

All trials were recorded by a camera located over the pool and videos were acquired and analyzed by an automated tracking system (AnyMaze 5.0, Stoelting). Escape latency (in seconds) and distance travelled to reach the platform (in meters) were scored. Thigmotaxis was defined as the swimming time within the zone closer to the pool wall (10 cm from pool wall).

Immunohistochemistry: Fos staining. One hour after completing the last training session in the MWM, each animal was deeply anaesthetized with a mixture of Zoletil (500 mg/kg, Virbac Italia) and Xylazine (100 mg/kg, Bayer, Germany) and transcardially perfused with 40 ml of saline solution (NaCl 0.9%) followed by 40 ml of 4% formaldehyde in PBS (4 °C). Brains were rapidly removed and post-fixed for 24 h in 4% formaldehyde and then transferred to 30% sucrose in PBS until sectioning. 40 µm-coronal sections were obtained using a cryostat (Leica CM 1520, Leica Microsystems, Wetzlar, Germany) and were stored at − 20 °C in cryoprotectant solution. For the c-Fos-immunoreactivity (c-Fos-IR), free-floating sections were incubated for 5 min in 3% hydrogen peroxide in PBS and rinsed three times in PBS containing 0.1% Triton X-100 (PBST). After 1 h of incubation in PBST containing 1% BSA and 1% NGS sections were incubated overnight in anti-phospho-c-Fos rabbit monoclonal antibody (5348S; Cell signaling Technology, USA) diluted 1:8000 in PBST–BSA–NGS, at 4 °C and with constant orbital rotation. Sections were washed three times in PBST and incubated in biotinylated secondary antibody diluted 1:500 in PBST-1% BSA (goat anti-rabbit IgG; Vector Laboratories, USA) for 2 h at room temperature. After three washes in PBST, sections were transferred for 1 h in avidin–biotinylated peroxidase complex diluted 1:500 in PBST (ABC Kit; Vector Laboratories, USA) and rinsed three times in PBS. Finally, the reaction was visualized using nickel intensified diaminobenzidine (DAB peroxidase substrate kit, Vector Laboratories, USA). The reaction was stopped after exactly 4 min by washing with 0.1 M PBS (pH 7.6). Sections were mounted on slides, dehydrated through a graded series of alcohols, cleared and coverslipped. Sections from groups to be directly compared were processed at the same time and using the same conditions and reagents to reduce variability. In all experiments, the number of cells displaying c-Fos immunoreactivity was measured in dCA1, taking twelve alternating brain sections (from − 1.22 mm to − 1.92 mm relative to bregma), encompassing the whole antero-posterior axis. Regions were defined according to the mouse brain atlas[54].

Digital reconstruction and c-Fos quantification. Digital images were acquired at 10X magnification, using a microscope (Nikon Eclipse 80I) equipped with a CCD camera. After images acquisition, single images of 2560 × 1920 pixel were stitched together in a mosaic view of the entire dCA1 region and counting of the stained nuclei was carried out using the public domain software ImageJ (http://rsb.info.nih.gov/ij/). Briefly, for each section, stained nuclei were automatically detected based on their intensity of staining relative to background and their size. Detailed counting of c-Fos positive cells was performed drawing from 8 to 12 contiguous regions of interested (ROIs), covering the whole dCA1 on each section. Each ROI had a 200 µm width and ROIs were placed consecutively along the dCA1 proximo-distal axis (distal CA1: away from the dentate gyrus, close to the subiculum; proximal CA1close to dentate gyrus and CA2)[36,55]. The anchor point for the first ROI was always set at the beginning of the dCA1 along the midline of the brain, using the ventricle as the starting point marker. The dCA1 was covered by 8 ROIs in the most anterior sections, 10 ROIs in the medial region, whereas in the most posterior region was covered by 12 ROIs per section. Although missing ROIs were present in every animal the mean number of ROIs sampled was similar in the different groups (control: 87 ± 5.7; massed: 89.8 ± 10.8; distributed: 90.4 ± 7.4). ROIs in the whole dCA1 were also classified based on their number of c-Fos positive cells, according to the following intervals: 0–10; 11–20; 21–30; 31–40; 41–50; 51–60; 61–70; 71–80; 81–90; 91–100 c-Fos + cells per ROI. For each experimental subject, the frequency of ROIs in each interval was then calculated and reported as percentage of the total number of ROIs for that subject.

Regional c-Fos expression was evaluated dividing the whole dCA1 in eight different subregions: antero-distal (AD), antero-central (AC), medio-distal (MD), medio-central (MC), medio-proximal (MP), postero-distal (PD), postero-central (PC), postero-proximal (PP). Each subregion includes 16 ROIs except for the medio-proximal compartment (10 ROIs), according to the dCA1 shape.

Analysis of c-Fos expression pattern. Data obtained from digital image reconstruction and c-Fos quantification were exported in a tab-delimited spreadsheet and imported in MATLAB. MATLAB heatmap representation was used to obtain the 3D heatmap representation of c-Fos positive cells for each ROI and section (Fig. 3). Custom-made scripts (Mata and Matrixa) were used to identify the ROIs with a cell count equal or above 40 cells (threshold chosen based on the differences observed in the ROIs frequency analysis) and neighboring other ROIs (within 5 Euclidean distance) with the same cell count (Fig. 4 b–d). Finally custom-made scripts (Histcut_23; Pixels_m_23; Common_23) were used to highlight the ROIs with a cell count equal or above 23 (mean of c-Fos positive cells per ROI in control animals) and with a shared position within each experimental group (Fig. 5). All scripts are included as supplementary materials.

Machine learning based classification. A MATLAB based library was used to train the classification model (https://www.mathworks.com/help/stats/choose-a-classifier.html). The model is a supervised machine learning algorithm called Quadratic Discriminant (QD) that is based on discriminant analysis learning.

We applied the QD classifier adopting the function cross_val_score with cv = 10 to perform tenfold cross-validation (available in MATLAB R2022a). The classifier was trained using the information from each subject about the c-Fos positive cells number along the anterior–posterior axis (section number), c-Fos positive cells number along the proximo-distal axis (ROI number), total number of c-Fos positive cells from each hemisphere (cell count hemisphere 1; cell count hemisphere 2), total number of c-Fos positive cells averaged between the two hemispheres (cell count both hemispheres), the presence and the number of the ROIs above threshold (ROIs expressing c-Fos$^+$ cells ≥ 23), number of the ROIs above threshold adjacent to each other from hemisphere 1, 2 and the average between the two hemispheres (neighboring cell hemisphere 1; neighboring cell hemisphere 2; neighboring cell both hemispheres). To calculate feature importance in classifier decision, we used the attribute feature selection that expresses the fraction of relative importance for each feature.

Data collection and statistical analysis. All data are presented as mean ± standard error. For the MWM experiment, escape latency and distance travelled were analyzed using both two-way and one-way repeated measures ANOVA with session (six levels: session 1 to 6) as repeated measure. Time spent in thigmotaxis between S1 and S6 was analyzed by using a two-tailed paired t-test. A one-way ANOVA was used to compare c-Fos expression along the proximo-distal and the antero-posterior axes in mice from the massed and distributed trained groups, followed by Tukey HSD multiple comparison test when appropriate. ROIs frequency intervals were analyzed using a nonparametric analysis (Mann–Whitney U test).

Data availability

All data supporting described findings can be obtained from the corresponding author (A.M.) upon reasonable request.

Code availability

Codes for these experiments are available in the supplementary material.

Received: 1 March 2023; Accepted: 1 August 2023
Published online: 16 August 2023

References

1. Goodrick, C. L. Maze learning of mature-young and aged rats as a function of distribution of practice. *J. Exp. Psychol.* **98**, 344–349 (1973).
2. Domjan, M. Effects of the intertrial interval on taste-aversion learning in rats. *Physiol. Behav.* **25**, 117–125 (1980).
3. Shea, C. H., Lai, Q., Black, C. & Park, J.-H. Spacing practice sessions across days benefits the learning of motor skills. *Hum. Mov. Sci.* **19**, 737–760 (2000).
4. Giurfa, M. *et al.* Olfactory conditioning of the sting extension reflex in honeybees: Memory dependence on trial number, interstimulus interval, intertrial interval, and protein synthesis. *Learn. Mem.* **16**, 761–765 (2009).
5. Menzel, R., Manz, G., Menzel, R. & Greggers, U. Massed and spaced learning in honeybees: The role of CS, US, the intertrial interval, and the test interval. *Learn. Mem.* **8**, 198–208 (2001).
6. Hser, Y. & Wickens, T. D. The effects of the spacing of test trials and study trials in paired-association learning. *Educ. Psychol.* **9**, 99–120 (1989).
7. Cepeda, N. J., Pashler, H., Vul, E., Wixted, J. T. & Rohrer, D. Distributed practice in verbal recall tasks: A review and quantitative synthesis. *Psychol. Bull.* **132**, 354–380 (2006).
8. Sisti, H. M., Glass, A. L. & Shors, T. J. Neurogenesis and the spacing effect: Learning over time enhances memory and the survival of new neurons. *Learn. Mem.* **14**, 368–375 (2007).
9. Mastrorilli, V., Centofante, E., Antonelli, F., Rinaldi, A. & Mele, A. The neural substrate of spatial memory stabilization depends on the distribution of the training sessions. *Proc. Natl. Acad. Sci. U. S. A.* **119**, e2120717119 (2022).
10. Smolen, P., Zhang, Y. & Byrne, J. H. The right time to learn: Mechanisms and optimization of spaced learning. *Nat. Rev. Neurosci.* **17**, 77–88 (2016).
11. Toppino, T. C. & Gerbier, E. About practice. In *Psychology of Learning and Motivation* (ed. Ross, B. H.) 113–189 (Academic Press, San Diego, 2014). https://doi.org/10.1016/B978-0-12-800090-8.00004-4.
12. Naqib, F., Sossin, W. S. & Farah, C. A. Molecular determinants of the spacing effect. *Neural Plast.* **2012**, 581291 (2012).
13. Pagani, M. R., Oishi, K., Gelb, B. D. & Zhong, Y. The phosphatase SHP2 regulates the spacing effect for long-term memory induction. *Cell* **139**, 186–198 (2009).
14. Philips, G. T., Ye, X., Kopec, A. M. & Carew, T. J. MAPK establishes a molecular context that defines effective training patterns for long-term memory formation. *J. Neurosci.* **33**, 7565–7573 (2013).
15. Bourtchuladze, R. *et al.* Deficient long-term memory in mice with a targeted mutation of the cAMP-responsive element-binding protein. *Cell* **79**, 59–68 (1994).
16. Josselyn, S. A. *et al.* Long-term memory is facilitated by cAMP response element-binding protein overexpression in the amygdala. *J. Neurosci.* **21**, 2404–2412 (2001).
17. Genoux, D. *et al.* Protein phosphatase 1 is a molecular constraint on learning and memory. *Nature* **418**, 970–975 (2002).
18. Seese, R. R., Wang, K., Yao, Y. Q., Lynch, G. S. & Gall, C. M. Spaced training rescues memory and ERK1/2 signaling in fragile X syndrome model mice. *Proc. Natl. Acad. Sci.* **111**, 16907–16912 (2014).
19. Masamizu, Y. *et al.* Two distinct layer-specific dynamics of cortical ensembles during learning of a motor task. *Nat. Neurosci.* **17**, 987–994 (2014).
20. DeNardo, L. A. *et al.* Temporal evolution of cortical ensembles promoting remote memory retrieval. *Nat. Neurosci.* **22**, 460–469 (2019).
21. Yiu, A. P. *et al.* Neurons are recruited to a memory trace based on relative neuronal excitability immediately before training. *Neuron* **83**, 722–735 (2014).
22. Chowdhury, A. & Caroni, P. Time units for learning involving maintenance of system-wide cFos expression in neuronal assemblies. *Nat. Commun.* **9**, 4122 (2018).
23. Badreddine, N. *et al.* Spatiotemporal reorganization of corticostriatal networks encodes motor skill learning. *Cell Rep.* **39**, 110623 (2022).
24. Matamales, M. *et al.* Local D2- to D1-neuron transmodulation updates goal-directed learning in the striatum. *Science* **367**, 549–555 (2020).
25. Morris, R. G., Garrud, P., Rawlins, J. N. & O'Keefe, J. Place navigation impaired in rats with hippocampal lesions. *Nature* **297**, 681–683 (1982).
26. Soltesz, I. & Losonczy, A. CA1 pyramidal cell diversity enabling parallel information processing in the hippocampus. *Nat. Neurosci.* **21**, 484–493 (2018).
27. Danielson, N. B. *et al.* Sublayer-specific coding dynamics during spatial navigation and learning in hippocampal area CA1. *Neuron* **91**, 1–14 (2016).
28. Henriksen, E. J. *et al.* Spatial representation along the proximodistal axis of CA1. *Neuron* **68**, 127–137 (2010).
29. Cembrowski, M. S. & Spruston, N. Heterogeneity within classical cell types is the rule: Lessons from hippocampal pyramidal neurons. *Nat. Rev. Neurosci.* **20**, 193–204 (2019).
30. Dandolo, L. C. & Schwabe, L. Time-dependent memory transformation along the hippocampal anterior–posterior axis. *Nat. Commun.* **9**, 1205 (2018).
31. Beer, Z. *et al.* The memory for time and space differentially engages the proximal and distal parts of the hippocampal subfields CA1 and CA3. *PLOS Biol.* **16**, e2006100 (2018).

32. Schoenfeld, R., Schiffelholz, T., Beyer, C., Leplow, B. & Foreman, N. Variations of the Morris water maze task to comparatively assess human and rodent place navigation. *Neurobiol. Learn. Mem.* **139**, 117–127 (2017).
33. Ruediger, S., Spirig, D., Donato, F. & Caroni, P. Goal-oriented searching mediated by ventral hippocampus early in trial-and-error learning. *Nat. Neurosci.* **15**, 1563–1571 (2012).
34. Bello-Medina, P. C., Sánchez-Carrasco, L., González-Ornelas, N. R., Jeffery, K. J. & Ramírez-Amaya, V. Differential effects of spaced vs. massed training in long-term object-identity and object-location recognition memory. *Behav. Brain Res.* **250**, 102–113 (2013).
35. Spreng, M., Rossier, J. & Schenk, F. Spaced training facilitates long-term retention of place navigation in adult but not in adolescent rats. *Behav. Brain Res.* **128**, 103–108 (2002).
36. Igarashi, K. M., Ito, H. T., Moser, E. I. & Moser, M.-B. Functional diversity along the transverse axis of hippocampal area CA1. *FEBS Lett.* **588**, 2470–2476 (2014).
37. Fanselow, M. S. & Dong, H.-W. Are the dorsal and ventral hippocampus functionally distinct structures?. *Neuron* **65**, 7–19 (2010).
38. Witter, M. P., Wouterlood, F. G., Naber, P. A. & van Haeften, T. Anatomical organization of the parahippocampal-hippocampal network. *Ann. N. Y. Acad. Sci.* **911**, 1–24 (2006).
39. van Groen, T., Miettinen, P. & Kadish, I. The entorhinal cortex of the mouse: Organization of the projection to the hippocampal formation. *Hippocampus* **13**, 133–149 (2003).
40. Mizuseki, K., Diba, K., Pastalkova, E. & Buzsáki, G. Hippocampal CA1 pyramidal cells form functionally distinct sublayers. *Nat. Neurosci.* **14**, 1174–1181 (2011).
41. Eichenbaum, H., Wiener, S., Shapiro, M. & Cohen, N. The organization of spatial coding in the hippocampus: A study of neural ensemble activity. *J. Neurosci.* **9**, 2764–2775 (1989).
42. Hampson, R. E., Simeral, J. D. & Deadwyler, S. A. Distribution of spatial and nonspatial information in dorsal hippocampus. *Nature* **402**, 610–614 (1999).
43. Deadwyler, S., Bunn, T. & Hampson, R. Hippocampal ensemble activity during spatial delayed-nonmatch-to-sample performance in rats. *J. Neurosci.* **16**, 354–372 (1996).
44. Redish, A. D. *et al.* Independence of firing correlates of anatomically proximate hippocampal pyramidal cells. *J. Neurosci.* **21**, RC134 (2001).
45. Nakamura, N. H. *et al.* Hippocampal cells encode places by forming small anatomical clusters. *Neuroscience* **166**, 994–1007 (2010).
46. Pavlides, C. *et al.* Hippocampal functional organization: A microstructure of the place cell network encoding space. *Neurobiol. Learn. Mem.* **161**, 122–134 (2019).
47. Bergstrom, H. C. *et al.* The structure of Pavlovian fear conditioning in the amygdala. *Brain Struct. Funct.* **218**, 1569–1589 (2013).
48. Bergstrom, H. C., McDonald, C. G. & Johnson, L. R. Pavlovian fear conditioning activates a common pattern of neurons in the lateral amygdala of individual brains. *PLoS ONE* **6**, e15698 (2011).
49. Jacques, A. *et al.* Functional neuronal topography: A statistical approach to micro mapping neuronal location. *Front. Neural Circuits* **12**, 84 (2018).
50. Chadwick, M. J., Hassabis, D., Weiskopf, N. & Maguire, E. A. Decoding individual episodic memory traces in the human hippocampus. *Curr. Biol.* **20**, 544–547 (2010).
51. Hassabis, D. *et al.* Decoding neuronal ensembles in the human hippocampus. *Curr. Biol.* **19**, 546–554 (2009).
52. Guzowski, J. F., Setlow, B., Wagner, E. K. & McGaugh, J. L. Experience-dependent gene expression in the rat hippocampus after spatial learning: A comparison of the immediate-early genes arc, c- fos, and zif268. *J. Neurosci.* **21**, 5089–5098 (2001).
53. Torromino, G. *et al.* Offline ventral subiculum-ventral striatum serial communication is required for spatial memory consolidation. *Nat. Commun.* **10**, 5721 (2019).
54. Franklin, B. J. & Paxinos, G. *The Mouse Brain in Stereotaxic Coordinates* (Academic Press, San Diego, 1997).
55. Amaral, D. G. & Witter, M. P. Hippocampal formation. In *The Rat Nervous System* (ed. Paxinos, G.) 443–493 (Academic Press, San Diego, 1995).

Acknowledgements

This research was supported by a NARSAD independent investigator grant from the Brain and Behavioral Research Foundation (to A.M.), the AARG-NTF-22-971925 grant from Alzheimer's Association (to A.R.), a HBP (to A.M. and A.R.), the European Union's Horizon 2020 Framework Programme for Research and Innovation under the Specific Grant Agreement numbers 945539 (Human Brain Project SGA3) (to EC, MM, and CAL) and by the Italian National Recovery and Resilience Plan (PNRR), M4C2, funded by the European Union - NextGenerationEU (Project IR0000011, CUP B51E22000150006, "EBRAINS-Italy) (to MM, and CAL).

Author contributions

All authors contributed to the study conception and design. Material preparation, data collection and analysis were performed by E.C., L.F., and C.A.L.. The first draft of the manuscript was written by E.C., A.R. and A.M. all authors commented on previous versions of the manuscript. All authors read and approved the final manuscript.

Competing interests

The authors declare no competing interests.

Additional information

Supplementary Information The online version contains supplementary material available at https://doi.org/10.1038/s41598-023-39882-0.

Correspondence and requests for materials should be addressed to A.M.

6.2 Gene Silencing of circRmst in Primary Cortical Neuron Cultures: Functional and Morphometric Analyses

6.2.1 Introduction

In the last decade, circular RNAs (circRNAs) have become a subject of growing interest. Thanks to advancements in molecular biology techniques and the development of new sequencing methodologies, these transcripts have been rediscovered as potential regulators of gene expression. Their expression levels, localization, and functions have been associated with various physiological and pathological phenotypes. Despite numerous studies, the potential functions of circRNAs remain to be fully understood and characterized. Several studies have detected the expression of circular RNAs in human biofluids and extracellular vesicles (Lasda and Parker 2016). Due to their high stability, they could be used as biomarkers for diagnosing conditions that currently require invasive procedures. Moreover, recent proposals from the scientific community suggest the use of circRNAs as therapeutic agents or targets (He et al. 2021). Therefore, studies on circular RNAs could have significant implications in the clinical field.

Our study has been focused on characterizing these molecules in neuronal differentiation.

The Rmst gene locus undergoes significant splicing events, resulting in various linear isoforms (long non-coding Rmst, lncRmst) and several circular isoforms (circRmst). Molecular characterization analyses allowed us to define the size (1.5 Kb) and structure of circRmst. Additionally, we identified a smaller variant, which we have named circRmst 0.8 Kb. Expression studies during neuronal differentiation and mouse brain development revealed a fine regulation of the expression of these molecules. Through bioinformatics analyses and biochemical assays, we were able to confirm the in vivo interaction of both circRmst isoforms

with the transcription factor Sox2. The Sox2 protein acts as a regulator of the pluripotent state of stem cells and is involved in activating the neurogenic differentiation program in neural progenitors. In pathological conditions, such as glioblastoma, Sox2 is highly expressed and used as a diagnostic marker. Considering that several studies attribute to circRNAs the ability to bind proteins and microRNAs, but knowledge of the functional significance of such interactions is still limited, we have begun studying the role of the circRmst/Sox2 complex during neu,.ronal differentiation.

We have been able to identify a cell line in which to conduct gene silencing experiments. Additionally, we observe a new cytoplasmic localization of Sox2 in primary cortical neuron cultures. These findings suggest that there may be a regulation of the Sox2 protein mediated by its interaction with circRmst in the cytoplasm of cortical neurons. For this reason, we aim to investigate this newly identified localization of Sox2 and characterize a new functional role in the cytoplasm. The proposed functional and morphometric studies will allow us to explore the biological significance of the decoy activity exerted by circRmst during neuronal differentiation. The results of this study could contribute to research in the biomedical field. Indeed, there are various proposals for using circular RNAs as therapeutic agents.

6.2.2 Aim of the study

The results obtained from previous research validated the in vivo interaction between circRmst and Sox2 in both mouse brain tissues and murine cortical neuronal cultures. Additionally, we confirmed the expression of the Sox2 protein

in cytoplasmic compartments of neuronal cultures. Therefore, We propose the following functional characterization experiments:

1. Gene Silencing of circRmst 1.5 Kb and circRmst 0.8 Kb in Cortical Neuronal Cultures (Knockdown Experiments, KD): The goal of this experiment is to evaluate the decoy function of circRmst in relation to Sox2 protein. This interaction could regulate Sox2 localization and/or turnover. By assessing the expression of Sox2 target genes, I will evaluate any deregulation in its transcriptional activity. Immunofluorescence experiments will allow me to study changes in the differentiation process, particularly by using glial and neuronal markers to analyze variations in the cellular composition of the culture. Neuron-specific markers will be used to investigate the differentiation status of cortical neurons. Morphometric parameters such as neurite length, thickness, diameter, and spine density will be analyzed to quantitatively study alterations in differentiation.

2. Co-localization Experiments of the circRmst/Sox2 Complex in Control and KD Conditions: Observing the interaction between circRmst and Sox2 would provide experimental evidence supporting the interaction observed through RIP. Additionally, we could evaluate the effectiveness of gene silencing of circRmst molecules and characterize the decoy role of circular transcripts on Sox2 activity. The proposed experiments are necessary functional studies to validate the molecular mechanism and support the hypothesis of the involvement of the circRmst/Sox2 complex in the neuronal differentiation process.

CircRNAs are covalently closed molecules generated by an alternative splicing mechanism known as back-splicing. Initially considered a byproduct of alternative

splicing, circRNAs are now recognized as key regulatory molecules in physiological processes. Several studies suggest that circRNAs can bind to and regulate the activity of proteins and microRNAs, possess codogenic capabilities, and modulate the immune response. They are evolutionarily conserved molecules, and despite being expressed at lower levels than linear coding transcripts, many circRNAs are highly enriched in the mammalian nervous system. During neurogenesis and synaptogenesis, circRNA expression levels vary significantly, suggesting their potential involvement in synapse formation and activity processes. Moreover, altered circRNA expression profiles have been detected in various nervous system disorders.

The Rmst gene locus is of particular interest as it is highly regulated during neuronal differentiation. Several circular RNA molecules are produced during this process, but their function is still unknown. In contrast, the linear isoform of the Rmst locus, lncRmst, regulates the neurogenesis process in neural progenitors. This molecule acts as a molecular scaffold in recruiting the transcription factor Sox2 to neurogenic gene promoters through direct interaction.

Initial structural and sequence studies allowed us to identify two circular RNA transcripts from the murine Rmst locus. The first isoform, 1.5 Kb in length, already characterized in other studies, originates from two alternative splicing events, a back-splicing and a trans-splicing, involving two linear transcripts. The second, identified for the first time, is composed of a single back-splicing event and is 0.8 Kb in length. Expression studies of these two isoforms and lncRmst in cortical neuron cultures and mouse neural tissues at various developmental stages revealed strong regulation of these molecules during neuronal differentiation and pre- and post-natal development. Furthermore, subcellular fractionation experiments in cortical cells showed an enrichment of these molecules' expression

in the cytoplasm. Various functions have been suggested for circular RNAs in the cytoplasm. We, therefore, sought potential interactors.

Literature analyses, bioinformatic studies, and structural analysis allowed us to identify Sox2 binding sites in the exons that compose both circRmst 1.5 Kb and circRmst 0.8 Kb transcripts. Initially, we validated the predicted interaction in vivo through RNA immunoprecipitation (RIP) experiments conducted on cytoplasmic lysates from mouse brains, which confirmed the binding of these isoforms to the Sox2 protein. Since the interaction was observed in cytoplasmic fractions, we investigated the novel localization of Sox2 in compartments outside the nucleus. Immunofluorescence experiments in primary cortical neuron cultures identified Sox2 localization in neuronal processes for the first time, as well as an increase in the cytoplasmic expression of the protein over time.

We hypothesize a role for circRmst 1.5 Kb and circRmst 0.8 Kb in regulating Sox2 molecules in the cytoplasm. Considering that nuclear Sox2 levels must be finely regulated during neuronal differentiation, circular RNAs may act as decoys and modulate Sox2 localization and/or function in the cytoplasm. We, therefore, aim to study the biological significance of the observed interaction in the cytoplasm and the localization of Sox2 in neuronal processes. We will perform gene silencing experiments to evaluate the functional role of the circRmst/Sox2 interaction in neuronal differentiation.

Preliminary data have allowed us to identify a murine cell line to test the effectiveness of siRNA molecules constructed on the back-splicing junction to uniquely silence circRmst 1.5 Kb and circRmst 0.8 Kb isoforms. We will also silence the linear isoform as a control to ensure no off-target effects. After determining the appropriate dose and type of siRNA to use, we will transfect the interfering siRNA molecules into primary cortical neuron cultures. Transfection will

occur in the early days of neuronal differentiation, and various analyses will be conducted to evaluate changes in the culture's differentiation capacity. Subsequently, we will perform immunofluorescence experiments for neuronal and glial markers. These analyses will allow us to study variations in the percentage of cell types that compose the culture.

We hypothesize that an imbalance in Sox2 levels due to the loss of circRmst-mediated regulation may affect the transcriptional activity of the protein in the nucleus and activate glial differentiation genes. We will evaluate Sox2 protein expression levels and localization through Western blot and immunofluorescence analyses. These experiments will allow us to determine whether the circRmst/Sox2 interaction influences protein stability and localization. Morphometric analyses will be useful for assessing changes in the culture's differentiation capacity. We will use markers for neuronal extensions, such as axons and dendrites, and measure length, thickness, and density using targeted quantitative analysis programs. Finally, we aim to conduct co-localization experiments of the circRmst/Sox2 complex to validate RIP experiments and assess the effects of KD.

6.2.3 Materials and methods

Primary cultures of cortical neurons from CD1 mouse embryos harvested at embryonic day 17/18 (E17, E18).
Neuronal tissues from CD1 mice (hippocampus, cerebellum, cortex) harvested at various embryonic stages (E14, E17, E18), at different postnatal days (P0, P10, P30), and in adulthood (P45, P90).
Whole brains from CD1 mice harvested on embryonic days E17, E18, and postnatal day 0.

6.2.4 Results

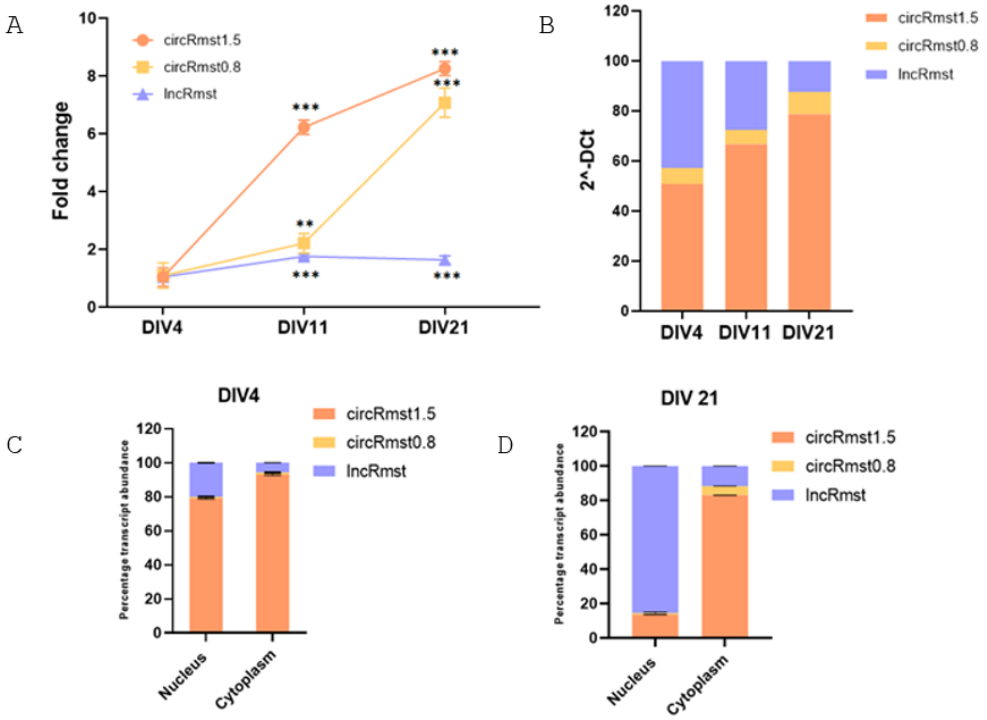

Figure 27 Expression studies of circRmst 1.5 and circRmst 0.8 in neuronal differentiation circRmst 1.5 and circRmst 0.8 levels increase progressively during neuronal differentiation and accumulate in mature neurons, with circRmst 1.5 the most abundant in DIV21 neurons. circRmst 1.5 and circRmst 0.8 are enriched in the cytoplasm, with an enhanced cytoplasmic localization at DIV21. A. RT-qPCR analysis was performed on whole-cell lysates of CNs at DIV4, DIV11 and DIV21. Relative expressions of circular and linear isoforms are reported. Fold Change = 2^-DDCt; GAPDH as endogenous control; Unpaired two-tailed t-test *P ≤ 0,05; **P ≤ 0,01; ***P ≤ 0,001; (B) 2^-DCt for relative expression of each isoform. C -D The relative abundance of circRmst 1.5, circRmst 0.8 and lncRmst in the cytoplasmic and nuclear fractions are reported. RT-qPCR analysis was performed on CNs at DIV4 (C) and DIV 21(D). n = 4 cultures (DIV4), n = 2 cultures (DIV11 and DIV21), Data are shown as means ± SD.

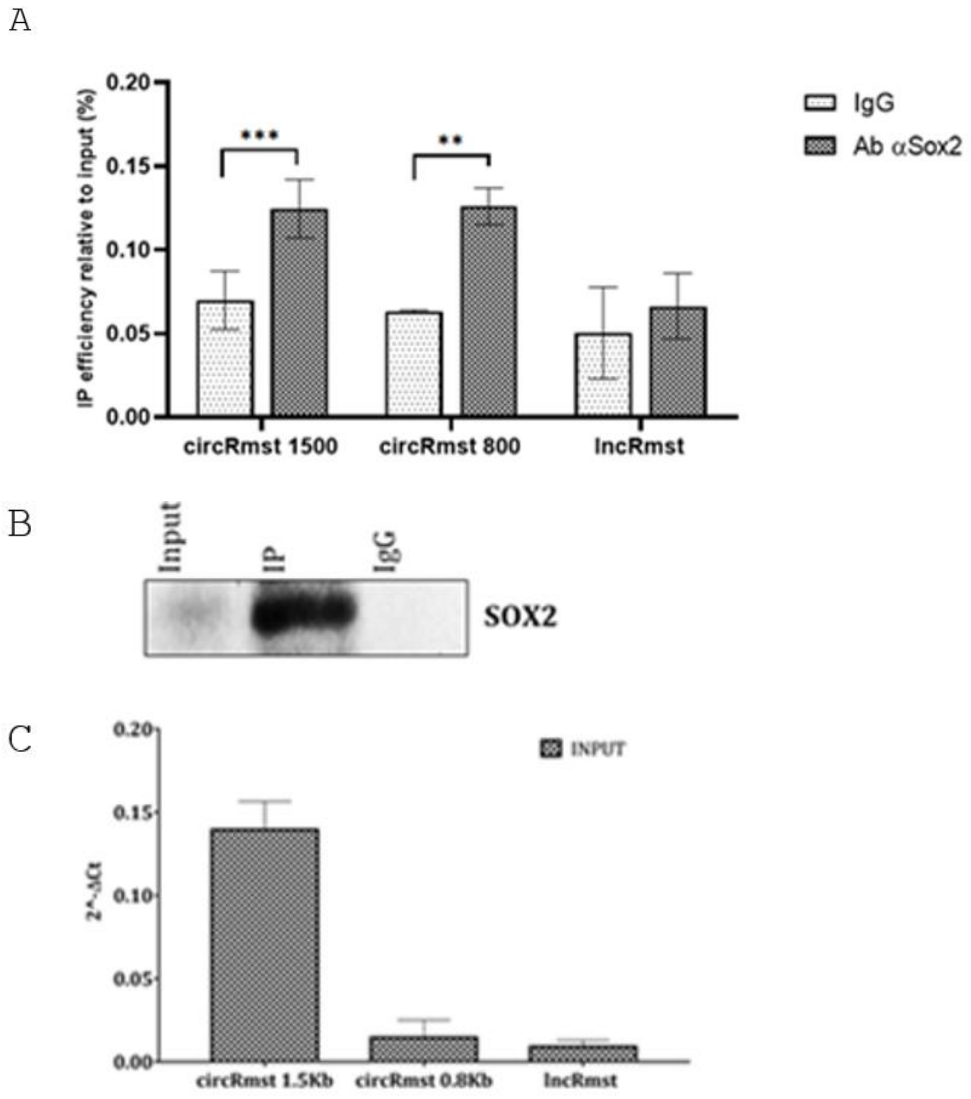

Figure 28 circRmst 1.5 and circRmst 0.8 interacts with cytoplasmic SOX2. RIP analysis was performed in cytoplasmic fractions from P0 mouse whole brain A) RNA levels are analyzed by RT-qPCR and data are expressed as relative enrichment of Rmst isoform levels between SOX2 IP and Input. n = 3 P0 mouse whole brain lysate. Data are shown as means ± SD; Unpaired two-tailed t-test *P ≤ 0,05; **P ≤ 0,01; ***P ≤ 0,001; B)WB analysis of cytoplasmic SOX2 expression in Input, IP and IgG samples (brain RIP). C) The abundances of circular and linear transcripts in the Input fractions of brain RIP experiments are reported. Data are expressed as 2^-DCt and shown as means ± SD; transcript levels were normalized to GAPDH.

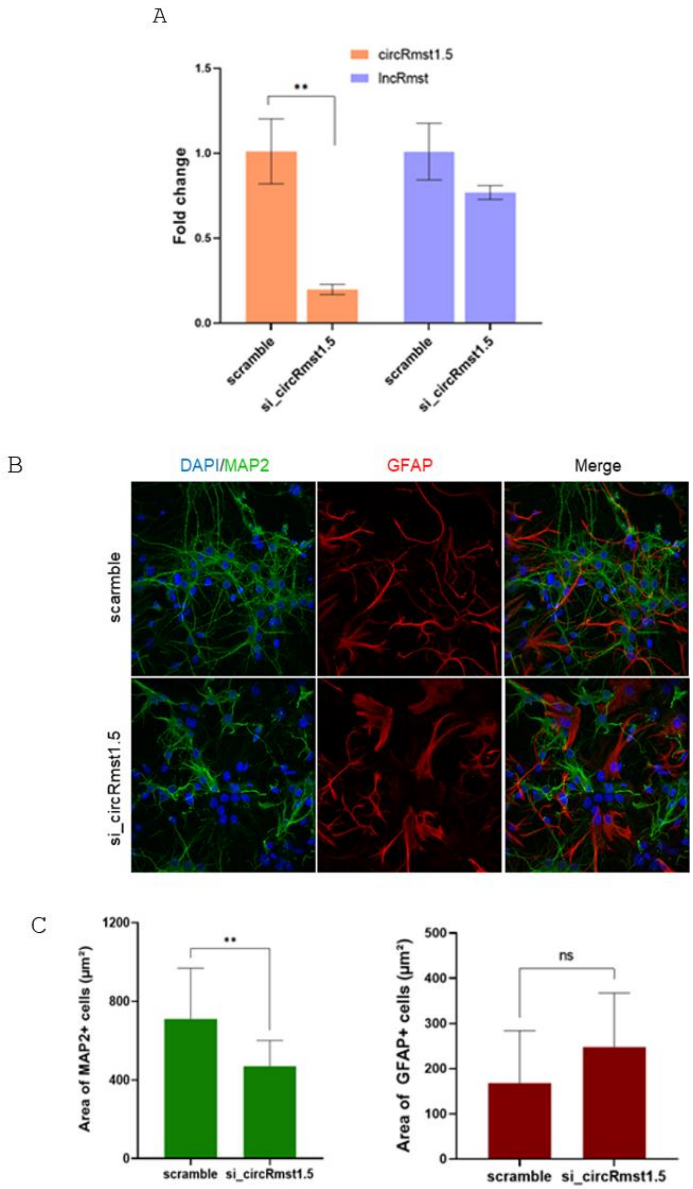

Figure 29 Knock-Down of circRmst 1.5 on primary cortical neurons. The KD of circRmst 1.5 in primary CNs affect neuronal morphology and network A) BSJ -directed siRNAs specifically reduce circRmst 1.5 levels. Analysis by RT-qPCR in DIV7 CNs, 72 hrs from siRNA transfection. n = 2 cultures (DIV4), Data are shown as means ± SD; Unpaired two-tailed t-test *P ≤ 0,05; **P ≤ 0,01; ***P ≤ 0,001 B) IF staining for MAP2 (green) or GFAP (red), of DIV7 CNs transfected with scramble siRNAs (control) or si_circRmst1.5 (circRmst1.5 KD). C) Quantitative analysis on MAP2+ and GFAP+ cells indicates a reduced neuronal network. Data are expressed in um^2 and normalized on cell number

detected in each field (n=15). Two-way ANOVA followed by Tukey's multiple comparisons test, ***p < 0.001, **p < 0.01, *p < 0.05; data are plotted as mean ± SD).

6.3 Effect of different stress paradigms on innate avoidance behavior in CD1 male mice

6.3.1 Introduction

Organisms encounter a range of environmental conditions that can disrupt their internal balance. To effectively address these internal and external "stressors," organisms must activate a coordinated physiological and psychological response, choosing the most suitable behavioral strategies. This reaction is referred to as the stress response and involves a complex and highly conserved network of systems. Stress is inherently subjective, and the types of stressful situations an organism faces can vary widely. Stressors may be acute and intense (e.g., predation), chronic and severe (e.g., drought), or mild (e.g., brief exposure to light), with each type requiring a distinct adaptive response. On a systemic level, the physiological stress response includes: 1) an immediate reaction mediated by the autonomic nervous system (ANS) and the hypothalamic-pituitary-adrenal (HPA) axis, and 2) a delayed response essential for recovery and adaptation (De Kloet et al. 2005; 2008). When faced with stressors, the initial response is triggered by the ANS, activated by sensory inputs, brainstem pathways conveying these stimuli, and limbic system pathways responding to psychological stressors. The sympathetic nervous system, through activation of the splanchnic nerve, stimulates adrenomedullary cells to release catecholamines (epinephrine and norepinephrine). These hormones bind to adrenergic receptors, causing increases in respiration, blood pressure, and heart rate, as well as activation of catabolic pathways. This reaction, known as the "fight or flight response," is generally short-lived due to reflex parasympathetic activation (Berger et al. 2019). Additionally, external and internal sensory information is processed by the brain and converted into endocrine responses within the paraventricular nucleus of the hypothalamus (PVN). Neurons in the PVN produce and release corticotropin-

releasing hormone (CRH), which then prompts the pituitary gland to release adrenocorticotropic hormone (ACTH) into the bloodstream. ACTH acts on the adrenal glands, leading to the release of glucocorticoids (GCs; corticosterone in rodents and cortisol in humans) from the adrenal cortices. GCs affect various body tissues to either mobilize or store energy to address the stress challenge (De Kloet et al. 2004). The ability to end the stress response relies on glucocorticoid negative feedback targeting key neural regions such as the PVN, anterior pituitary gland, medial prefrontal cortex (mPFC), amygdala, and hippocampus. There are two types of GCs receptors: (1) the high-affinity mineralocorticoid receptor (MR), found mainly in the hippocampus, and (2) the low-affinity glucocorticoid receptor (GR), which is widely distributed across the brain, especially in the hippocampus, amygdala, and prefrontal cortex—regions essential for negative feedback mechanisms regulating HPA axis activation (Reul et al. 1985; Roozendaal et al. 2002). In the absence of stressors and when the body is at rest, MRs are typically occupied, while GC levels are too low to bind to GRs. However, elevated GC levels during stress can activate GRs as well (De Kloet et al. 2004). MRs and GRs exert both (1) slow, genomic effects and (2) fast, non-genomic effects. Genomic actions involve binding to GC receptors, which act as transcription factors to induce long-term changes in gene expression (De Kloet et al. 1998). Non-genomic effects occur within minutes of glucocorticoid release and likely involve actions at the cell membrane. As transcriptional regulators, the initial effects on adaptive behavior involve altered gene expression related to enzymes and receptors for biogenic amines and neuropeptides (Sabban et al. 2001), growth factors (Schaaf et al. 1997; Hansson et al. 2000), and cell-adhesion factors (Sandi, 2004). Corticosteroids, particularly through GRs, have minimal impact on cellular properties under resting conditions. However, when cells deviate from their resting state, the effects become apparent, and GR activation can reverse noradrenaline-induced excitation (Joëls et al. 1989). Non-genomic signaling provides a rapid negative feedback mechanism for the hypothalamic-pituitary-adrenal axis. The

production and release of CRH by PVN neurons are subject to both fast and delayed negative control by corticosterone. The rapid effects of corticosteroid hormones in the hippocampus exert a swift negative control over CRH and ACTH release (Dallman 2005). This effect is temporary; once corticosteroid levels stabilize, the negative influence dissipates, only to return later with the onset of genomic actions. During the initial phase of the central stress response, increasing corticosterone levels enhance hippocampal excitability and amplify the effects of other stress hormones. These permissive effects of corticosterone may aid in the quick encoding of stress-related information, appraisal processes, and selection of behavioral responses to stressors (McGaugh et al. 2002; Oitzl et al. 1992; Oitzl et al. 1994). Overall, MR activity helps maintain cellular communication, excitability, and network stability. In contrast, GR activation, in addition to MR, leads to a delayed suppression or normalization of network activity, contributing to the regulation of GC levels within physiological ranges (Erdmann et al. 2008; Kretz et al. 1999), through both genomic and non-genomic mechanisms. For instance, basal corticosteroid levels facilitate the induction of long-term potentiation (LTP) in the hippocampus (Diamond et al. 1992). In contrast, elevated corticosterone levels, stress, or exposure to new environments can impair LTP and promote long-term depression (LTD) (Kim et al. 2002; Pavlides et al. 1996; Xu et al. 1998).

Although the physiological stress response is highly conserved, scientific literature reveals considerable variability in stress responses depending on strain in laboratory mouse models (Cappucci et al. 2018).

6.3.2 Aim of the study

Although the physiological stress response is evolutionarily conserved, there is significant variability in behavioral responses to stressful experiences in mice, which can depend on both the type of stress and the strain of the animal (Cappucci et al. 2018). To address this, we aimed to evaluate the effect of different stress paradigms in CD1 male mice.

While much of the scientific literature is based on data from C57 mice, the literature about the behavioral stress response in CD1 mice shows considerable contradictions, and it remains unclear which coping strategies these animals employ following a stressful experience (Almatroudi et al. 2018; Ota et al. 2015; Scheich et al. 2017).

To this aim, male CD1 mice were subjected to various restraint stress paradigm and we assessed the impact of these stressors on their innate avoidance behavior by testing the animals in the EPM assay.

6.3.3 Materials and methods

Animals: Male outbred CD1 mice, 8-15 weeks old, weighing 40-60g were supplied from a colony maintained at Sapienza University of Rome, obtained from Charles River breeding pairs. Mice were housed in groups of 2-4 mice per cage (26.8 x 21.5 x 14.1 cm) or 5-8 mice per cage (42.5 x 26.6 x 18.5 cm) allocated in the animal facility of the Department of Biology and Biotechnology "Charles Darwin", Sapienza University of Rome, Italy. Male Wistar rats of 3-9 months supplied from Charles River, housed in couple in standard rat cages (42.5 x 26.6 x 18.5 cm), were used for the predator exposure procedure. All animals were maintained at a constant temperature (21±2°C) and umidity (45-60%), on a 12h light/dark cycle

(lights on at 07:30) with *ad libitum* access to food and water. All behavioral procedures were performed during the light period (9:00-18:00). Procedures were conducted under the authorization N. 796/2017-PR and N.967/2018-PR from the Italian Ministry of Health, according to Italian (DL.116/92) and European laws and regulations on the use of animals in research, and NIH guidelines on animal care.

Stress paradigms: The animals were randomly assigned to different experimental groups. The stress protocol involves a period of restraint, in which the animal is placed inside a black, ventilated plexiglass tube (3 cm in diameter; 15 cm in length) that prevents the animal from moving freely. All groups were weighed and gently handled for 3 minutes a day during the 4-5 days preceding the start of the stress protocol. Before the start of each session, the animals were allowed to acclimate in the room for about 1 hour, then they were briefly handled and weighed. The chronic stress group was subjected to restraint for two hours per day for 10 consecutive days. The acute stress group was subjected to restraint stress for 2 hours or 30 minutes.

Prior to the initiation of the predator exposure paradigm, animals were handled by an experienced experimenter for either 3 minutes per day over 5 days, or for 4 minutes twice daily over 2 days. The testing apparatus consisted of a transparent box (42.5 × 26.6 × 18.5 cm) that housed a protective cylinder (13 cm in diameter; 13 cm in length), featuring a 3 cm opening on one end and metal bars spaced 0.8 cm apart on the curved surface. The procedure included 4 habituation sessions, which were conducted either once daily over 4 consecutive days) or twice daily over 2 days, followed by an exposure session on the fifth day. Before each session, mice were brought into the experimental room and given 30 minutes to acclimate. During each habituation session, mice were allowed to explore the apparatus freely for 10 minutes, with the protective cylinder positioned so that the opening faced upwards, facilitating unrestricted exploration of the stress environment. The

chamber was lined with fresh animal bedding. Upon completion of the habituation phase, on the following day, mice were exposed to a rat for a single 10-minute session. During this exposure session, the stress chamber was lined with a mix of 50% clean bedding and 50% rat litter. Mice were placed inside the protective cylinder, which was then inverted to close the opening, and a rat was swiftly introduced into the chamber. The rat was free to move around the cylinder and interact with the mouse. The chamber was secured with a metal grid lid, and the cylinder was fastened to prevent displacement by the predator. After 10 minutes, the predator was removed and returned to its home cage to rest for at least 15 minutes before the next exposure. The exposed mice were then placed back in their home cage, the bedding in the apparatus was changed, and the equipment was cleaned with 70% ethanol. Control mice underwent the same procedure without the presence of the predator and always had clean bedding. Additionally, controls were always tested before stressed mice to ensure they were not exposed to any olfactory cues left by the rat in the testing room.

The rats also underwent a habituation process before the testing phase. Initially, they were acclimated to the experimental room for 15 minutes each day over two days. They were then food-restricted for two days, receiving only 20g of standard rodent food per day. To prevent the predator from becoming accustomed to the mice, each rat was subjected to a maximum of three exposures per day per week.

All stress sessions were conducted between 10 AM and 4 PM. The animals in the control group were briefly handled and returned to their cages before the start of the restraint session for the acute, chronic and predator exposure stress groups.

Elevated plus maze: The apparatus was made of black Plexiglas and consisted of two open and two closed arms connected by a central square platform (5 x 5 cm); each arm was 5 cm wide and 35 cm long and the closed arms were surrounded

by 15 cm high black walls. The maze was positioned 50 cm from the ground and placed in a mildly lit room (100lux), with white curtains all around. Each mouse was placed on the central platform facing the open arm and allowed to freely explore the apparatus. Between consecutive tests, the apparatus was cleaned with 70% ethanol solution. The time spent in open and closed arms and total distance were later manually scored from the recorded videotapes using ANY-maze (ANY-maze, Stoelting Co., USA). The mouse was considered inside a specific compartment when all four paws were inside the compartment. Each mouse was isolated for 30 minutes, then it was placed on the central platform facing the open arm and allowed to freely explore for 5 minutes. Elevated plus maze was performed 24h later the end of chronic and predator exposure stress and 30 minutes later the end of acute restraint.

6.3.4 Results

To evaluate the effect of different stress paradigms on innate avoidance behavior, different groups of CD1 male mice were subjected to acute or chronic restraint stress or predator exposure stress protocols. The chronic restraint stress paradigm does not affect time spent in open arms and distance travelled in elevated plus maze (Fig 30 A-B; OA time t=0.5674, df=22, p=0.576; Distance, t=1.857, df=22, p=0.076, unpaired two-tailed t-test). Similarly, 2h or 30min of acute restraint stress do not affect time spent in open arms and distance travelled in elevated plus maze (Fig 30 C-F; OA time following 2h of acute restraint stress, t=0.4931, df=19, p=0.627; Distance, t=0.7753, df=19, p=0.447; OA time following 30min of acute restraint stress, t=0.2881, df=16, p=0.776; Distance, t=0.1757, df=16, p=0.862, unpaired two-tailed t-test). Furthermore, predator exposure stress paradigm do not affect time spent in open arms and distance travelled in

EPM (Fig 30 G-H; OA time, t=0.4761, df=10 p=0.644; Distance, t=1.735, df=10, p=0.113, unpaired two-tailed t-test).

Together, these data suggest that Chronic and acute restraint and predator exposure stress paradigms are not able to affect innate avoidance behavior tested in EPM in adult CD1 male mice. Anyway, it will be appropriate to increase the number of experimental subjects to compensate for the high variability present in the outbred strain.

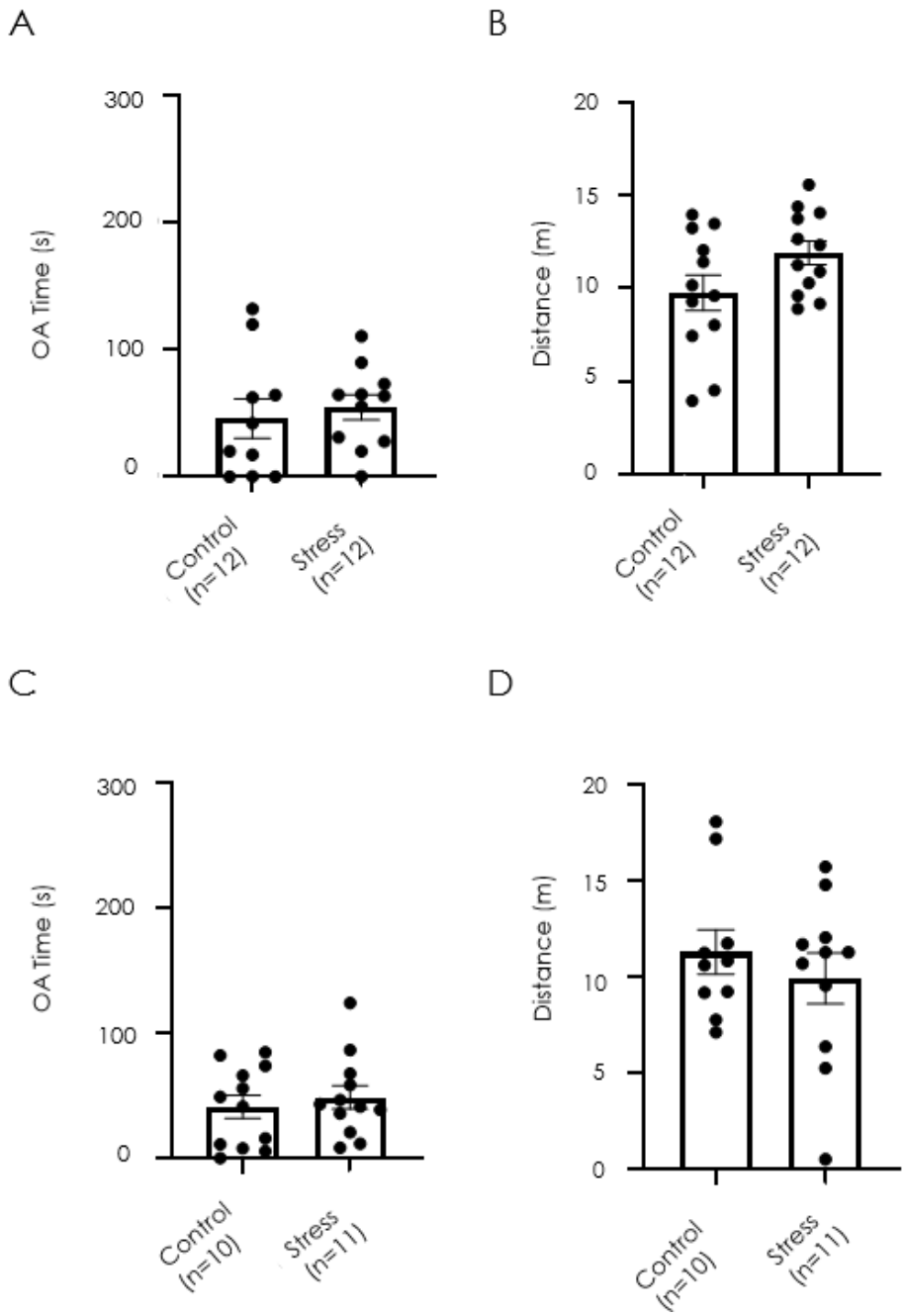
A
B
C
D
OA Time (s)
Distance (m)
300
200
100
0
20
15
10
5
Control (n=12)
Stress (n=12)
Control (n=10)
Stress (n=11)

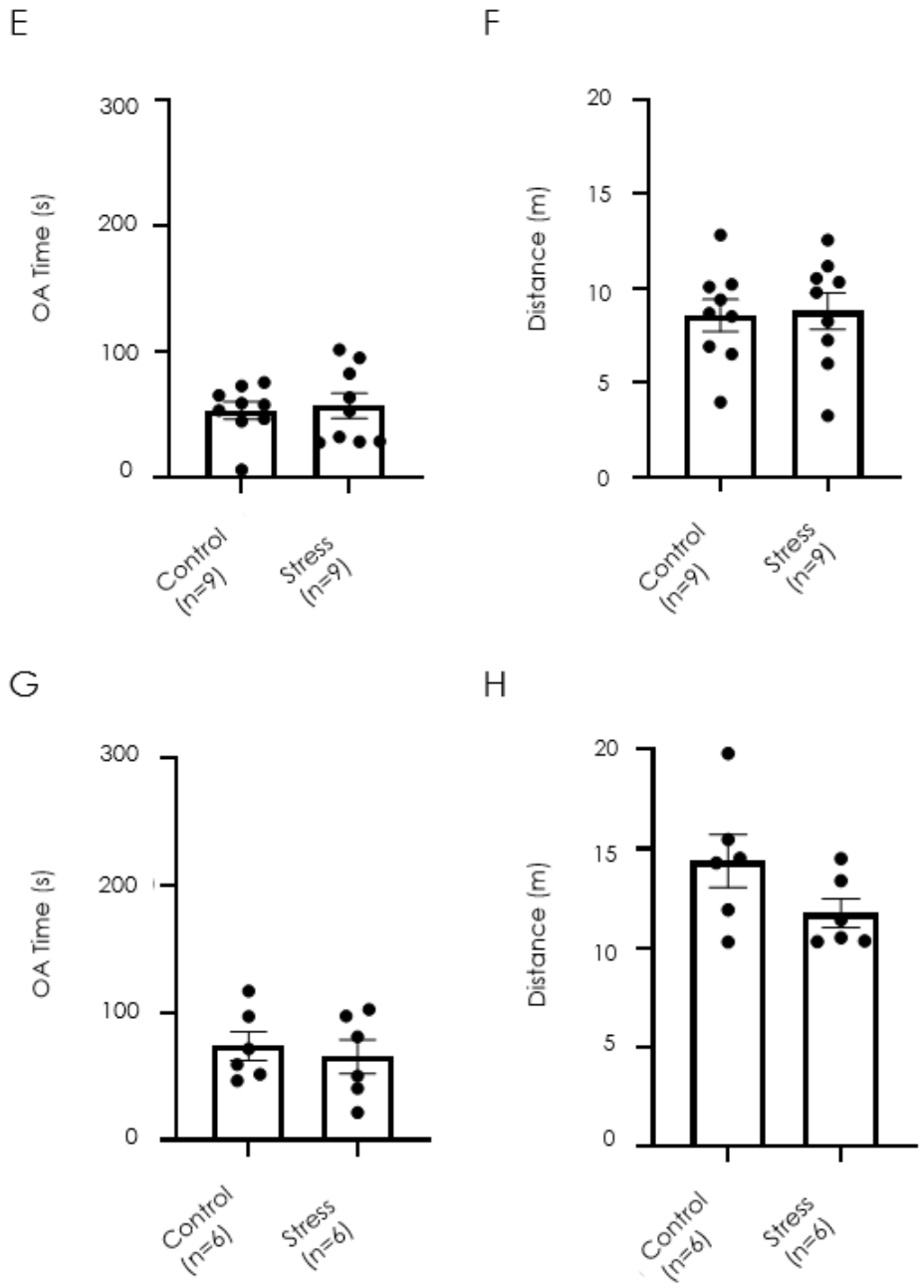

Figure 30 Different stress paradigms do not affect anxiety-like behaviour and distance travelled in EPM in adult CD1 male mice. **(A-B)** Chronic restraint stress protocol, **(C-D)** 2h of the acute restraint stress protocol, **(E-F)** 30 minutes of the acute restraint stress protocol and **(G-H)** Predator exposure stress protocol. Bars represent mean ± SEM, while the dots indicate the values for each individual animal.

6.3.5 Discussion

In this experiment, the effect of different stress protocols on anxiety-like behavior in male outbred CD1 mice was evaluated. Specifically, the chronic stress group was subjected to restraint stress for two hours per day for 10 consecutive days and tested in the EPM 24 hours later, while the acute stress group was subjected to restraint stress for either 2 hours or 30 minutes and tested in the EPM after 30 minutes. As for the group subjected to predator exposure stress, it was tested in the EPM 24 hours after the end of the stress exposure. The absence of an effect of stress on CD1 outbred male mice is a topic that has attracted attention in neuroscientific and behavioral research. CD1 mice are an outbred genetic line, meaning they are not selected for specific genetic traits, which makes them genetically more variable compared to inbred lines. This genetic variability could be one reason why the effects of stress on this population are not uniform or may not be observed at all. Scientific literature has documented well-defined effects of chronic or acute stress on various aspects of behavior and physiology in rodents, including alterations in anxiety, depression, memory, and neurogenesis (de Kloet et al., 2005; Nestler et al., 2010). However, studies on CD1 mice have shown contrasting results, with some reporting no significant effect of chronic stress on anxiety or depression-related behaviors, while others observe effects in specific subgroups (Almatroudi et al. 2018; Ota et al. 2015; Scheich et al. 2017). Studies on inbred mice such as C57BL/6 have shown that chronic stress can lead to increased anxiety-like behavior (de Kloet et al., 2005; Nestler et al., 2010). However, studies on CD1 mice do not always replicate these results, suggesting that genetic and environmental heterogeneity may play a critical role in modulating stress effects. This phenomenon has also been observed in studies using stress paradigms such as "chronic social defeat stress" or "restraint stress," where behavioral effects can vary significantly among individuals within the same outbred population (Almatroudi et al. 2018; Ota et al. 2015; Scheich et al. 2017). In this

study, we have indeed observed that protocols of acute or chronic restraint stress, as well as predator exposure stress, do not influence anxiety behavior in adult CD1 male mice tested in the elevated plus maze. The absence of an effect of stress in CD1 outbred mice may be attributed to their high genetic variability, which can lead to different stress responses. For this reason, it will be appropriate to increase the number of experimental subjects to compensate for the high variability present in the outbred strain. This suggests that outbred animal models, while useful for studying the diversity of physiological and behavioral responses, may present challenges in detecting specific effects compared to more homogeneous inbred models.

7 References

Adhikari, Avishek, Mihir A. Topiwala, and Joshua A. Gordon. 2010. 'Synchronized Activity between the Ventral Hippocampus and the Medial Prefrontal Cortex during Anxiety'. *Neuron* 65 (2): 257–69. https://doi.org/10.1016/j.neuron.2009.12.002.

Adhikari, Mihir A. Topiwala and Joshua A. Gordon. 2011. 'Single Units in the Medial Prefrontal Cortex with Anxiety-Related Firing Patterns Are Preferentially Influenced by Ventral Hippocampal Activity'. *Neuron* 71 (5): 898–910. https://doi.org/10.1016/j.neuron.2011.07.027.

Albert, Paul R., Faranak Vahid-Ansari, and Christine Luckhart. 2014. 'Serotonin-Prefrontal Cortical Circuitry in Anxiety and Depression Phenotypes: Pivotal Role of Pre- and Post-Synaptic 5-HT1A Receptor Expression'. *Frontiers in Behavioral Neuroscience* 8 (June). https://doi.org/10.3389/fnbeh.2014.00199.

Alegre-Cortés, Javier, María Sáez, Roberto Montanari, and Ramon Reig. 2021. 'Medium Spiny Neurons Activity Reveals the Discrete Segregation of Mouse Dorsal Striatum'. *eLife* 10 (February):e60580. https://doi.org/10.7554/eLife.60580.

Almada, Rafael C., Andreas J. Genewsky, Daniel E. Heinz, Paul M. Kaplick, Norberto C. Coimbra, and Carsten T. Wotjak. 2018. 'Stimulation of the Nigrotectal Pathway at the Level of the Superior Colliculus Reduces Threat Recognition and Causes a Shift From Avoidance to Approach Behavior'. *Frontiers in Neural Circuits* 12 (May). https://doi.org/10.3389/fncir.2018.00036.

Almatroudi, Abdulrahman, Mehrnoosh Ostovar, Christopher P Bailey, Stephen M Husbands, and Sarah J Bailey. 2018. 'Antidepressant-like Effects of BU10119, a Novel Buprenorphine Analogue with Mixed κ/μ Receptor Antagonist Properties, in Mice'. *British Journal of Pharmacology* 175 (14): 2869–80. https://doi.org/10.1111/bph.14060.

Anacker, Christoph, Victor M. Luna, Gregory S. Stevens, Amira Millette, Ryan Shores, Jessica C. Jimenez, Briana Chen, and René Hen. 2018. 'Hippocampal Neurogenesis Confers Stress Resilience by Inhibiting the Ventral Dentate Gyrus'. *Nature* 559 (7712): 98–102. https://doi.org/10.1038/s41586-018-0262-4.

Armbruster, Blaine N., Xiang Li, Mark H. Pausch, Stefan Herlitze, and Bryan L. Roth. 2007. 'Evolving the Lock to Fit the Key to Create a Family of G Protein-Coupled Receptors Potently Activated by an Inert Ligand'. *Proceedings of the National Academy of Sciences of the United States of America* 104 (12): 5163–68. https://doi.org/10.1073/pnas.0700293104.

Arnaudova, Inna, Merel Kindt, Michael Fanselow, and Tom Beckers. 2017. 'Pathways towards the Proliferation of Avoidance in Anxiety and Implications for Treatment'. *Behaviour Research and Therapy*, Avoidance and Decision Making: Implications for the Understanding and Treatment of Anxiety, 96 (September):3–13. https://doi.org/10.1016/j.brat.2017.04.004.

Aupperle, Robin L., and Martin P. Paulus. 2010. 'Neural Systems Underlying Approach and Avoidance in Anxiety Disorders'. *Dialogues in Clinical Neuroscience* 12 (4): 517–31. https://doi.org/10.31887/DCNS.2010.12.4/raupperle.

Ball, Tali M., and Lisa A. Gunaydin. 2022. 'Measuring Maladaptive Avoidance: From Animal Models to Clinical Anxiety'. *Neuropsychopharmacology: Official Publication of the American College of Neuropsychopharmacology* 47 (5): 978–86. https://doi.org/10.1038/s41386-021-01263-4.

Balleine, Bernard W., Mauricio R. Delgado, and Okihide Hikosaka. 2007. 'The Role of the Dorsal Striatum in Reward and Decision-Making'. *Journal of Neuroscience* 27 (31): 8161–65. https://doi.org/10.1523/JNEUROSCI.1554-07.2007.

Bandelow, Borwin, and Sophie Michaelis. 2015. 'Epidemiology of Anxiety Disorders in the 21st Century'. *Dialogues in Clinical Neuroscience* 17 (3): 327–35. https://doi.org/10.31887/DCNS.2015.17.3/bbandelow.

Bariselli, Sebastiano, Christelle Glangetas, Stamatina Tzanoulinou, and Camilla Bellone. 2016. 'Ventral Tegmental Area Subcircuits Process Rewarding and Aversive Experiences'. *Journal of Neurochemistry* 139 (6): 1071–80. https://doi.org/10.1111/jnc.13779.

Hormigo, Sebastian, German Vega-Flores, and Manuel A. Castro-Alamancos. 2016. 'Basal Ganglia Output Controls Active Avoidance Behavior'. *Journal of Neuroscience* 36 (40): 10274–84. https://doi.org/10.1523/JNEUROSCI.1842-16.2016.

Bello-Medina, Paola C., Gonzalo Flores, Gina L. Quirarte, James L. McGaugh, and Roberto A. Prado Alcalá. 2016. 'Mushroom Spine Dynamics in Medium Spiny Neurons of Dorsal Striatum Associated with Memory of Moderate and Intense Training'. *Proceedings of the National Academy of Sciences* 113 (42): E6516–25. https://doi.org/10.1073/pnas.1613680113.

Berger, Ilona, Martin Werdermann, Stefan R. Bornstein, and Charlotte Steenblock. 2019. 'The Adrenal Gland in Stress – Adaptation on a Cellular Level'. *The Journal of Steroid Biochemistry and Molecular Biology* 190 (June):198–206. https://doi.org/10.1016/j.jsbmb.2019.04.006.

Blanchard, D. Caroline, and Robert J. Blanchard. 2008. 'Chapter 2.4 Defensive Behaviors, Fear, and Anxiety'. In *Handbook of Behavioral Neuroscience*, edited by Robert J. Blanchard, D. Caroline Blanchard, Guy Griebel, and

David Nutt, 17:63–79. Handbook of Anxiety and Fear. Elsevier. https://doi.org/10.1016/S1569-7339(07)00005-7.

Boehme, Stephanie, Viktoria Ritter, Susan Tefikow, Ulrich Stangier, Bernhard Strauss, Wolfgang H. R. Miltner, and Thomas Straube. 2014. 'Brain Activation during Anticipatory Anxiety in Social Anxiety Disorder'. *Social Cognitive and Affective Neuroscience* 9 (9): 1413–18. https://doi.org/10.1093/scan/nst129.

Bortolanza, Mariza, Evellyn C. Wietzikoski, Suelen L. Boschen, Patricia A. Dombrowski, Mary Latimer, Duncan A. A. MacLaren, Philip Winn, and Claudio Da Cunha. 2010. 'Functional Disconnection of the Substantia Nigra Pars Compacta from the Pedunculopontine Nucleus Impairs Learning of a Conditioned Avoidance Task'. *Neurobiology of Learning and Memory* 94 (2): 229–39. https://doi.org/10.1016/j.nlm.2010.05.011.

Bryant, Kathleen G., and Jacqueline M. Barker. 2020. 'Arbitration of Approach-Avoidance Conflict by Ventral Hippocampus'. *Frontiers in Neuroscience* 14:615337. https://doi.org/10.3389/fnins.2020.615337.

Burton, Amanda C., Kae Nakamura, and Matthew R. Roesch. 2015. 'From Ventral-Medial to Dorsal-Lateral Striatum: Neural Correlates of Reward-Guided Decision-Making'. *Neurobiology of Learning and Memory*, Memory and decision making, 117 (January):51–59. https://doi.org/10.1016/j.nlm.2014.05.003.

Butler, Ryan K., L. Casey White, Dani Frederick-Duus, Kris F. Kaigler, Jim R. Fadel, and Marlene A. Wilson. 2012. 'Comparison of the Activation of Somatostatin- and Neuropeptide Y-Containing Neuronal Populations of the Rat Amygdala Following Two Different Anxiogenic Stressors'. *Experimental Neurology*, Special issue: Mechanisms of protein misfolding in stressors, 238 (1): 52–63. https://doi.org/10.1016/j.expneurol.2012.08.002.

Cai, Yuan, and Christopher P. Ford. 2018. 'Dopamine Cells Differentially Regulate Striatal Cholinergic Transmission across Regions through Corelease of Dopamine and Glutamate'. *Cell Reports* 25 (11): 3148-3157.e3. https://doi.org/10.1016/j.celrep.2018.11.053.

Calhoon, Gwendolyn G., and Kay M. Tye. 2015. 'Resolving the Neural Circuits of Anxiety'. *Nature Neuroscience* 18 (10): 1394–1404. https://doi.org/10.1038/nn.4101.

Cameron, H. A., and R. D. McKay. 2001. 'Adult Neurogenesis Produces a Large Pool of New Granule Cells in the Dentate Gyrus'. *The Journal of Comparative Neurology* 435 (4): 406–17. https://doi.org/10.1002/cne.1040.

Cappucci, Ugo, Giulia Torromino, Assunta Maria Casale, Jeremy Camon, Fabrizio Capitano, Maria Berloco, Andrea Mele, Sergio Pimpinelli, Arianna Rinaldi, and Lucia Piacentini. 2018. 'Stress-Induced Strain and Brain Region-

Specific Activation of LINE-1 Transposons in Adult Mice'. *Stress* 21 (6): 575–79. https://doi.org/10.1080/10253890.2018.1485647.

Carvalho, Milene C., Caio M. Moreira, Janaína M. Zanoveli, and Marcus L. Brandão. 2012. 'Central, but Not Basolateral, Amygdala Involvement in the Anxiolytic-like Effects of Midazolam in Rats in the Elevated plus Maze'. *Journal of Psychopharmacology (Oxford, England)* 26 (4): 543–54. https://doi.org/10.1177/0269881110389209.

Castellan-Baldan, Lissandra, Mateus da Costa Kawasaki, Sandro José Ribeiro, Fabrício Calvo, Vani Maria Alves Corrêa, and Norberto Cysne Coimbra. 2006. 'Topographic and Functional Neuroanatomical Study of GABAergic Disinhibitory Striatum–Nigral Inputs and Inhibitory Nigrocollicular Pathways: Neural Hodology Recruiting the Substantia Nigra, Pars Reticulata, for the Modulation of the Neural Activity in the Inferior Colliculus Involved with Panic-like Emotions'. *Journal of Chemical Neuroanatomy* 32 (1): 1–27. https://doi.org/10.1016/j.jchemneu.2006.05.002.

Centofante, Eleonora, Luca Fralleoni, Carmen A. Lupascu, Michele Migliore, Arianna Rinaldi, and Andrea Mele. 2023. 'Specific Patterns of Neural Activity in the Hippocampus after Massed or Distributed Spatial Training'. *Scientific Reports* 13 (1): 13357. https://doi.org/10.1038/s41598-023-39882-0.

Cepeda, Carlos, Véronique M. André, Irene Yamazaki, Nanping Wu, Max Kleiman-Weiner, and Michael S. Levine. 2008. 'Differential Electrophysiological Properties of Dopamine D1 and D2 Receptor-Containing Striatal Medium-Sized Spiny Neurons'. *European Journal of Neuroscience* 27 (3): 671–82. https://doi.org/10.1111/j.1460-9568.2008.06038.x.

Challis, Collin, Janette Boulden, Avin Veerakumar, Julie Espallergues, Fair M. Vassoler, R. Christopher Pierce, Sheryl G. Beck, and Olivier Berton. 2013. 'Raphe GABAergic Neurons Mediate the Acquisition of Avoidance after Social Defeat'. *Journal of Neuroscience* 33 (35): 13978–88. https://doi.org/10.1523/JNEUROSCI.2383-13.2013.

Charara, Ali, Mamadou Sidibé, and Yoland Smith. 2003. 'Basal Ganglia Circuitry and Synaptic Connectivity'. In *Surgical Treatment of Parkinson's Disease and Other Movement Disorders*, edited by Daniel Tarsy, Jerrold L. Vitek, and Andres M. Lozano, 19–39. Totowa, NJ: Humana Press. https://doi.org/10.1007/978-1-59259-312-5_2.

Chavez, M. E., R. Saladocastillo, M. Sanchezalavez, G. L. Quirarte, and R. A. Pradoalcala. 1995. 'Post-Training Injection of GABAergic Antagonists into the Striatum Produces Retrograde Amnesia'. *Neurobiology of Learning and Memory* 63 (3): 296–300. https://doi.org/10.1006/nlme.1995.1035.

Cui, Guohong, Sang Beom Jun, Xin Jin, Michael D. Pham, Steven S. Vogel, David M. Lovinger, and Rui M. Costa. 2013. 'Concurrent Activation of Striatal Direct and Indirect Pathways during Action Initiation'. *Nature* 494 (7436): 238–42. https://doi.org/10.1038/nature11846.

Dallman, Mary F. 2005. 'Fast Glucocorticoid Actions on Brain: Back to the Future'. *Frontiers in Neuroendocrinology* 26 (3): 103–8. https://doi.org/10.1016/j.yfrne.2005.08.001.

Davis, M., and P. J. Whalen. 2001. 'The Amygdala: Vigilance and Emotion'. *Molecular Psychiatry* 6 (1): 13–34. https://doi.org/10.1038/sj.mp.4000812.

Davis, Michael, David L. Walker, Leigh Miles, and Christian Grillon. 2010. 'Phasic vs Sustained Fear in Rats and Humans: Role of the Extended Amygdala in Fear vs Anxiety'. *Neuropsychopharmacology* 35 (1): 105–35. https://doi.org/10.1038/npp.2009.109.

De Leonibus, Elvira, Pauline Lafenetre, Alberto Oliverio, and Andrea Mele. 2003. 'Pharmacological Evidence of the Role of Dorsal Striatum in Spatial Memory Consolidation in Mice'. *Behavioral Neuroscience* 117 (4): 685–94. https://doi.org/10.1037/0735-7044.117.4.685.

Degroot, Aldemar, and Dallas Treit. 2004. 'Anxiety Is Functionally Segregated within the Septo-Hippocampal System'. *Brain Research* 1001 (1): 60–71. https://doi.org/10.1016/j.brainres.2003.10.065.

De Kloet, E. Ron de, Marian Joëls, and Florian Holsboer. 2005. 'Stress and the Brain: From Adaptation to Disease'. *Nature Reviews Neuroscience* 6 (6): 463–75. https://doi.org/10.1038/nrn1683.

De Kloet, E Ronald de, and Roel Derijk. 2004. 'Signaling Pathways in Brain Involved in Predisposition and Pathogenesis of Stress-Related Disease: Genetic and Kinetic Factors Affecting the MR/GR Balance'. *Annals of the New York Academy of Sciences* 1032 (1): 14–34. https://doi.org/10.1196/annals.1314.003.

De Kloet, E. Ronald de, Henk Karst, and Marian Joëls. 2008. 'Corticosteroid Hormones in the Central Stress Response: Quick-and-Slow'. *Frontiers in Neuroendocrinology*, Rapid Actions of Steroid Hormones, 29 (2): 268–72. https://doi.org/10.1016/j.yfrne.2007.10.002.

De Kloet, E. Ronald de, Erno Vreugdenhil, Melly S. Oitzl, and Marian Joëls. 1998. 'Brain Corticosteroid Receptor Balance in Health and Disease*'. *Endocrine Reviews* 19 (3): 269–301. https://doi.org/10.1210/edrv.19.3.0331.

DeLong, Mahlon R. 1990. 'Primate Models of Movement Disorders of Basal Ganglia Origin'. *Trends in Neurosciences* 13 (7): 281–85. https://doi.org/10.1016/0166-2236(90)90110-V.

Devan, Bryan D., and Norman M. White. 1999. 'Parallel Information Processing in the Dorsal Striatum: Relation to Hippocampal Function'. *Journal of Neuroscience* 19 (7): 2789–98. https://doi.org/10.1523/JNEUROSCI.19-07-02789.1999.

Dg, Tervo, Hwang By, Viswanathan S, Gaj T, Lavzin M, Ritola Kd, Lindo S, et al. 2016. 'A Designer AAV Variant Permits Efficient Retrograde Access to Projection Neurons'. *Neuron* 92 (2). https://doi.org/10.1016/j.neuron.2016.09.021.

Diamond, David M., M. Catherine Bennett, Monika Fleshner, and Gregory M. Rose. 1992. 'Inverted-U Relationship between the Level of Peripheral Corticosterone and the Magnitude of Hippocampal Primed Burst Potentiation'. *Hippocampus* 2 (4): 421–30. https://doi.org/10.1002/hipo.450020409.

Dixon, Matthew L., Ravi Thiruchselvam, Rebecca Todd, and Kalina Christoff. 2017. 'Emotion and the Prefrontal Cortex: An Integrative Review'. *Psychological Bulletin* 143 (10): 1033–81. https://doi.org/10.1037/bul0000096.

Duval, Elizabeth R., Arash Javanbakht, and Israel Liberzon. 2015. 'Neural Circuits in Anxiety and Stress Disorders: A Focused Review'. *Therapeutics and Clinical Risk Management*, January. https://www.tandfonline.com/doi/abs/10.2147/TCRM.S48528.

Erdmann, G., S. Berger, and G. Schütz. 2008. 'Genetic Dissection of Glucocorticoid Receptor Function in the Mouse Brain'. *Journal of Neuroendocrinology* 20 (6): 655–59. https://doi.org/10.1111/j.1365-2826.2008.01717.x.

Farrell, Martilias S., Ying Pei, Yehong Wan, Prem N. Yadav, Tanya L. Daigle, Daniel J. Urban, Hyeong-Min Lee, et al. 2013. 'A Gαs DREADD Mouse for Selective Modulation of cAMP Production in Striatopallidal Neurons'. *Neuropsychopharmacology* 38 (5): 854–62. https://doi.org/10.1038/npp.2012.251.

Felix-Ortiz, A. C., A. Burgos-Robles, N. D. Bhagat, C. A. Leppla, and K. M. Tye. 2016. 'Bidirectional Modulation of Anxiety-Related and Social Behaviors by Amygdala Projections to the Medial Prefrontal Cortex'. *Neuroscience* 321 (May):197–209. https://doi.org/10.1016/j.neuroscience.2015.07.041.

Felix-Ortiz, Ada C., Anna Beyeler, Changwoo Seo, Christopher A. Leppla, Craig P. Wildes, and Kay M. Tye. 2013. 'BLA to vHPC Inputs Modulate Anxiety-Related Behaviors'. *Neuron* 79 (4): 658–64. https://doi.org/10.1016/j.neuron.2013.06.016.

Fino, Elodie, Marie Vandecasteele, Sylvie Perez, Frédéric Saudou, and Laurent Venance. 2018. 'Region-Specific and State-Dependent Action of Striatal GABAergic Interneurons'. *Nature Communications* 9 (1): 3339. https://doi.org/10.1038/s41467-018-05847-5.

'Frontiers | What Is the Degree of Segregation between Striatonigral and Striatopallidal Projections?' n.d. Accessed 11 July 2024. https://www.frontiersin.org/journals/neuroanatomy/articles/10.3389/fnana.2010.00136/full.

Gabbott, Paul L. A., Tracy A. Warner, Paul R. L. Jays, Phillip Salway, and Sarah J. Busby. 2005. 'Prefrontal Cortex in the Rat: Projections to Subcortical Autonomic, Motor, and Limbic Centers'. *The Journal of Comparative Neurology* 492 (2): 145–77. https://doi.org/10.1002/cne.20738.

Gangarossa, Giuseppe, Julie Espallergues, Philippe Mailly, Dimitri De Bundel, Alban de Kerchove d'Exaerde, Denis Hervé, Jean-Antoine Girault, Emmanuel Valjent, and Patrik Krieger. 2013. 'Spatial Distribution of D1R- and D2R-Expressing Medium-Sized Spiny Neurons Differs along the Rostro-Caudal Axis of the Mouse Dorsal Striatum'. *Frontiers in Neural Circuits* 7:124. https://doi.org/10.3389/fncir.2013.00124.

Gerfen, Charles R., and D. James Surmeier. 2011. 'Modulation of Striatal Projection Systems by Dopamine'. *Annual Review of Neuroscience* 34:441–66. https://doi.org/10.1146/annurev-neuro-061010-113641.

Gittis, Aryn H., Alexandra B. Nelson, Myo T. Thwin, Jorge J. Palop, and Anatol C. Kreitzer. 2010. 'Distinct Roles of GABAergic Interneurons in the Regulation of Striatal Output Pathways'. *Journal of Neuroscience* 30 (6): 2223–34. https://doi.org/10.1523/JNEUROSCI.4870-09.2010.

Goodman, J., and M. G. Packard. 2016. 'Chapter 35 - Memory Systems of the Basal Ganglia'. In *Handbook of Behavioral Neuroscience*, edited by Heinz Steiner and Kuei Y. Tseng, 24:725–40. Handbook of Basal Ganglia Structure and Function, Second Edition. Elsevier. https://doi.org/10.1016/B978-0-12-802206-1.00035-0.

Gould, Todd D., David T. Dao, and Colleen E. Kovacsics. 2009. 'The Open Field Test'. In *Mood and Anxiety Related Phenotypes in Mice: Characterization Using Behavioral Tests*, edited by Todd D. Gould, 1–20. Totowa, NJ: Humana Press. https://doi.org/10.1007/978-1-60761-303-9_1.

Groenewegen, Henk J. 2003. 'The Basal Ganglia and Motor Control'. *Neural Plasticity* 10 (1–2): 108384. https://doi.org/10.1155/NP.2003.107.

Grupe, Dan W., and Jack B. Nitschke. 2013. 'Uncertainty and Anticipation in Anxiety: An Integrated Neurobiological and Psychological Perspective'. *Nature Reviews Neuroscience* 14 (7): 488–501. https://doi.org/10.1038/nrn3524.

Hansson, Anita C., Antonio Cintra, Natale Belluardo, Wolfgang Sommer, Maheep Bhatnagar, Michael Bader, Detlev Ganten, and Kjell Fuxe. 2000. 'Gluco- and Mineralocorticoid Receptor-Mediated Regulation of Neurotrophic Factor Gene Expression in the Dorsal Hippocampus and the Neocortex of the Rat'. *European Journal of Neuroscience* 12 (8): 2918–34. https://doi.org/10.1046/j.1460-9568.2000.00185.x.

Harder, Henry G., Shannon Wagner, and Josh Rash. 2016. *Mental Illness in the Workplace: Psychological Disability Management*. London: Routledge. https://doi.org/10.4324/9781315595009.

He, Ya-Di, Wen Tao, Tao He, Bang-Yu Wang, Xiu-Mei Tang, Liang-Ming Zhang, Zhen-Quan Wu, et al. 2021. 'A Urine Extracellular Vesicle circRNA Classifier for Detection of High-Grade Prostate Cancer in Patients with Prostate-Specific Antigen 2–10 Ng/mL at Initial Biopsy'. *Molecular Cancer* 20 (1): 96. https://doi.org/10.1186/s12943-021-01388-6.

Hedreen, John C., and Marlon R. Delong. 1991. 'Organization of Striatopallidal, Striatonigral, and Nigrostriatal Projections in the Macaque'. *Journal of Comparative Neurology* 304 (4): 569–95. https://doi.org/10.1002/cne.903040406.

Hill, Alexis S., Amar Sahay, and René Hen. 2015. 'Increasing Adult Hippocampal Neurogenesis Is Sufficient to Reduce Anxiety and Depression-Like Behaviors'. *Neuropsychopharmacology: Official Publication of the American College of Neuropsychopharmacology* 40 (10): 2368–78. https://doi.org/10.1038/npp.2015.85.

Hintiryan, Houri, Ian Bowman, David L. Johnson, Laura Korobkova, Muye Zhu, Neda Khanjani, Lin Gou, et al. 2021. 'Connectivity Characterization of the Mouse Basolateral Amygdalar Complex'. *Nature Communications* 12 (1): 2859. https://doi.org/10.1038/s41467-021-22915-5.

Hintiryan, Houri, Nicholas N. Foster, Ian Bowman, Maxwell Bay, Monica Y. Song, Lin Gou, Seita Yamashita, et al. 2016. 'The Mouse Cortico-Striatal Projectome'. *Nature Neuroscience* 19 (8): 1100–1114. https://doi.org/10.1038/nn.4332.

Hormigo, Sebastian, German Vega-Flores, and Manuel A. Castro-Alamancos. 2016. 'Basal Ganglia Output Controls Active Avoidance Behavior'. *Journal of Neuroscience* 36 (40): 10274–84. https://doi.org/10.1523/JNEUROSCI.1842-16.2016.

Hu, Hailan, Yihui Cui, and Yan Yang. 2020. 'Circuits and Functions of the Lateral Habenula in Health and in Disease'. *Nature Reviews Neuroscience* 21 (5): 277–95. https://doi.org/10.1038/s41583-020-0292-4.

Hunnicutt, Barbara J., Bart C. Jongbloets, William T. Birdsong, Katrina J. Gertz, Haining Zhong, and Tianyi Mao. 2016. 'A Comprehensive Excitatory Input Map of the Striatum Reveals Novel Functional Organization'. *eLife* 5 (November):e19103. https://doi.org/10.7554/eLife.19103.

Huston, Joseph P., Maria A. de Souza Silva, Bianca Topic, and Christian P. Müller. 2013. 'What's Conditioned in Conditioned Place Preference?' *Trends in Pharmacological Sciences* 34 (3): 162–66. https://doi.org/10.1016/j.tips.2013.01.004.

Ipser, Jonathan C., Leesha Singh, and Dan J. Stein. 2013. 'Meta-Analysis of Functional Brain Imaging in Specific Phobia'. *Psychiatry and Clinical Neurosciences* 67 (5): 311–22. https://doi.org/10.1111/pcn.12055.

Javaid, Syed Fahad, Ibrahim Jawad Hashim, Muhammad Jawad Hashim, Emmanuel Stip, Mohammed Abdul Samad, and Alia Al Ahbabi. 2023. 'Epidemiology of Anxiety Disorders: Global Burden and Sociodemographic Associations'. *Middle East Current Psychiatry* 30 (1): 44. https://doi.org/10.1186/s43045-023-00315-3.

Joëls, Marian, and E. Ronald de Kloet. 1989. 'Effects of Glucocorticoids and Norepinephrine on the Excitability in the Hippocampus'. *Science* 245 (4925): 1502–5. https://doi.org/10.1126/science.2781292.

Kessler, Ronald C., Maria Petukhova, Nancy A. Sampson, Alan M Zaslavsky, and Hans-Ullrich Wittchen. 2012. 'Twelve-Month and Lifetime Prevalence and Lifetime Morbid Risk of Anxiety and Mood Disorders in the United States'. *International Journal of Methods in Psychiatric Research* 21 (3): 169–84. https://doi.org/10.1002/mpr.1359.

Kheirbek, Mazen A., Liam J. Drew, Nesha S. Burghardt, Daniel O. Costantini, Lindsay Tannenholz, Susanne E. Ahmari, Hongkui Zeng, André A. Fenton, and René Hen. 2013. 'Differential Control of Learning and Anxiety along the Dorsoventral Axis of the Dentate Gyrus'. *Neuron* 77 (5): 955–68. https://doi.org/10.1016/j.neuron.2012.12.038.

Kim, Jeansok J., and David M. Diamond. 2002. 'The Stressed Hippocampus, Synaptic Plasticity and Lost Memories'. *Nature Reviews Neuroscience* 3 (6): 453–62. https://doi.org/10.1038/nrn849.

Kirkby, Robert J., and Daniel P. Kimble. 1968. 'Avoidance and Escape Behavior Following Striatal Lesions in the Rat'. *Experimental Neurology* 20 (2): 215–27. https://doi.org/10.1016/0014-4886(68)90095-2.

Kirkby, Robert J., and Stephen Polgar. 1974. 'Active Avoidance in the Laboratory Rat Following Lesions of the Dorsal or Ventral Caudate Nucleus'. *Physiological Psychology* 2 (3): 301–6. https://doi.org/10.3758/BF03333025.

Kita, H., and S. T. Kitai. 1988. 'Glutamate Decarboxylase Immunoreactive Neurons in Rat Neostriatum: Their Morphological Types and Populations'. *Brain Research* 447 (2): 346–52. https://doi.org/10.1016/0006-8993(88)91138-9.

Kita, H., T. Kosaka, and C. W. Heizmann. 1990. 'Parvalbumin-Immunoreactive Neurons in the Rat Neostriatum: A Light and Electron Microscopic Study'. *Brain Research* 536 (1–2): 1–15. https://doi.org/10.1016/0006-8993(90)90002-s.

Kretz, Oliver, Holger M. Reichardt, Günther Schütz, and Rudolf Bock. 1999. 'Corticotropin-Releasing Hormone Expression Is the Major Target for Glucocorticoid Feedback-Control at the Hypothalamic Level'. *Brain Research* 818 (2): 488–91. https://doi.org/10.1016/S0006-8993(98)01277-3.

Kroenke, Kurt, Robert L. Spitzer, Janet B.W. Williams, Patrick O. Monahan, and Bernd Löwe. 2007. 'Anxiety Disorders in Primary Care: Prevalence, Impairment, Comorbidity, and Detection'. *Annals of Internal Medicine* 146 (5): 317–25. https://doi.org/10.7326/0003-4819-146-5-200703060-00004.

Krout, Karl E., Arthur D. Loewy, G.W. Max Westby, and Peter Redgrave. 2001. 'Superior Colliculus Projections to Midline and Intralaminar Thalamic Nuclei of the Rat'. *Journal of Comparative Neurology* 431 (2): 198–216. https://doi.org/10.1002/1096-9861(20010305)431:2<198::AID-CNE1065>3.0.CO;2-8.

Kügler, S., E. Kilic, and M. Bähr. 2003. 'Human Synapsin 1 Gene Promoter Confers Highly Neuron-Specific Long-Term Transgene Expression from an Adenoviral Vector in the Adult Rat Brain Depending on the Transduced Area'. *Gene Therapy* 10 (4): 337–47. https://doi.org/10.1038/sj.gt.3301905.

Lanciego, José L., Natasha Luquin, and José A. Obeso. 2012. 'Functional Neuroanatomy of the Basal Ganglia'. *Cold Spring Harbor Perspectives in Medicine* 2 (12): a009621. https://doi.org/10.1101/cshperspect.a009621.

Lasda, Erika, and Roy Parker. 2016. 'Circular RNAs Co-Precipitate with Extracellular Vesicles: A Possible Mechanism for circRNA Clearance'. *PLOS ONE* 11 (2): e0148407. https://doi.org/10.1371/journal.pone.0148407.

LeBlanc, Kimberly H., Tanisha D. London, Ilona Szczot, Miriam E. Bocarsly, Danielle M. Friend, Katrina P. Nguyen, Marda M. Mengesha, Marcelo Rubinstein, Veronica A. Alvarez, and Alexxai V. Kravitz. 2020. 'Striatopallidal Neurons Control Avoidance Behavior in Exploratory Tasks'. *Molecular Psychiatry* 25 (2): 491–505. https://doi.org/10.1038/s41380-018-0051-3.

Lee, Anni S., Ronald S. Duman, and Christopher Pittenger. 2008. 'A Double Dissociation Revealing Bidirectional Competition between Striatum and Hippocampus during Learning'. *Proceedings of the National Academy of Sciences* 105 (44): 17163–68. https://doi.org/10.1073/pnas.0807749105.

Lee, In Bum, Eugene Lee, Na-Eun Han, Marko Slavuj, Jeong Wook Hwang, Ahrim Lee, Taeyoung Sun, et al. 2024. 'Persistent Enhancement of Basolateral Amygdala-Dorsomedial Striatum Synapses Causes Compulsive-like Behaviors in Mice'. *Nature Communications* 15 (1): 219. https://doi.org/10.1038/s41467-023-44322-8.

Lenz, Jeffrey D., and Mary Kay Lobo. 2013. 'Optogenetic Insights into Striatal Function and Behavior'. *Behavioural Brain Research*, Optogenetics, 255 (October):44–54. https://doi.org/10.1016/j.bbr.2013.04.018.

Leonibus, Elvira De, Alberto Oliverio, and Andrea Mele. 2005. 'A Study on the Role of the Dorsal Striatum and the Nucleus Accumbens in Allocentric and Egocentric Spatial Memory Consolidation'. *Learning & Memory* 12 (5): 491–503. https://doi.org/10.1101/lm.94805.

Lerner, Talia N., Carrie Shilyansky, Thomas J. Davidson, Kathryn E. Evans, Kevin T. Beier, Kelly A. Zalocusky, Ailey K. Crow, et al. 2015. 'Intact-Brain Analyses Reveal Distinct Information Carried by SNc Dopamine Subcircuits'. *Cell* 162 (3): 635–47. https://doi.org/10.1016/j.cell.2015.07.014.

Linke, Rüdiger. 1999. 'Differential Projection Patterns of Superior and Inferior Collicular Neurons onto Posterior Paralaminar Nuclei of the Thalamus

Surrounding the Medial Geniculate Body in the Rat'. *European Journal of Neuroscience* 11 (1): 187–203. https://doi.org/10.1046/j.1460-9568.1999.00422.x.

Loewke, Adrienne C., Adelaide R. Minerva, Alexandra B. Nelson, Anatol C. Kreitzer, and Lisa A. Gunaydin. 2021. 'Frontostriatal Projections Regulate Innate Avoidance Behavior'. *Journal of Neuroscience* 41 (25): 5487–5501. https://doi.org/10.1523/JNEUROSCI.2581-20.2021.

Machado-de-Sousa, João Paulo, Flávia de Lima Osório, Andrea P. Jackowski, Rodrigo A. Bressan, Marcos H. N. Chagas, Nelson Torro-Alves, André L. D. DePaula, José A. S. Crippa, and Jaime E. C. Hallak. 2014. 'Increased Amygdalar and Hippocampal Volumes in Young Adults with Social Anxiety'. *PLOS ONE* 9 (2): e88523. https://doi.org/10.1371/journal.pone.0088523.

MacKay-Lyons, Marilyn. 2002. 'Central Pattern Generation of Locomotion: A Review of the Evidence'. *Physical Therapy* 82 (1): 69–83. https://doi.org/10.1093/ptj/82.1.69.

Marín, Oscar, Stewart A. Anderson, and John L. R. Rubenstein. 2000. 'Origin and Molecular Specification of Striatal Interneurons'. *Journal of Neuroscience* 20 (16): 6063–76. https://doi.org/10.1523/JNEUROSCI.20-16-06063.2000.

Matamales, Miriam, Jürgen Götz, and Jesus Bertran-Gonzalez. 2016. 'Quantitative Imaging of Cholinergic Interneurons Reveals a Distinctive Spatial Organization and a Functional Gradient across the Mouse Striatum'. *PloS One* 11 (6): e0157682. https://doi.org/10.1371/journal.pone.0157682.

McGaugh, James L, and Benno Roozendaal. 2002. 'Role of Adrenal Stress Hormones in Forming Lasting Memories in the Brain'. *Current Opinion in Neurobiology* 12 (2): 205–10. https://doi.org/10.1016/S0959-4388(02)00306-9.

Moreira, Caio M., Sueli Masson, Milene C. Carvalho, and Marcus L. Brandão. 2007. 'Exploratory Behaviour of Rats in the Elevated Plus-Maze Is Differentially Sensitive to Inactivation of the Basolateral and Central Amygdaloid Nuclei'. *Brain Research Bulletin* 71 (5): 466–74. https://doi.org/10.1016/j.brainresbull.2006.10.004.

Muller, Jay F., Franco Mascagni, and Alexander J. McDonald. 2009. 'Dopaminergic Innervation of Pyramidal Cells in the Rat Basolateral Amygdala'. *Brain Structure and Function* 213 (3): 275–88. https://doi.org/10.1007/s00429-008-0196-y.

Nagel, Georg, Martin Brauner, Jana F. Liewald, Nona Adeishvili, Ernst Bamberg, and Alexander Gottschalk. 2005. 'Light Activation of Channelrhodopsin-2 in Excitable Cells of Caenorhabditis Elegans Triggers Rapid Behavioral Responses'. *Current Biology* 15 (24): 2279–84. https://doi.org/10.1016/j.cub.2005.11.032.

Nestler, Eric J., and Steven E. Hyman. 2010. 'Animal Models of Neuropsychiatric Disorders'. *Nature Neuroscience* 13 (10): 1161–69. https://doi.org/10.1038/nn.2647.

Nguyen, Claire, Sarah Mondoloni, Tinaïg Le Borgne, Ines Centeno, Maxime Come, Joachim Jehl, Clément Solié, et al. 2021. 'Nicotine Inhibits the VTA-to-Amygdala Dopamine Pathway to Promote Anxiety'. *Neuron* 109 (16): 2604-2615.e9. https://doi.org/10.1016/j.neuron.2021.06.013.

Nguyen, David, Erind Alushaj, Suzanne Erb, and Rutsuko Ito. 2019. 'Dissociative Effects of Dorsomedial Striatum D1 and D2 Receptor Antagonism in the Regulation of Anxiety and Learned Approach-Avoidance Conflict Decision-Making'. *Neuropharmacology* 146 (March):222–30. https://doi.org/10.1016/j.neuropharm.2018.11.040.

Oitzl, Melly S., Marc Fluttert, and E. Ron de Kloet. 1994. 'The Effect of Corticosterone on Reactivity to Spatial Novelty Is Mediated by Central Mineralocorticosteroid Receptors'. *European Journal of Neuroscience* 6 (7): 1072–79. https://doi.org/10.1111/j.1460-9568.1994.tb00604.x.

Oitzl, Melly S., and E. Ronald de Kloet. 1992. 'Selective Corticosteroid Antagonists Modulate Specific Aspects of Spatial Orientation Learning'. *Behavioral Neuroscience* 106 (1): 62–71. https://doi.org/10.1037/0735-7044.106.1.62.

Ota, Yuki, Yukio Ago, Tatsunori Tanaka, Shigeru Hasebe, Yui Toratani, Yusuke Onaka, Hitoshi Hashimoto, Kazuhiro Takuma, and Toshio Matsuda. 2015. 'Anxiolytic-like Effects of Restraint during the Dark Cycle in Adolescent Mice'. *Behavioural Brain Research* 284 (May):103–11. https://doi.org/10.1016/j.bbr.2015.02.010.

Packard, Mark G., and Barbara J. Knowlton. 2002. 'Learning and Memory Functions of the Basal Ganglia'. *Annual Review of Neuroscience* 25 (Volume 25, 2002): 563–93. https://doi.org/10.1146/annurev.neuro.25.112701.142937.

Padilla-Coreano, Nancy, Scott S. Bolkan, Georgia M. Pierce, Dakota R. Blackman, William D. Hardin, Alvaro L. Garcia-Garcia, Timothy J. Spellman, and Joshua A. Gordon. 2016. 'Direct Ventral Hippocampal-Prefrontal Input Is Required for Anxiety-Related Neural Activity and Behavior'. *Neuron* 89 (4): 857–66. https://doi.org/10.1016/j.neuron.2016.01.011.

Papez, J. W. 1995. 'A Proposed Mechanism of Emotion. 1937'. *The Journal of Neuropsychiatry and Clinical Neurosciences* 7 (1): 103–12. https://doi.org/10.1176/jnp.7.1.103.

Parfitt, Gustavo Morrone, Robin Nguyen, Jee Yoon Bang, Afif J. Aqrabawi, Matthew M. Tran, D. Kanghoon Seo, Blake A. Richards, and Jun Chul Kim. 2017. 'Bidirectional Control of Anxiety-Related Behaviors in Mice: Role of Inputs Arising from the Ventral Hippocampus to the Lateral Septum and Medial Prefrontal Cortex'. *Neuropsychopharmacology: Official Publication*

of the American College of Neuropsychopharmacology 42 (8): 1715–28. https://doi.org/10.1038/npp.2017.56.

Pavlides, Constantine, Sonoko Ogawa, Akihisa Kimura, and Bruce S. McEwen. 1996. 'Role of Adrenal Steroid Mineralocorticoid and Glucocorticoid Receptors in Long-Term Potentiation in the CA1 Field of Hippocampal Slices'. *Brain Research* 738 (2): 229–35. https://doi.org/10.1016/S0006-8993(96)00776-7.

Paxinos and Franklin's the Mouse Brain in Stereotaxic Coordinates, Compact. 2019. https://shop.elsevier.com/books/paxinos-and-franklins-the-mouse-brain-in-stereotaxic-coordinates-compact/franklin/978-0-12-816159-3.

Pellow, Sharon, Philippe Chopin, Sandra E. File, and Mike Briley. 1985. 'Validation of Open : Closed Arm Entries in an Elevated plus-Maze as a Measure of Anxiety in the Rat'. *Journal of Neuroscience Methods* 14 (3): 149–67. https://doi.org/10.1016/0165-0270(85)90031-7.

Prado-Alcalá, R. A., Z. J. Grinberg, Z. L. Arditti, M. M. García, H. G. Prieto, and H. Brust-Carmona. 1975. 'Learning Deficits Produced by Chronic and Reversible Lesions of the Corpus Striatum in Rats'. *Physiology & Behavior* 15 (3): 283–87. https://doi.org/10.1016/0031-9384(75)90095-5.

Prado-Alcalá, Roberto A., Andrea Cristina Medina, Paola C. Bello-Medina, and Gina L. Quirarte. 2017. 'Inhibition of Transcription and Translation in the Striatum after Memory Reactivation: Lack of Evidence of Reconsolidation'. *Neurobiology of Learning and Memory*, Memory reconsolidation and memory updating, 142 (July):21–29. https://doi.org/10.1016/j.nlm.2016.12.018.

Ragozzino, Michael E., Katharine E. Ragozzino, Sheri J. Y. Mizumori, and Raymond P. Kesner. 2002. 'Role of the Dorsomedial Striatum in Behavioral Flexibility for Response and Visual Cue Discrimination Learning'. *Behavioral Neuroscience* 116 (1): 105–15. https://doi.org/10.1037/0735-7044.116.1.105.

REUL, J. M. H. M., and E. R. DE KLOET. 1985. 'Two Receptor Systems for Corticosterone in Rat Brain: Microdistribution and Differential Occupation'. *Endocrinology* 117 (6): 2505–11. https://doi.org/10.1210/endo-117-6-2505.

Revest, J.-M., D. Dupret, M. Koehl, C. Funk-Reiter, N. Grosjean, P.-V. Piazza, and D. N. Abrous. 2009. 'Adult Hippocampal Neurogenesis Is Involved in Anxiety-Related Behaviors'. *Molecular Psychiatry* 14 (10): 959–67. https://doi.org/10.1038/mp.2009.15.

Roozendaal, Benno. 2002. 'Stress and Memory: Opposing Effects of Glucocorticoids on Memory Consolidation and Memory Retrieval'. *Neurobiology of Learning and Memory* 78 (3): 578–95. https://doi.org/10.1006/nlme.2002.4080.

Sabban, Esther L., and Richard Kvetňanský. 2001. 'Stress-Triggered Activation of Gene Expression in Catecholaminergic Systems: Dynamics of

Transcriptional Events'. *Trends in Neurosciences* 24 (2): 91–98. https://doi.org/10.1016/S0166-2236(00)01687-8.

Santabárbara, Javier, Isabel Lasheras, Darren M. Lipnicki, Juan Bueno-Notivol, María Pérez-Moreno, Raúl López-Antón, Concepción De la Cámara, Antonio Lobo, and Patricia Gracia-García. 2021. 'Prevalence of Anxiety in the COVID-19 Pandemic: An Updated Meta-Analysis of Community-Based Studies'. *Progress in Neuro-Psychopharmacology and Biological Psychiatry* 109 (July):110207. https://doi.org/10.1016/j.pnpbp.2020.110207.

Schaaf, Marcel J.M., Rob W.M. Hoetelmans, E. Ronald de Kloet, and Erno Vreugdenhil. 1997. 'Corticosterone Regulates Expression of BDNF and trkB but Not NT-3 and trkC mRNA in the Rat Hippocampus'. *Journal of Neuroscience Research* 48 (4): 334–41. https://doi.org/10.1002/(SICI)1097-4547(19970515)48:4<334::AID-JNR5>3.0.CO;2-C.

Scheich, B., P. Vincze, É. Szőke, É. Borbély, Á. Hunyady, J. Szolcsányi, Á. Dénes, Zs. Környei, B. Gaszner, and Zs. Helyes. 2017. 'Chronic Stress-Induced Mechanical Hyperalgesia Is Controlled by Capsaicin-Sensitive Neurones in the Mouse'. *European Journal of Pain* 21 (8): 1417–31. https://doi.org/10.1002/ejp.1043.

Schmued, Laurence C., and James H. Fallon. 1986. 'Fluoro-Gold: A New Fluorescent Retrograde Axonal Tracer with Numerous Unique Properties'. *Brain Research* 377 (1): 147–54. https://doi.org/10.1016/0006-8993(86)91199-6.

Schultz, Wolfram, Peter Dayan, and P. Read Montague. 1997. 'A Neural Substrate of Prediction and Reward'. *Science* 275 (5306): 1593–99. https://doi.org/10.1126/science.275.5306.1593.

Silveira, Maria Cristina L., Guy Sandner, and Frederico G. Graeff. 1993. 'Induction of Fos Immunoreactivity in the Brain by Exposure to the Elevated Plus-Maze'. *Behavioural Brain Research* 56 (1): 115–18. https://doi.org/10.1016/0166-4328(93)90028-O.

Stachniak, Tevye J., Anirvan Ghosh, and Scott M. Sternson. 2014. 'Chemogenetic Synaptic Silencing of Neural Circuits Localizes a Hypothalamus→Midbrain Pathway for Feeding Behavior'. *Neuron* 82 (4): 797–808. https://doi.org/10.1016/j.neuron.2014.04.008.

Stamatakis, Alice M., and Garret D. Stuber. 2012. 'Activation of Lateral Habenula Inputs to the Ventral Midbrain Promotes Behavioral Avoidance'. *Nature Neuroscience* 15 (8): 1105–7. https://doi.org/10.1038/nn.3145.

'Stress, Cognitive Impairment and Cell Adhesion Molecules | Nature Reviews Neuroscience'. n.d. Accessed 2 September 2024. https://www.nature.com/articles/nrn1555.

LeBlanc, Kimberly H., Tanisha D. London, Ilona Szczot, Miriam E. Bocarsly, Danielle M. Friend, Katrina P. Nguyen, Marda M. Mengesha, Marcelo

Rubinstein, Veronica A. Alvarez, and Alexxai V. Kravitz. 2020. 'Striatopallidal Neurons Control Avoidance Behavior in Exploratory Tasks'. *Molecular Psychiatry* 25 (2): 491–505. https://doi.org/10.1038/s41380-018-0051-3.

Sylvers, Patrick, Scott O. Lilienfeld, and Jamie L. LaPrairie. 2011. 'Differences between Trait Fear and Trait Anxiety: Implications for Psychopathology'. *Clinical Psychology Review* 31 (1): 122–37. https://doi.org/10.1016/j.cpr.2010.08.004.

Tang, Wei, Olexiy Kochubey, Michael Kintscher, and Ralf Schneggenburger. 2020. 'A VTA to Basal Amygdala Dopamine Projection Contributes to Signal Salient Somatosensory Events during Fear Learning'. *Journal of Neuroscience* 40 (20): 3969–80. https://doi.org/10.1523/JNEUROSCI.1796-19.2020.

Tepper, James M., Fatuel Tecuapetla, Tibor Koós, and Osvaldo Ibáñez-Sandoval. 2010. 'Heterogeneity and Diversity of Striatal GABAergic Interneurons'. *Frontiers in Neuroanatomy* 4:150. https://doi.org/10.3389/fnana.2010.00150.

Torromino, G., L. Autore, V. Khalil, V. Mastrorilli, M. Griguoli, A. Pignataro, E. Centofante, et al. 2019. 'Offline Ventral Subiculum-Ventral Striatum Serial Communication Is Required for Spatial Memory Consolidation'. *Nature Communications* 10 (1): 5721. https://doi.org/10.1038/s41467-019-13703-3.

Tovote, Philip, Jonathan Paul Fadok, and Andreas Lüthi. 2015. 'Neuronal Circuits for Fear and Anxiety'. *Nature Reviews Neuroscience* 16 (6): 317–31. https://doi.org/10.1038/nrn3945.

Tritsch, Nicolas X., and Bernardo L. Sabatini. 2012. 'Dopaminergic Modulation of Synaptic Transmission in Cortex and Striatum'. *Neuron* 76 (1): 33–50. https://doi.org/10.1016/j.neuron.2012.09.023.

Tye, Kay M., Rohit Prakash, Sung-Yon Kim, Lief E. Fenno, Logan Grosenick, Hosniya Zarabi, Kimberly R. Thompson, Viviana Gradinaru, Charu Ramakrishnan, and Karl Deisseroth. 2011. 'Amygdala Circuitry Mediating Reversible and Bidirectional Control of Anxiety'. *Nature* 471 (7338): 358–62. https://doi.org/10.1038/nature09820.

Tzschentke, Thomas M. 1998. 'Measuring Reward with the Conditioned Place Preference Paradigm: A Comprehensive Review of Drug Effects, Recent Progress and New Issues'. *Progress in Neurobiology* 56 (6): 613–72. https://doi.org/10.1016/S0301-0082(98)00060-4.

Urban, Daniel J., and Bryan L. Roth. 2015. 'DREADDs (Designer Receptors Exclusively Activated by Designer Drugs): Chemogenetic Tools with Therapeutic Utility'. *Annual Review of Pharmacology and Toxicology* 55 (Volume 55, 2015): 399–417. https://doi.org/10.1146/annurev-pharmtox-010814-124803.

Vermani, Monica, Madalyn Marcus, and Martin A. Katzman. 2011. 'Rates of Detection of Mood and Anxiety Disorders in Primary Care: A Descriptive, Cross-Sectional Study'. *The Primary Care Companion for CNS Disorders* 13 (2): 27211. https://doi.org/10.4088/PCC.10m01013.

Vertes, Robert P. 2004. 'Differential Projections of the Infralimbic and Prelimbic Cortex in the Rat'. *Synapse (New York, N.Y.)* 51 (1): 32–58. https://doi.org/10.1002/syn.10279.

Vink, Matthijs, René S. Kahn, Mathijs Raemaekers, Martijn van den Heuvel, Maria Boersma, and Nick F. Ramsey. 2005. 'Function of Striatum beyond Inhibition and Execution of Motor Responses'. *Human Brain Mapping* 25 (3): 336–44. https://doi.org/10.1002/hbm.20111.

Voorn, Pieter, Louk J. M. J. Vanderschuren, Henk J. Groenewegen, Trevor W. Robbins, and Cyriel M. A. Pennartz. 2004. 'Putting a Spin on the Dorsal–Ventral Divide of the Striatum'. *Trends in Neurosciences* 27 (8): 468–74. https://doi.org/10.1016/j.tins.2004.06.006.

Walf, Alicia A., and Cheryl A. Frye. 2007. 'The Use of the Elevated plus Maze as an Assay of Anxiety-Related Behavior in Rodents'. *Nature Protocols* 2 (2): 322–28. https://doi.org/10.1038/nprot.2007.44.

Wall, Nicholas R., Mauricio De La Parra, Edward M. Callaway, and Anatol C. Kreitzer. 2013. 'Differential Innervation of Direct- and Indirect-Pathway Striatal Projection Neurons'. *Neuron* 79 (2): 347–60. https://doi.org/10.1016/j.neuron.2013.05.014.

Wallace, Michael L., Arpiar Saunders, Kee Wui Huang, Adrienne C. Philson, Melissa Goldman, Evan Z. Macosko, Steven A. McCarroll, and Bernardo L. Sabatini. 2017. 'Genetically Distinct Parallel Pathways in the Entopeduncular Nucleus for Limbic and Sensorimotor Output of the Basal Ganglia'. *Neuron* 94 (1): 138-152.e5. https://doi.org/10.1016/j.neuron.2017.03.017.

Wang, Dong V., Fang Wang, Jun Liu, Lu Zhang, Zhiru Wang, and Longnian Lin. 2011. 'Neurons in the Amygdala with Response-Selectivity for Anxiety in Two Ethologically Based Tests'. *PloS One* 6 (4): e18739. https://doi.org/10.1371/journal.pone.0018739.

Wang, Hong, and Virginia M. Pickel. 2002. 'Dopamine D2 Receptors Are Present in Prefrontal Cortical Afferents and Their Targets in Patches of the Rat Caudate-Putamen Nucleus'. *Journal of Comparative Neurology* 442 (4): 392–404. https://doi.org/10.1002/cne.10086.

Wendler, Etieli, Jessica C. C. Gaspar, Tatiana L. Ferreira, Janaína K. Barbiero, Roberto Andreatini, Maria A. B. F. Vital, Charles D. Blaha, Philip Winn, and Claudio Da Cunha. 2014. 'The Roles of the Nucleus Accumbens Core, Dorsomedial Striatum, and Dorsolateral Striatum in Learning: Performance and Extinction of Pavlovian Fear-Conditioned Responses and Instrumental Avoidance Responses'. *Neurobiology of Learning and Memory* 109 (March):27–36. https://doi.org/10.1016/j.nlm.2013.11.009.

Wu, Zhijian, Aravind Asokan, and R. Jude Samulski. 2006. 'Adeno-Associated Virus Serotypes: Vector Toolkit for Human Gene Therapy'. *Molecular Therapy* 14 (3): 316–27. https://doi.org/10.1016/j.ymthe.2006.05.009.

Xu, Lin, Roger Anwyl, and Michael J. Rowan. 1998. 'Spatial Exploration Induces a Persistent Reversal of Long-Term Potentiation in Rat Hippocampus'. *Nature* 394 (6696): 891–94. https://doi.org/10.1038/29783.

Yin, Henry H., and Barbara J. Knowlton. 2004. 'Contributions of Striatal Subregions to Place and Response Learning'. *Learning & Memory* 11 (4): 459–63. https://doi.org/10.1101/lm.81004.

Yin Henry and Knowlton Barbara. 2006. 'The Role of the Basal Ganglia in Habit Formation'. *Nature Reviews Neuroscience* 7 (6): 464–76. https://doi.org/10.1038/nrn1919.

Yin, Henry H., Shweta Prasad Mulcare, Monica R. F. Hilário, Emily Clouse, Terrell Holloway, Margaret I. Davis, Anita C. Hansson, David M. Lovinger, and Rui M. Costa. 2009. 'Dynamic Reorganization of Striatal Circuits during the Acquisition and Consolidation of a Skill'. *Nature Neuroscience* 12 (3): 333–41. https://doi.org/10.1038/nn.2261.

Zhao, Hua, Bei-Lin Zhang, Shao-Jun Yang, and Benjamin Rusak. 2015. 'The Role of Lateral Habenula–Dorsal Raphe Nucleus Circuits in Higher Brain Functions and Psychiatric Illness'. *Behavioural Brain Research*, Special Issue: Serotonin, 277 (January):89–98. https://doi.org/10.1016/j.bbr.2014.09.016.

Zhou, Fu-Ming, Charles J. Wilson, and John A. Dani. 2002. 'Cholinergic Interneuron Characteristics and Nicotinic Properties in the Striatum'. *Journal of Neurobiology* 53 (4): 590–605. https://doi.org/10.1002/neu.10150.

Zingg B, Chou XL, Zhang ZG, Mesik L, Liang F, Tao HW, Zhang LI. AAV-Mediated Anterograde Transsynaptic Tagging: Mapping Corticocollicular Input-Defined Neural Pathways for Defense Behaviors. Neuron. 2017 Jan 4;93(1):33-47. doi: 10.1016/j.neuron.2016.11.045. Epub 2016 Dec 15. PMID: 27989459; PMCID: PMC5538794.

8 Other activities and scientific contribution

8.1 Summary

In addition to the laboratory activities and other experimental work, I had the opportunity to attend numerous seminars in the fields of neuroscience and neurobiology. I also engaged in tutoring activities for undergraduate and master's students in the Master's degree program in Neurobiology and conducted teaching activities during practical lessons in the courses "Behavioral Neuroscience Methods" and "Psychobiology and Elements of Pharmacology" for the Master's degree program in Neurobiology at Sapienza University of Rome. Additionally, I was awarded a collaboration grant to tutor students in the "Foundations of Neuroscience" course for the degree program in "Mathematical Sciences for Artificial Intelligence." Finally, I contributed to a scientific publication and presented some of the data produced during my Ph.D. at an international conference in the field of neuroscience.

8.2 Seminars

JØRGEN JENNUM. A WINDOW FOR UNDERSTANDING NEURODEGENERATIVE DISEASE. WEBINAR. 25/01/2022

MARTA MOREY RAMONELL. DEVELOPMENTAL WIRING AND ADULT PLASTICITY OF NEURAL CIRCUITS. SAPIENZA UNIVERSITÀ DI ROMA AULA BOVET. 25/03/2022

RAFFAELE FERRI. CLINICAL NEUROPHYSIOLOGY OF ISOLATED REM SLEEP BEHAVIOR DISORDER: A WINDOW ON NEURODEGENERATION. WEBINAR. 24/01/2022.

GRAZIANO FIORITO. L'ESPRESSIONE DELLE EMOZIONI. AULA RM111 - AULA MAGNA, EDIFICIO C, REGINA ELENA. 22/04/2022

ALFONSO ARAQUE. TRIPARTITE SYNAPSES: ASTROCYTE REGULATION OF SYNAPTIC AND NETWORK FUNCTION. AULA ODEION, MUSEO DELL'ARTE (BUILDING CU003). 01/04/2022

MARTINE AMMASSARI-TEULE. AUTISM, AUTOPHAGY AND GENDER. WEBINAR. 17/06/2022

MATTHEW HILL. CANNABINOIDS, THE AMYGDALA AND STRESS. WEBINAR. 23/09/2022

KAREL SVOBODA. NEURAL CIRCUITS AND MECHANISMS UNDERLYING PLANNING AND MOVEMENT. WEBINAR. 23/09/2022

SILVIA SPADACENTA. THE COMMON MARMOSET AS A MODEL OF HUMAN SOCIAL INTERACTIONS. AULA MAGNA – RM111 (EDIFICIO C REGINA ELENA). 20/12/2022

GISELLA VETERE. DECODING MEMORY ACQUISITION AND CONSOLIDATION IN MICE. AULA BOVET, EDIFICIO EX FISIOLOGIA GENERALE, CU026, DIPARTIMENTO BBCD, SAPIENZA UNIVERSITÀ DI ROMA. 19/12/2022

ALFREDO BERARDELLI E ALBERTO OLIVERIO. IL CERVELLO E I SUOI MECCANISMI COGNITIVI. PALAZZO DEL RETTORATO DELLA SAPIENZA UNIVERSITÀ DI ROMA. 19/01/2023

MARIO CARTA. THE CELLULAR CODING OF TEMPERATURE IN THE MAMMALIAN CORTEX. AULA LUCIANI CU027. 05/05/2023

RAY DOLAN. INFERENCE, NEURAL REPLAY AND COGNITIVE MAPS. AULA ODEION. 25/05/2023

MARILENA GRIGUOLI. ROLE OF SEPTAL CHOLINERGIC NEURONS AND NEUROLIGIN 3 IN SOCIAL NOVELTY DISCRIMINATION. WEBINAR. 14/07/2023

8.3 Training courses

IZSLER. LEGISLAZIONE NAZIONALE ED ETICA. Virtual. 28/10/2022

IZSLER. BIOLOGIA E GESTIONE DEGLI ANIMALI DA LABORATORIO. Virtual. 28/10/2022

Esperto Radiazioni Ottiche Artificiali (ROA) e Tecnico sicurezza laser (TSL). Formazione generale sull'uso e sulla sicurezza di laser da laboratorio. La Sapienza. 11/1/2024

UniteImaSapienza. Formazione generale salute e sicurezza sul lavoro per lavoratori ed equiparati. 19/3/2024

Training course on confocal microscope. 25-16/1/2024. La Sapienza.

8.4 Event organization

Organization of the site visit of the advisory board at the Charles Darwin Department of Biology and Biotechnology. 21-23 September 2022

8.5 Tutoring activities

Alessia Frenza. Master's student in the Neurobiology program. 2021-2023

Caterina Virginia Addario Chieco. Bachelor's student in biological sciences and Master's student in the Neurobiology program. 2021-2024

Francesco Gregorio. Master's student in the Neurobiology program. 2023-2024

Tutoring for the course "Fundamentals of Neuroscience" for the degree in "Mathematical Sciences for Artificial Intelligence". 2023

8.6 Teaching activities

Teaching activities for practical lessons in "Behavioral Neuroscience Methods" and "Psychobiology and Elements of Pharmacology" for the Master's Degree in Neurobiology at La Sapienza University of Rome. 2022-2024

8.7 Scholarship

Recipient of a 40-hours tutoring scholarship for the course "Fundamentals of Neuroscience" for the degree in "Mathematical Sciences for Artificial Intelligence" (Call No. 4/2023). 2023

8.8 Peer review activities

Frontiers in Neuroscience - Reviewed 1 research article. 2024

8.9 Publications

E. Centofante, **L. Fralleoni**, C. Lupasco, M. Migliore, A. Rinaldi & A. Mele. *Specific patterns of neural activity in the hippocampus after massed or distributed spatial training*. Scientific Reports, 13, 13357 (2023). https://doi.org/10.1038/s41598-023-39882-0

8.10 Abstracts

L. Fralleoni, A. Frenza, C.V. Addario Chieco, F. Gregorio, A. Rinaldi. *Bidirectional control of BLA-DMS and PFC-DMS projectons on innate avoidance behaviour in*

mice. Federation of European Neuroscience Societies (FENS), Vienna, Austria. 2024

E. Centofante, **L. Fralleoni**, C. Lupasco, A. Rinaldi, M. Migliore, A. Mele. Different hippocampal activation pattern following massed or distributed spatial training in mice. Accepted for the 49th Meeting of the European Brain and Behaviour Society (EBBS) - Virtual, Losanne, Switzerland, 4-8 September 2021.

S. Gasparini, D. Cimino, **L. Fralleoni**, V. Licursi, A. Rinaldi, C. Mannironi, C. Presutti. CircRNAs: a potential involvement in the pathophysiology of autism spectrum disorder. Neuroepigenetics: From Cells to Behaviour and Disease, EMBO – EMBL Virtual Symposium, 28-30 October 2020.

S. Gasparini, D. Cimino**, L. Fralleoni**, V. Licursi, A. Rinaldi, C. Presutti, C. Mannironi. Characterization of circular RNAs dysregulated in autism spectrum disorder. The complex life of RNA EMBO - EMBL, 7-9 October 2020.